11-16-2015

Heat Transfer Analysis of Slot Jet Impingement onto Roughened Surfaces

Rashid Ali Alshatti
University of South Florida, q8_r@hotmail.com

Heat Transfer Analysis of Slot Jet Impingement onto Roughened Surfaces

by

Rashid Ali Alshatti

A dissertation submitted in partial fulfillment
of the requirements for the degree of
Doctor of Philosophy in Mechanical Engineering
Department of Mechanical Engineering
College of Engineering
University of South Florida

Co-Major Professor: Muhammad M. Rahman, Ph.D.
Co-Major Professor: Delcie Durham, Ph.D.
Frank Pyrtle, III, Ph.D.
Aydin K. Sunol, Ph.D.
Kamal Alsharif, Ph.D.

Date of Approval:
November 10, 2015

Keywords: Steady, Transient, Water, Silicon, Patterned

DEDICATION

This dissertation is dedicated to my family for their endless support and inspiration. Also, I would like to dedicate this work to my major advisor, Dr. Muhammad M. Rahman, for his guidance and patience throughout this journey. Finally, I would like to dedicate the dissertation to all my friends.

ACKNOWLEDGMENTS

I would like to acknowledge all of my committee members for all the guidance and support they have provided me as well as all of their time and effort to make this work possible. I also would like to thank the Mechanical Engineering Department at the University of South Florida for giving me the opportunity to continue my graduate study through a generous Graduate Teaching Assistantship.

TABLE OF CONTENTS

LIST OF FIGURES

ABSTRACT

The effect of surface roughness on jet impingement heat transfer was investigated in this research. A numerical analysis was conducted for free surface slot jet impinging normally onto a heated plate. Six different geometries and three different plate materials were investigated. The cooling fluid used for the analysis was water, and the flow was laminar with a range of Reynolds number (Re) from 500 to 1000. Temperature distribution, local and average heat transfer coefficient, and local and average Nusselt number were presented for each case.

The steady state heat transfer results show that the increase in Reynolds number (Re) increases the local heat transfer coefficient and the local Nusselt number. Impinging the jet nozzle directly onto a step has a better heat transfer enhancement than impinging the jet nozzle in between steps. Materials with low thermal conductivity exhibit large variation in temperature along the solid-fluid interface. The variations of the interface temperature become smaller between all cases when applying the isothermal boundary condition.

The transient heat transfer results show that the temperature of the interface increases with time until steady state condition is met. Materials with high thermal diffusivity reach the steady state condition with less time. The increase in surface roughness increases the time required to reach the steady state condition. The highest rates of heat transfer were found at locations where no fluid recirculation occurs. It takes less time to reach steady state condition when applying the isothermal boundary condition at the bottom surface of the plate.

CHAPTER 1: INTRODUCTION AND LITERATURE REVIEW

1.1 Introduction

Jet impingement has been used widely in the industry due to its ease of implementation and reliability. It is considered an excellent heat and mass transfer technique. Jet impingement has been used in a variety of applications, such as cooling, heating, and drying, due to its low cost and simple design. Some of the applications that benefit from the jet impingement technique are drying textiles, cooling turbine blades and electronic packages, and quenching and annealing metals. In the electronics design, every 10°C increase in junction temperature will decrease the life of the device by 50%. Therefore, it is very important to provide the best thermal management technique to maximize the device life.

Jet impingements can be categorized in several ways. Two main categories for jet impingement are free surface jet or submerged jet. Free surface jet is when liquid is discharged into an ambient gas while submerged jet is when liquid is discharged into liquid. Also, the geometry of the jet nozzle determines two more categories for jet impingement. The jet nozzle cross section can be either circular (axial or round) or rectangular (planar or slot). Other conditions influence how jet impingement is categorized, such as confinement or the presence of cross flow when multiple jets are present.

One of the challenges facing the jet impingement technique that has been studied in recent years is introducing surface features on the impinging plate. Due to the variety of applications that implement the jet impingement technique, the impinging plate might not always

be a flat surface, as was analyzed in most of the published studies. By introducing surface features, the fluid flow becomes complicated and the need for further studies can benefit the research area of jet impingement heat transfer.

1.2 Literature Review: Steady State Heat Transfer

Steady state jet impingement heat transfer has been studied for several decades. In the 1980s, Inada et al. [1] conducted numerical and experimental analysis for free surface jet impingement on a flat plate with constant heat flux. The authors obtained a temperature gradient equation at the wall with high accuracy within a certain range of values. Also, they found that the location for maximum heat transfer coefficient occurs when height to width of nozzle is equal to 0.7.

During the 1990s, several studies led by Ma were conducted on jet impingement. Ma et al. [2] analytically studied the heat transfer of free surface circular liquid jets. The authors obtained expressions for heat transfer coefficients for laminar flow using integral method. Then, Ma et al. [3] experimentally explored free surface circular jet impinging obliquely on a constant heat flux surface. The authors found maximum heat transfer increases with a decrease in inclination. Also, they found that the maximum heat transfer coefficient reduced by 22% with 45 degrees inclination.

Several others researched steady state jet impingement heat transfer. Chakroun et al. [4] experimentally investigated round air jet impinging upward onto a heated square plate. The authors found that heat transfer increased from 8.3% to 28% compared to smooth surface.

Through the 2000s, researchers continued to study jet impingement. Bula et al. [5] numerically researched a free surface axial jet impinging on a flat disk with discrete heat sources. The authors found that the maximum Nusselt number was located at stagnation point. Also, the

local heat transfer decreased rapidly afterwards. The authors found that the locations of heat sources strongly affected the locations of local heat transfer coefficients. In addition, Bula et al. [6] numerically examined a free surface slot jet impinging on a flat disk with discrete hot sources. The authors found that the heat flux has a small effect on the magnitude of average and local heat transfer coefficient and Nusselt number. Also, the authors suggested that material properties of the plate are the most important factors for ideal plate design thickness.

Additionally, Gau and Lee [7] experimentally investigated air slot jet impinging on a triangular rib-roughened wall. The authors found that a bubble forms between cavities preventing air from penetrating into the walls during the laminar region. Once the air becomes turbulent, it can penetrate cavities. The authors also found that heat transfer decreases when air bubble forms.

Ekkard and Kontrovitz [8] experimentally examined an array of jets impinging on a dimpled surface. The experiment conducted analyzed two plate configurations. The authors found that dimpled surfaces have lower heat transfer coefficient than smooth surfaces. Also, the authors found that the increase in cross-flow increases the heat transfer coefficient.

Sahoo and Sharif [9] numerically investigated confined slot jet impinging on a constant heat flux surface. The authors found that for the range of Reynolds numbers studied, buoyancy effects are not significant for the overall heat transfer process. Also, the authors suggested that the Richardson number becomes significant on the heat transfer process when jet Reynolds number is 30.

Chen et al. [10] theoretically studied free surface slot jets impinging normally on flat surfaces. The authors separated the laminar flow into four regions. Then, the authors developed formulas to solve for local heat transfer coefficients and temperature profiles for each region.

Li et al. [11] experimentally and numerically investigated flow patterns and heat transfer in a confined slot jet. The authors found that a different initial flow field creates two different flow patterns from the same boundary conditions. Also, the authors found that two flow patterns solutions can coexist with the same boundary conditions for Reynolds numbers from 275 to 400.

Lou et al. [12] numerically investigated the effects of geometric parameters on confined jet impingement. The authors found that the increase in nozzle width decreases both heat transfer coefficient and Nusselt number. Also, the authors found that surface roughness causes the working fluid to be trapped and reduces the heat transfer.

Katti and Prabhu [13] experimentally researched circular air jet normally impinging on axisymmetric detached ribs. The authors found that the heat transfer was enhanced from stagnation point until the first rib for all configurations. Also, the authors found that the increase in rib width decreased the Nusselt number downstream of the first rib.

Zhang et al. [14] experimentally and numerically examined liquid jet impinging on a shape memory alloy actuator. The authors observed flow field separation during the heating process. The authors also found that the pressure distribution depends on the motion of the actuator and jet velocity.

Akansu et al. [15] experimentally researched the effects of inclination for slot jet impinging on a flat surface. The authors found that the location for maximum heat transfer depends on the angle of inclination. Also, they found that as the inclination angle increases, the maximum heat transfer location shifts upward in the plate.

Ibuki et al. [16] experimentally investigated slot jet impinging normally or obliquely on a heated flat plate. The authors found that maximum heat transfer location shifts upward in the

plate with the increase in inclination. Also, the authors found that the effects on Nusselt number is not significant with the increase in inclination at the location downward the plate.

Naphon and Wongwises [17] experimentally explored liquid jet impinging on a rectangular fin heat sink of a central processing unit of a personal computer. The authors found that they were able to obtain lower temperatures for liquid jet impingement compared to conventional cooling systems.

Choo and Kim [18] experimentally compared confined and unconfined jet impingement. The authors found that thermal performance of confined and unconfined jets are similar under the same pumping power condition. Also, the authors found that thermal performance for confined jet is 20-30% lower than unconfined jet under the same flow rate condition.

Xing et al. [19] experimentally and numerically investigated different crossflow schemes of jet impingement on a flat and rib-roughened plate. The authors found that jet height to jet spacing ratio of three results the highest heat transfer coefficient. Also, the authors found that the increase of Reynolds number increases the heat transfer enhancement ratio.

Lee et al. [20] experimentally examined confined slot jet impinging on an isothermal flat plate. The authors found that the local Nusselt number decreases as distance from stagnation point increases. Also, the authors found that the decrease in the ratio of nozzle height to width increases the local Nusselt number at the stagnation point.

Liu et al. [21] experimentally researched arrays of jet impinging on target surfaces. The authors found that heat transfer enhanced near grooves. Also, the authors found that the average Nusselt number enhanced 15% by grooved surfaces, but overall, the average Nusselt number is comparable to smooth surface.

Tan et al. [22] experimentally investigated air jet impinging in a semi-confined channel. The authors analyzed three different configurations and found that rib-roughened channels enhanced the heat transfer by 30% compared to smooth surfaces. The authors found that the inverted v-shaped ribs are the best configuration for heat transfer enhancement.

1.3 Literature Review: Transient Heat Transfer

Transient jet impingement heat transfer has been investigated less in comparison to steady state heat transfer. Fujimoto et al. [23] numerically analyzed transient circular free surface liquid jets. The authors found that heat transfer increases with Reynolds number and decreases with distance away from stagnation point.

Rahman et al. [24] numerically studied transient free surface axial jet impinging on a uniformly heated disk. The authors found that local temperatures and heat flux increase with time at different rates. Also, the authors found that average heat transfer coefficient and Nusselt number decrease to a minimum value then increase to their steady state value. The authors also discovered that by increasing Reynolds number, it takes less time to reach steady state condition. Additionally, the research determined that materials with higher thermal diffusivity reach a steady state condition faster.

Liu et al. [25] experimentally explored transient heat transfer of air jet impinging onto confined disk. The authors found that as jet Reynolds number decreases, dimensionless chip temperature distribution becomes more uniform. The authors presented a correlation for transient heat flux for stationary disk. Also, the authors found the center of the chip where the maximum Nusselt number is located.

Yang and Tsai [26] numerically investigated the transient heat transfer of air jet impingement onto flat disk. The authors found that heat transfer coefficients can be maximized

by increasing turbulence values. Also, the authors discovered that the decrease in Reynolds number increases the time to reach steady state.

Rahman and Lallave [27] numerically analyzed transient heat transfer jet impinging on a rotating disk. The authors learned that as time goes toward steady state, interface temperature increases and Nusselt number decreases. The authors also discovered that the increase in Reynolds number increases Nusselt number and decreases the time required to reach steady state. Additionally, the authors found that the increase in Ekman number decreases the average Nusselt number.

Karwa et al. [28] experimentally investigated transient heat transfer of free surface jet impingement questing of a stainless steel cylinder. The authors found that the increase in jet velocity increases the heat fluxes in all regions. Also, the authors learned that as distance increases from the impingement region, heat flux decreases.

Rahman and Hernandez [29] numerically investigated the transient heat transfer of liquid jet impingement on a convex surface. The authors found that as time progresses, the interface temperature increases and heat transfer coefficient decreases. Also, the authors discovered that Reynolds number is the controlling parameter for the length of the transient process.

Lee et al. [30] experimentally and numerically investigated transient heat transfer of slot jet impingement. The authors found that increasing Reynolds number will increase the local Nusselt number. Also, the authors observed different flow behaviors at different Reynolds numbers and height to width of the jet nozzle ratios.

Yang et al. [31] numerically examined a row of jet impinging onto a cylindrical channel. The authors noticed variations of local Nusselt number with time. The authors discovered that the last jet in the row exhibits most of the temperature changes as time progresses.

1.4 Objectives

By analyzing the literature review for steady state heat transfer, one can notice that most of the research found in the literature was conducted for flat surfaces. The majority of the research conducted for surfaces with features used either air as the cooling fluid or some kind of confinement to the plate. Also, the transient heat transfer jet impingement was less researched compared to the steady state heat transfer. In addition, all the transient literature found in the previous section conducted for flat plate and the majority of them used circular jet nozzle.

It can be seen that a need exists for more research to be conducted analyzing the steady state and transient jet impingement heat transfer for roughened surfaces. The objective of the present research is to study the effects of surface features on heat transfer. The research analyzes different plate geometries and their effects on heat transfer. Also, the research compares different jet Reynolds number and different plate materials. Additionally, the variations of the step height and its effect on heat transfer are taken into consideration. The effects of constant heat flux boundary condition and isothermal boundary condition are studied. In summary, variations of the following parameters were taken into consideration in the current research:

- Plate geometry
- Reynolds number
- Plate material
- Height of surface features
- Boundary condition at the bottom surface of the plate

CHAPTER 2: STEADY STATE HEAT TRANSFER

2.1 Mathematical Model

The following mathematical analysis is presented for two-dimensional slot jet impinging normally onto a solid plate with surface roughness as shown in Figures (1-6). The bottom of the solid plate was uniformly heated for the base model; as a variation from the base model, the bottom of the plate was kept at constant temperature. The fluid used in this problem was water and assumed to be incompressible. A list of the symbols used in this section can be found in Appendix A. The following equations for conservation of mass, momentum, and energy are written in the Cartesian coordinate system [32, 33]:

$$\nabla \cdot \vec{V} = 0 \tag{1}$$

$$\left(\rho_f \vec{V} \cdot \nabla\right) \cdot \upsilon_x = -\frac{\partial p}{\partial x} + \mu \nabla^2 \upsilon_x \tag{2}$$

$$\left(\rho_f \vec{V} \cdot \nabla\right) \cdot \upsilon_y = -\rho_f g - \frac{\partial p}{\partial y} + \mu \nabla^2 \upsilon_y \tag{3}$$

$$\left(\rho_f c_{p_f} \vec{V} \cdot \nabla\right) \cdot T_f = k_f \nabla^2 T_f \tag{4}$$

The heat conduction inside the solid plate can be written as:

$$\nabla^2 T_s = 0 \tag{5}$$

The following boundary conditions are used to solve the previous equations:

At $x = 0, 0 \le y \le b + a$:

$$\frac{\partial T_s}{\partial x} = 0 \tag{6}$$

At $x = 0, b + a \le y \le b + a + H_n$:

$$\upsilon_x = 0, \frac{\partial T_f}{\partial x} = 0 \tag{7}$$

At $x = L, 0 \le y \le b + a$:

$$\frac{\partial T_s}{\partial x} = 0 \tag{8}$$

At $x = L, b + a \le y \le b + a + \delta$:

$$p = p_{atm}, \frac{\partial T_f}{\partial x} = 0 \tag{9}$$

At $y = 0, 0 \le x \le L$:

$$-k_s \frac{\partial T_s}{\partial y} = q_w \tag{10}$$

The isothermal boundary condition equation (10) can be written as:

At $y = 0, 0 \le x \le L$:

$$T_s = T_w \tag{11}$$

At $y = b + a + H_n, 0 \le x \le \frac{W}{2}$:

$$\upsilon_x = 0, \upsilon_y = -\upsilon_j, T_f = T_j \tag{12}$$

At solid-fluid interface:

$$T_s = T_f, \upsilon_x = 0, \upsilon_y = 0, k_s \frac{\partial T_s}{\partial \eta} = k_f \frac{\partial T_f}{\partial \eta} \tag{13}$$

At the free surface:

$$\frac{\partial y}{\partial x} = \frac{\upsilon_y}{\upsilon_x}, p = p_{atm} - \frac{\sigma \frac{d^2\delta}{dx^2}}{\left[1+\left(\frac{d\delta}{dx}\right)^2\right]^{3/2}}, \frac{\partial \upsilon_{fs}}{\partial n} = 0, \frac{\partial T_f}{\partial n} = 0 \tag{14}$$

where υ_{fs} is the velocity component along the free surface.

The local and average heat transfer coefficient can be written as:

$$h = \frac{q_w}{\left(T_{\text{int}} - T_j\right)} \tag{15}$$

$$h_{avg} = \frac{1}{L\left(\overline{T}_{\text{int}} - T_j\right)} \int_0^L h\left(T_{\text{int}} - T_j\right) dx \tag{16}$$

where $\overline{T}_{\text{int}}$ is the average temperature along the interface.

The local and average Nusselt number can be written as:

$$Nu = \frac{hW}{k_f} \tag{17}$$

$$Nu_{avg} = \frac{h_{avg}W}{k_f} \tag{18}$$

2.2 Numerical Computation

The numerical methodology used in this work was following the numerical computation used by [34, 35] and their works are comparable to experimental data found in the literature. The computation software FIDAP [36], a fluid dynamics analysis package, was used to solve the current problem. FIDAP is considered to be an excellent choice for solving free surface problems. The Galerkin finite element method was used to solve the governing equations along with the boundary conditions presented in section 2.1. The infinite number of degrees of freedom

can be broken down to a finite number of degrees using the finite element method. Velocity, pressure, and temperature fields were approximated in each four node quadrilateral element leading to a set of equations that defined the continuum. Introducing a new degree of freedom, which is the position of the free surface, at the nodes on the free surface led to a solution to the free surface problem. The Galerkin finite element method was used to discretize the governing transport equation and boundary conditions. Then, Newton-Raphson algorithm was used to carry out the solution of nonlinear algebraic equations if the guess for the free surface was close enough to the actual value. The solution was assumed to converge when the sum of the residuals for each degree of freedom was less than 1E-6.

All fluid and materials properties were obtained from Bejan [37]. The working fluid used in this research was water. Three different plate materials, which are silicon, copper, and constantan, were considered. The jet nozzle width (W), nozzle height (H_n), plate length (L), and plate thickness (b) were kept at 0.0017 m, 0.0055 m, 0.006475 m, and 0.00125 m, respectively, for all cases. Also, the temperature of the jet (T_j), the temperature of the bottom surface of the plate for the isothermal boundary condition (T_w), and heat flux for the constant heat flux boundary condition (q_w) were kept at 20°C, 50°C and 63 kW/m^2, respectively, for all cases as well. The range of Reynolds number (Re) studied was from 500 to 1000. The height of the step (a) is 0.00025 m for the base model and the range studied was from 0.000125 m to 0.000375 m.

Six different plate configurations were studied as shown in Figures (1-6). Cases A, C, and E are configurations where the jet nozzle is impinging directly onto the step. Cases B, D, and F are configurations where the jet nozzle is impinging in between steps. Due to the timely consuming computation and the symmetry of the problem, the computation was conducted for half of the problem, and the behavior was assumed to be the same when mirrored across the y-

coordinate. The FIDAP codes used for the base model for all cases can be found in Appendices (B-G).

2.3 Results and Discussion

The base model considered in the analysis is a uniformly heated silicon plate with step height of 0.00025 m and Reynolds number of 750. The velocity vector map and isothermal lines of the solid plate for the base model for all cases are shown in Figures (7-18). Figure 7 shows the velocity vector map for case A. The velocity is uniform in the free jet region, and then the water decelerates as it enters the impingement or stagnation region. The water then accelerates parallel to the plate to form the wall jet region as it exits the plate. Figure 8 shows the increase in temperature across the length and the depth of the solid plate for case A. The lowest temperature across the solid plate can be found at the impingement region. Figure 10 shows an increase in temperature for case B compared to case A due to the increase in recirculation before and after the step as shown in the velocity vector map in Figure 9. One can notice a shift in the wall jet region to the right due to a sudden geometry change obstructing the flow when forming the wall jet region. Figures (11, 12, 15, 16) show similar behavior found in Figures (7-8). Also, Figures (13, 14, 17, 18) show similar behavior found in Figures (9-10).

The interface temperature of the base model for all geometries is shown in Figure 19. The interface temperature increases along the plate length and decreases at locations of sudden geometry change. Impinging the jet nozzle directly onto the step shows an overall decrease of the interface temperature of the plate compared to cases B, D, and F where the jet is impinging in between steps. For cases A, C, and E, the fluid has more space away from the stagnation region to accelerate without any obstacles whereas in cases B, D, and F, the fluid gets trapped in the stagnation region in between steps and results in a recirculation of the fluid and builds a thick

layer that brings the overall interface temperature up. The local heat transfer of the base model for all geometries is shown in Figure 20. Case A shows the highest overall local heat transfer coefficient where case B shows the lowest overall local heat transfer coefficient. Highest points of local heat transfer coefficient can be found at the stagnation region and at points with sudden geometry change. The sudden change of the geometry breaks the thermal boundary layer resulting in an increase in local heat transfer coefficient. The Nusselt number of the base model for all geometries is shown in Figure 21. Cases A and E are the most advantageous geometries for removing large heat fluxes. By comparing between cases A, C, and E, it can be observed that increasing the contact surface area between the solid and the fluid interface enhances the heat transfer.

The interface temperature of the base model with Reynolds number of 500 for all geometries is shown in Figure 22. The overall trend remains the same, but there is an increase in overall interface temperature compared to Figure 19. The reason for the difference in temperature is due to the lower renewal rates of cooler liquid at the interface compared to the base model. The local heat transfer of the base model with Reynolds number of 500 for all geometries is shown in Figure 23. The local heat transfer coefficient values are lower than the base model for all cases. The Nusselt number of the base model with Reynolds number of 500 for all geometries is shown in Figure 24. Case A remains the best case compared to all other geometries for heat removal even at lower jet velocity.

The interface temperature of the base model with Reynolds number of 1000 for all geometries is shown in Figure 25. The increase in Reynolds number decreases the interface temperature for all cases. The reason for the decrease is higher liquid renewal rates at the interface causes better circulation compared to the base model. The local heat transfer of the base

model with Reyolds number of 1000 for all geometries is shown in Figure 26. The result of increasing jet velocity can be seen by the increase in local heat transfer coefficient in all cases. The Nusselt number of the base model with Reynolds number of 1000 for all geometries is shown in Figure 27. The increase in Reynolds number increases the Nusselt number for all cases.

The effect of Reynolds number on the average heat transfer coefficient for the base model is shown in Figure 28. As Reynolds number increases, the average heat transfer coefficient increases. Another observation is when the jet is directly impinging onto the step, case A performs the best; on the other hand, case D performs the best when the jet impinging occurs in between steps. Cases where the jet nozzle is impinging directly onto the step show better heat transfer enhancement with increase in surface area. Cases where the jet nozzle is impinging in between steps show better heat transfer enhancement with geometries that reduces the flow recirculation. The overall observation is that increasing Reynolds number enhances the circulation between the steps and improves the heat transfer.

The interface temperature of the base model with constantan as a plate material for all geometries is shown in Figure 29. It can be observed that there are larger temperature variations compared to Figure 19. The reason for the high variations in interface temperature is the low thermal conductivity of constantan. The low thermal conductivity of constantan makes it insulate the heat source and is influenced by the temperature of the fluid at the solid-fluid interface. The local heat transfer of the base model with constantan as a plate material for all geometries is shown in Figure 30. Impinging the jet nozzle directly onto the step produces higher peaks than in the base model. The Nusselt number of the base model with constantan as a plate material for all geometries is shown in Figure 31. There is a heat removal advantage at the location where the jet is directly impinging; the heat removal advantage decreases after half of the plate length.

The interface temperature of the base model with copper as a plate material for all geometries is shown in Figure 32. The interface temperature for the copper plate is more uniform across the plate length than in the base model shown in Figure 19. The reason for this trend is due to the high thermal conductivity of copper. The local heat transfer of the base model with copper as a plate material for all geometries is shown in Figure 33. The local heat transfer is uniform across the plate length compared to silicon and constantan. The Nusselt number of the base model with copper as a plate material for all geometries is shown in Figure 34. There are no huge variations of the Nusselt number across the plate length compared to silicon and constantan.

The interface temperature of the base model with a step height of 0.000125 m for all geometries is shown in Figure 35. The interface temperature follows the trend seen in Figure 19, but with lower overall interface temperatures for all geometries. The decrease in step height improves the circulation between the steps. Cases A, C, and E exhibit higher starting interface temperature while cases B, D, and F exhibit lower starting interface temperature. The local heat transfer of the base model with a step height of 0.000125 m for all geometries is shown in Figure 36. Reducing the step height brings all geometries closer to each other compared to Figure 20. The Nusselt number of the base model with a step height of 0.000125 m for all geometries is shown in Figure 37. The most benefited geometries from reducing the step height are the ones where the jet nozzle impinging offset to the steps. The enhancement in cases B, D, and F is due to the reduction of the step height which obstructing the fluid when forming the wall jet region.

The interface temperature of the base model with a step height of 0.000375 m for all geometries is shown in Figure 38. There is a slight decrease in the interface temperature at the beginning of the plate for cases A, C, and E compared to Figure 19. Another observation is that

cases B, D, and F exhibit an overall increase in the interface temperature along the plate length. The reason for the increase in temperature is the increase in recirculation of the fluid that occurs in between steps. The local heat transfer of the base model with a step height of 0.000375 m for all geometries is shown in Figure 39. Cases B and F exhibit the largest drop in local heat transfer coefficient along the plate length. The Nusselt number of the base model with a step height of 0.000375 m for all geometries is shown in Figure 40. Cases B and F perform the worst in heat transfer removal when increasing the step height.

Figure 41 shows the variations of the interface temperature across the plate length. The analysis was conducted for the base model with isothermal boundary condition instead of constant heat flux at the bottom of the plate. The wall temperature was set at 50°C. Results show the lowest temperatures that can be obtained are at the locations of the steps. Figure 42 shows the variations of local heat transfer coefficient for the isothermal boundary condition. Figure 43 shows the variations of the local Nusselt number for the isothermal boundary condition. The isothermal boundary condition strongly influences the behavior of the plots. All cases exhibit much similar behavior except the locations of the steps when compared to the constant heat flux boundary condition.

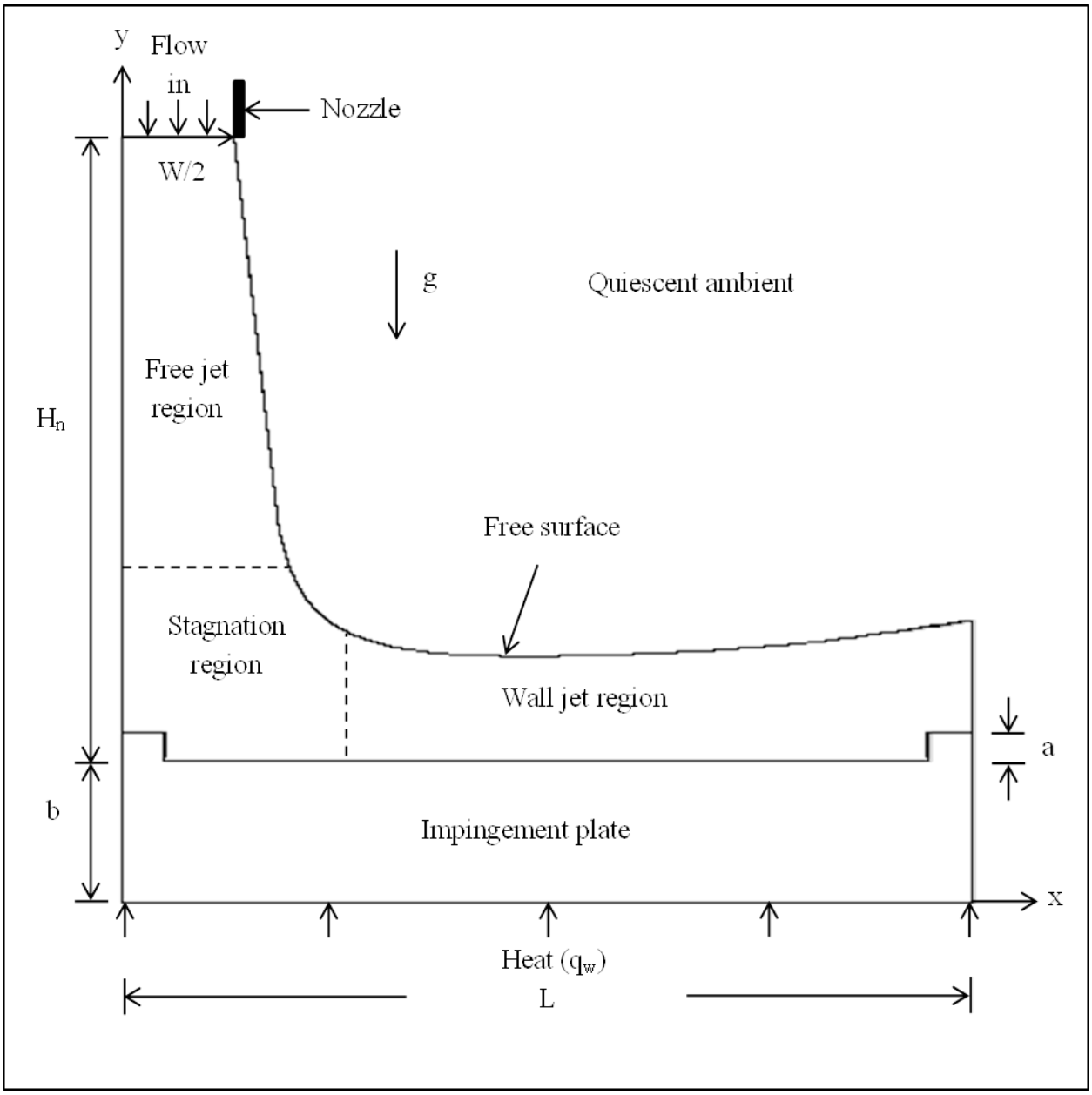

Figure 1: Schematic of Case A

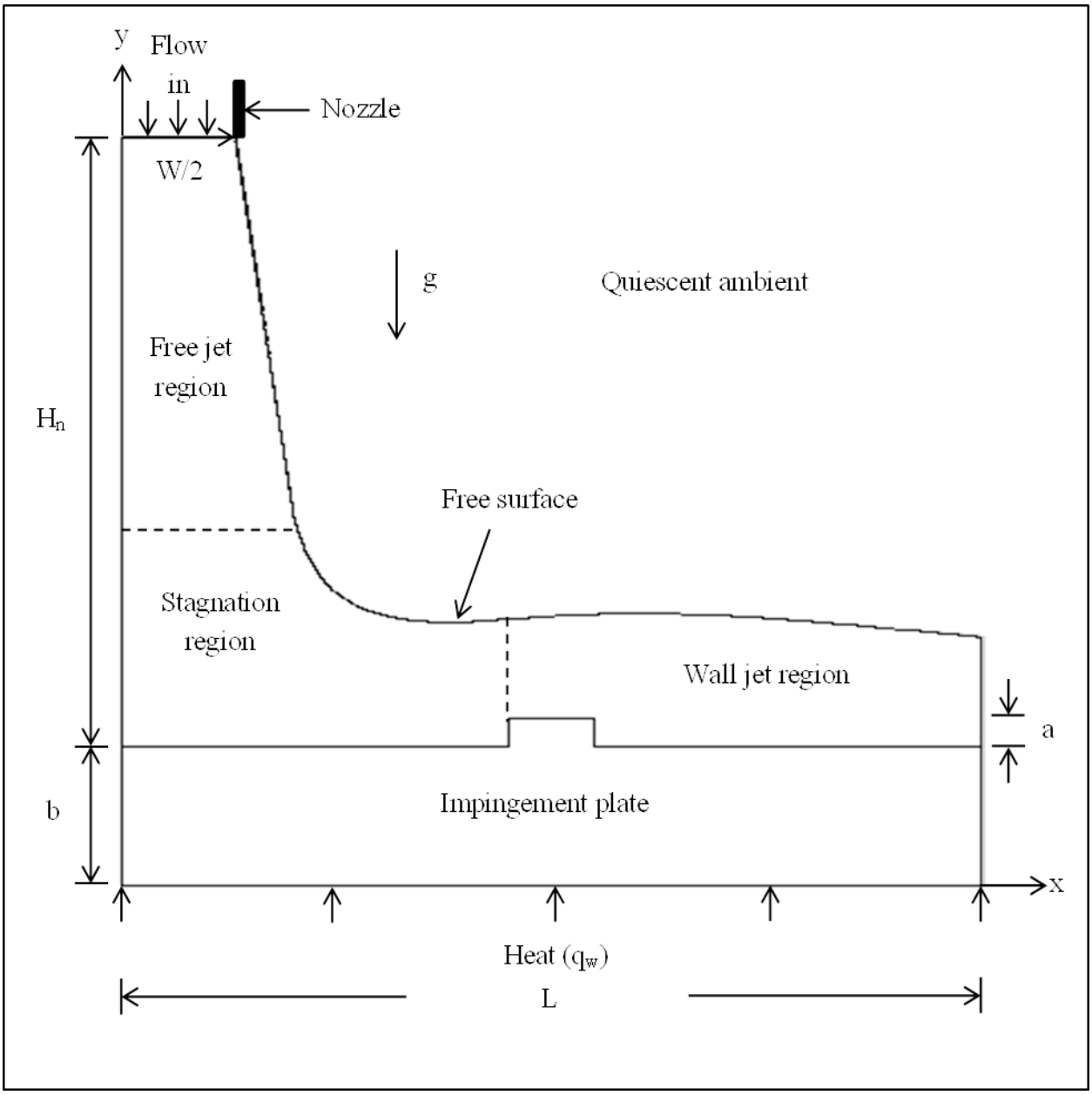

Figure 2: Schematic of Case B

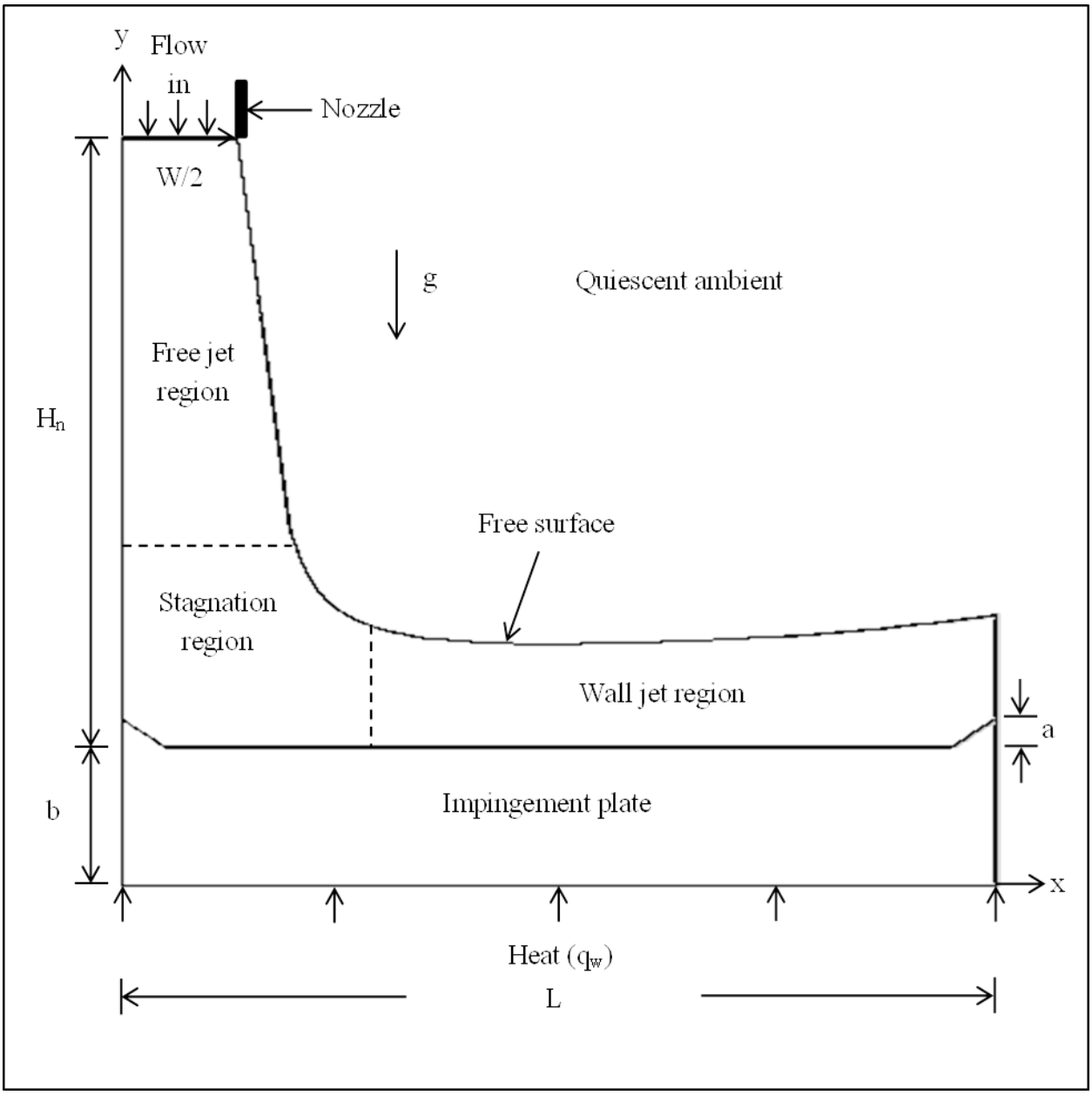

Figure 3: Schematic of Case C

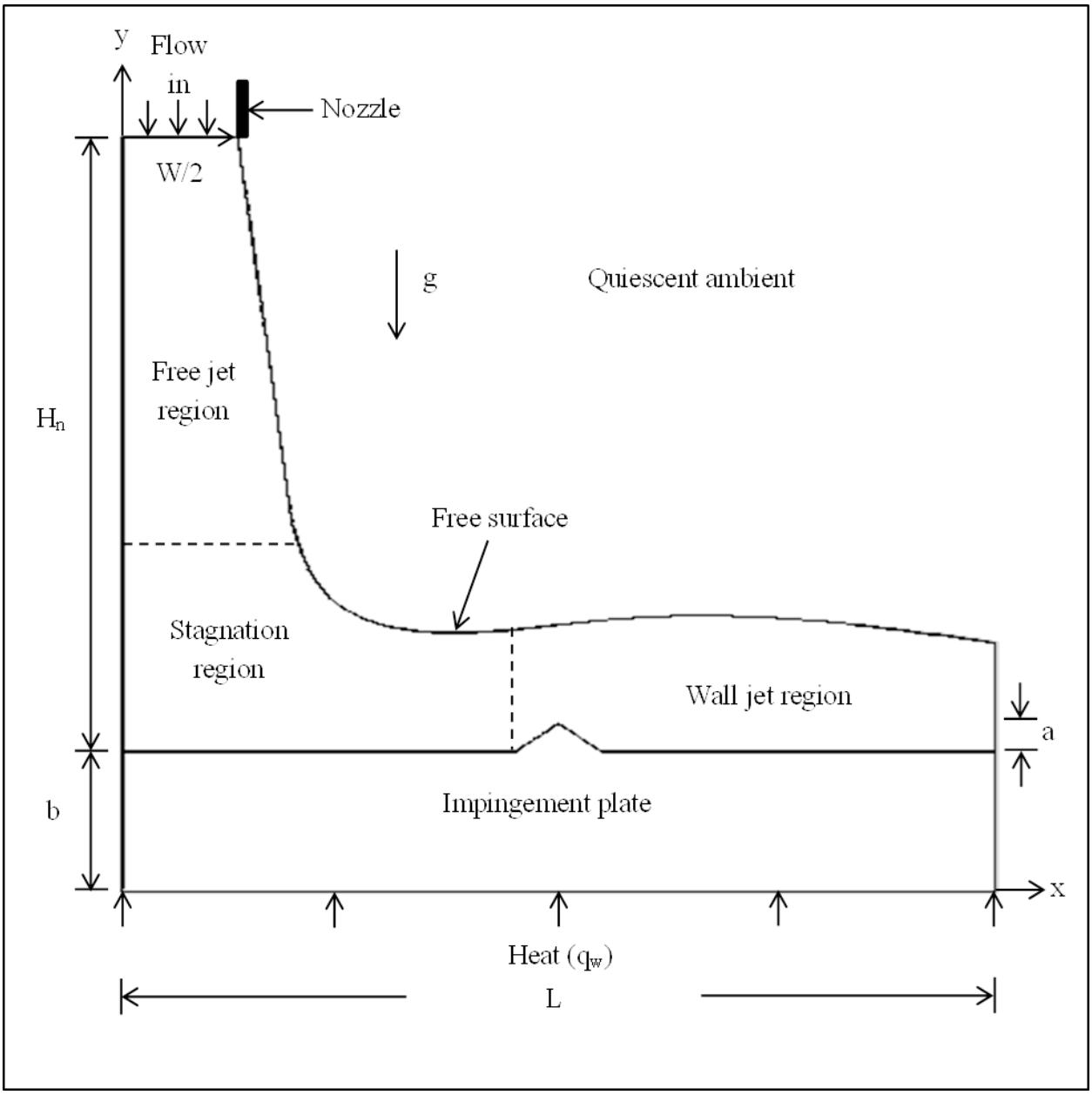

Figure 4: Schematic of Case D

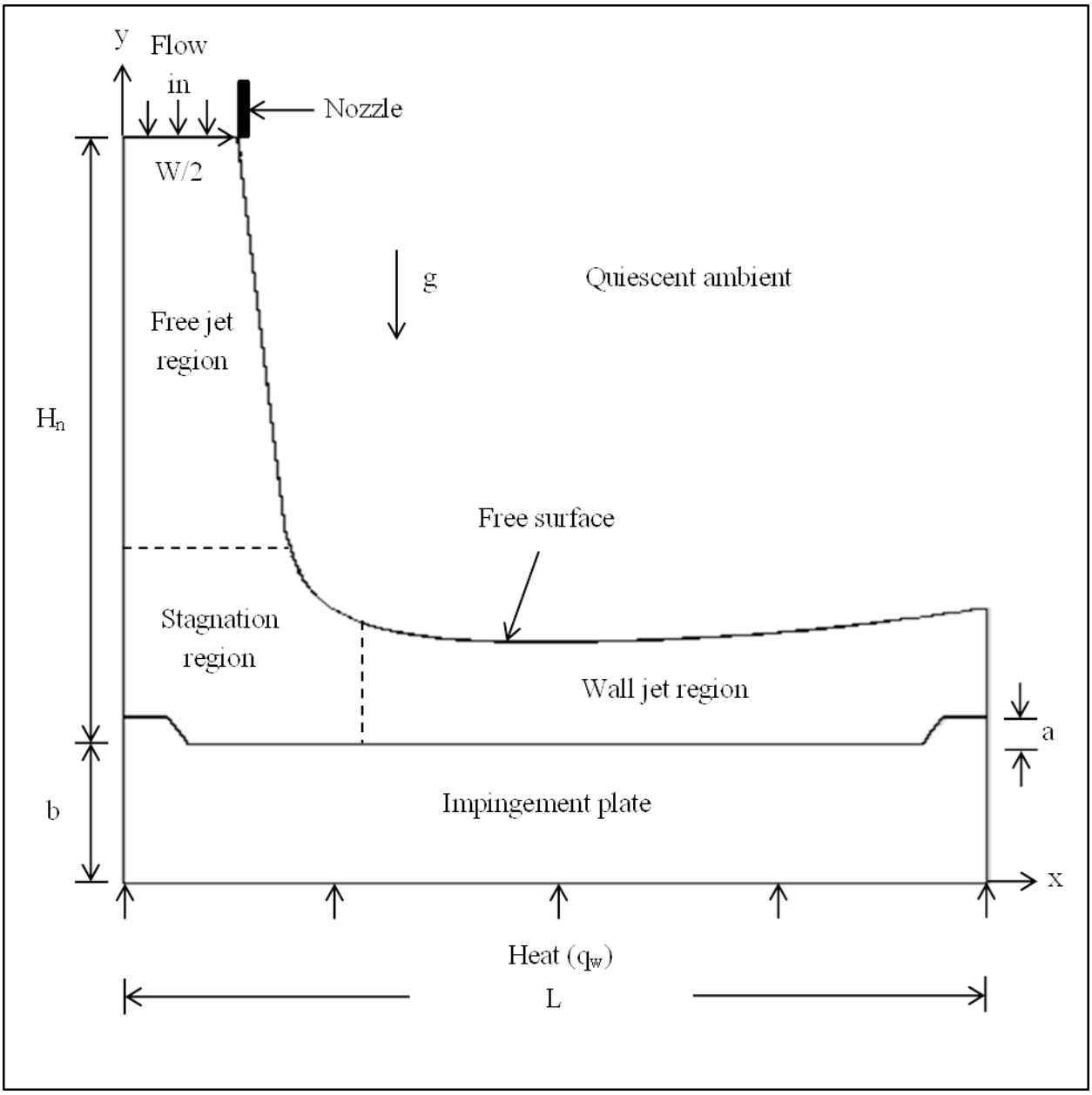

Figure 5: Schematic of Case E

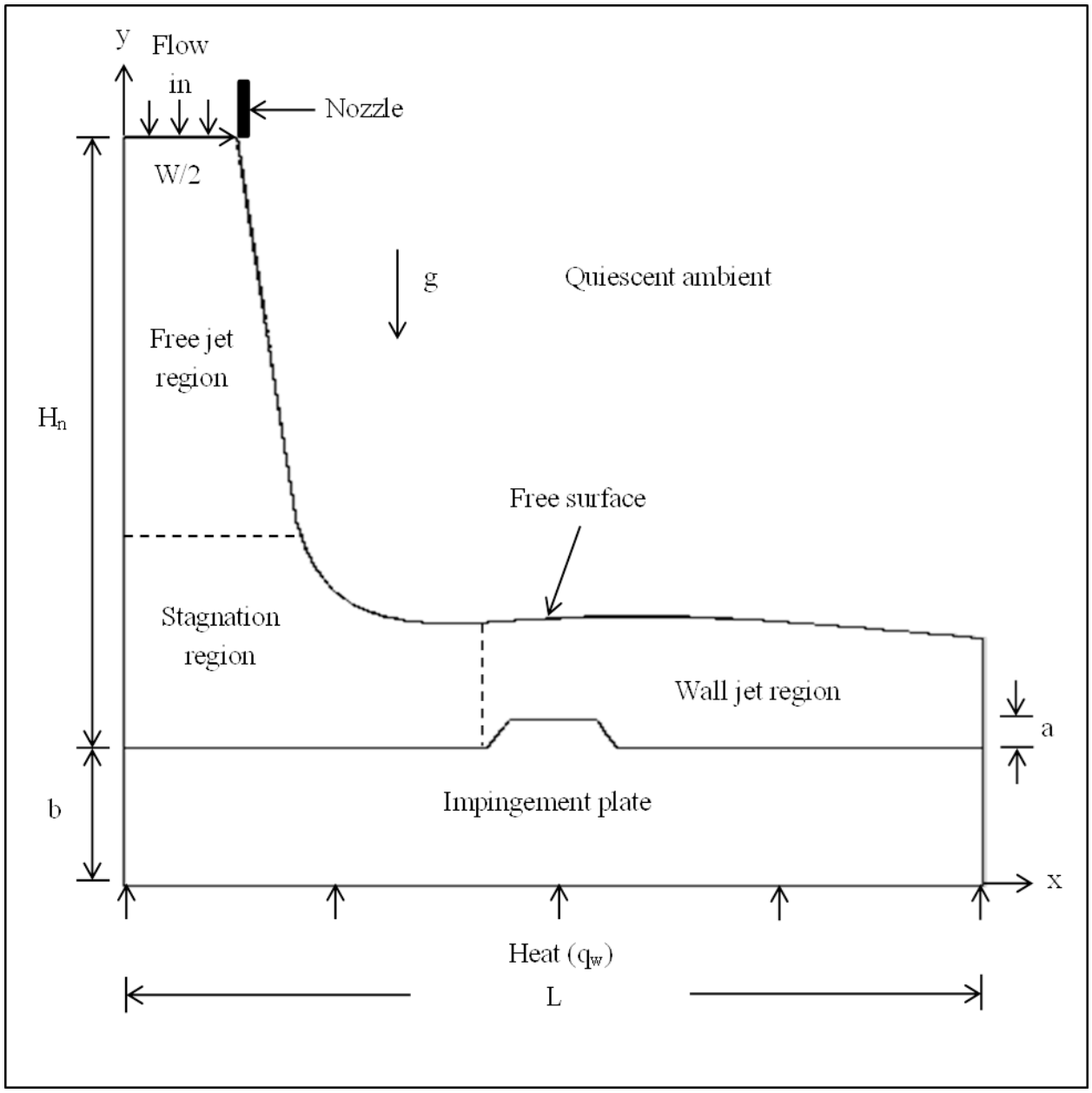

Figure 6: Schematic of Case F

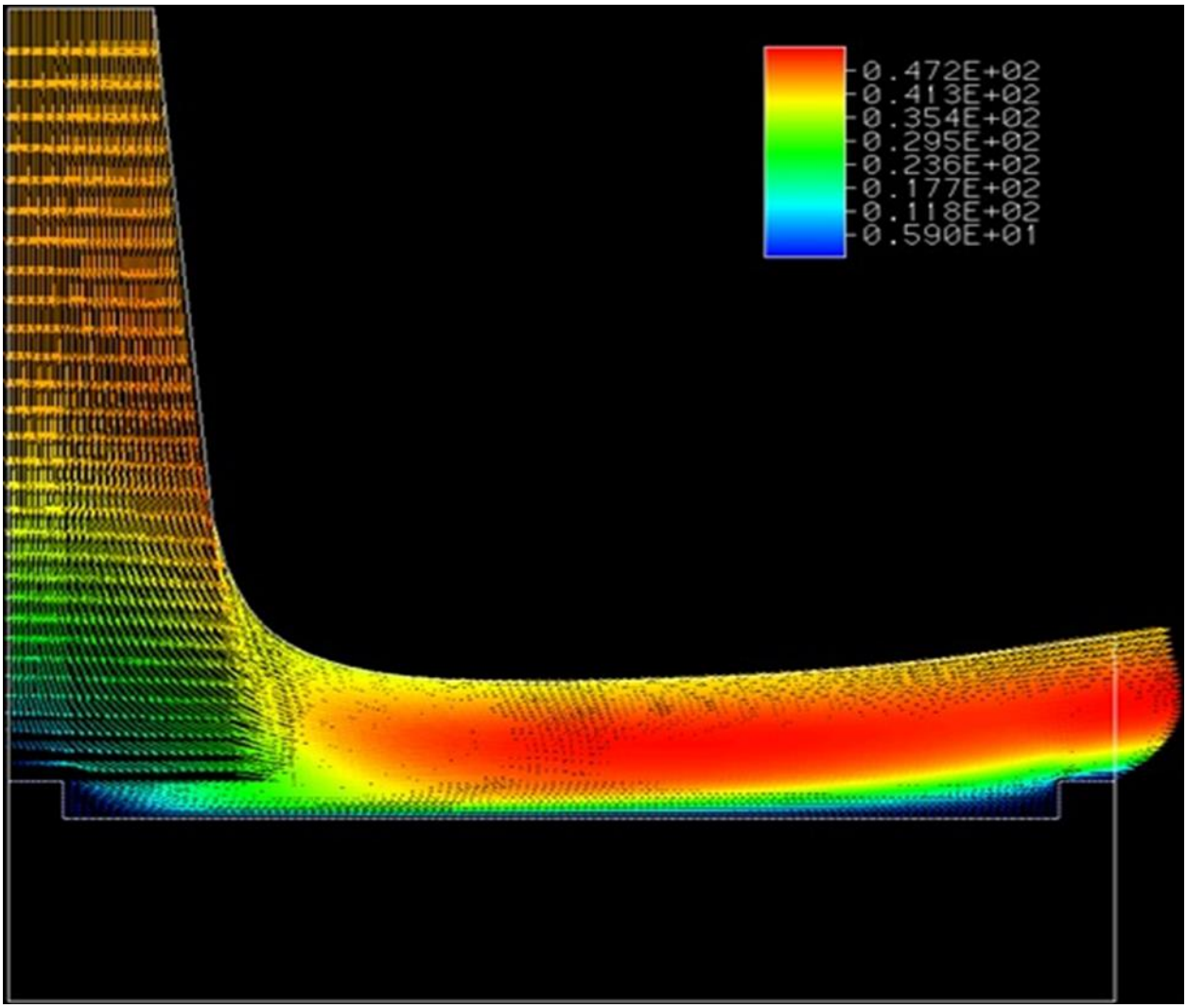

Figure 7: Velocity Vector of Case A

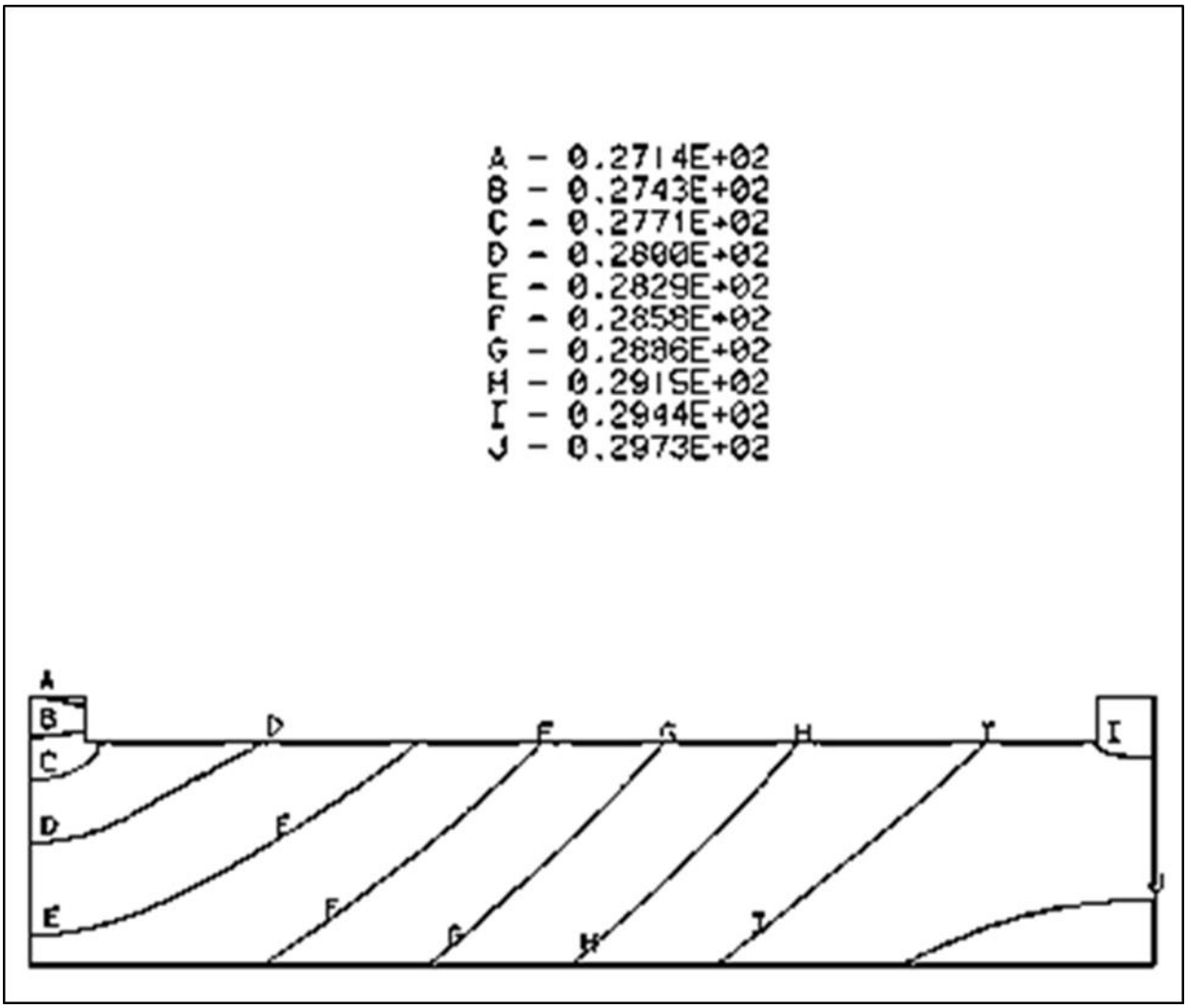

Figure 8: Isothermal Lines of Case A in Degrees Celsius

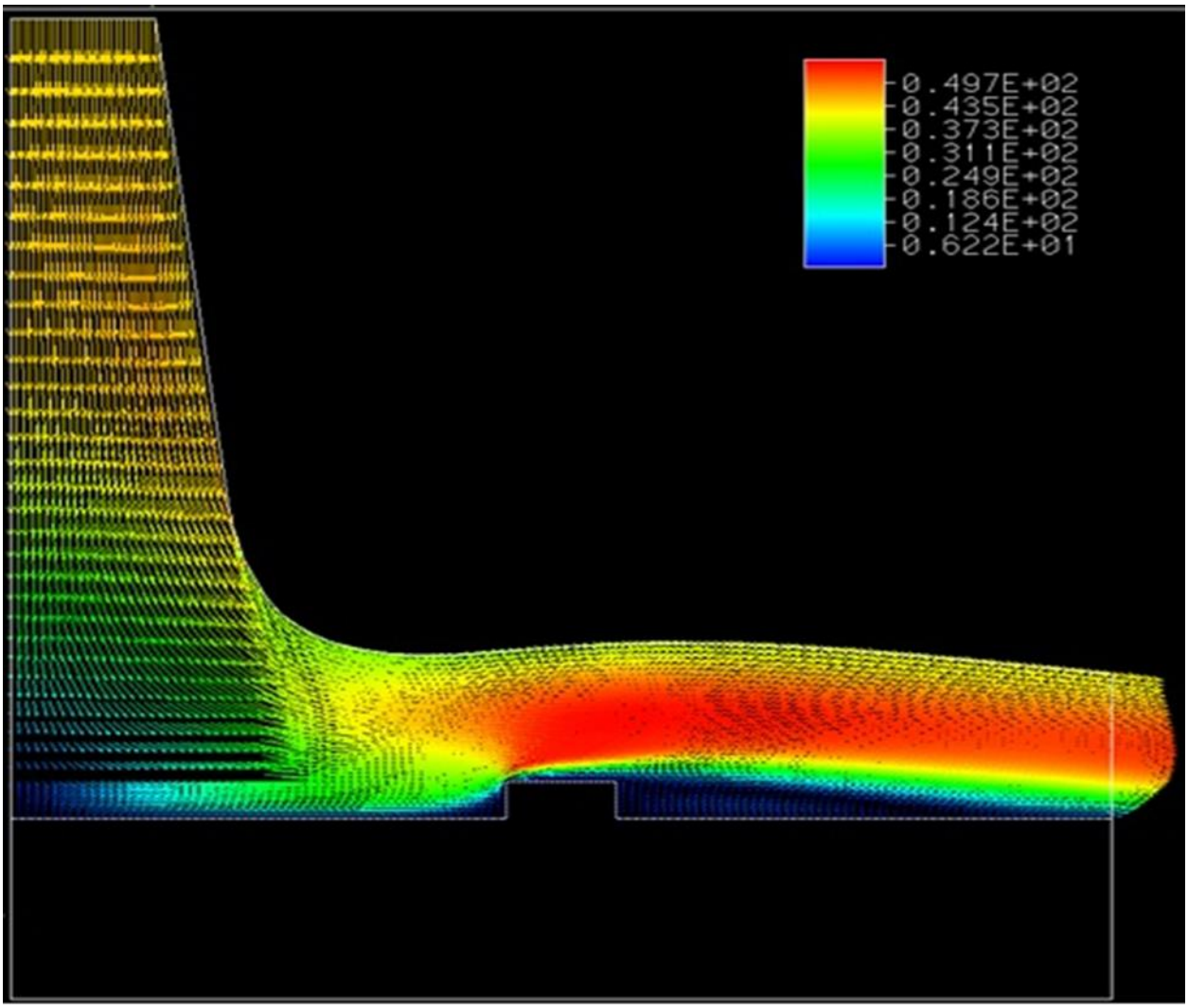

Figure 9: Velocity Vector of Case B

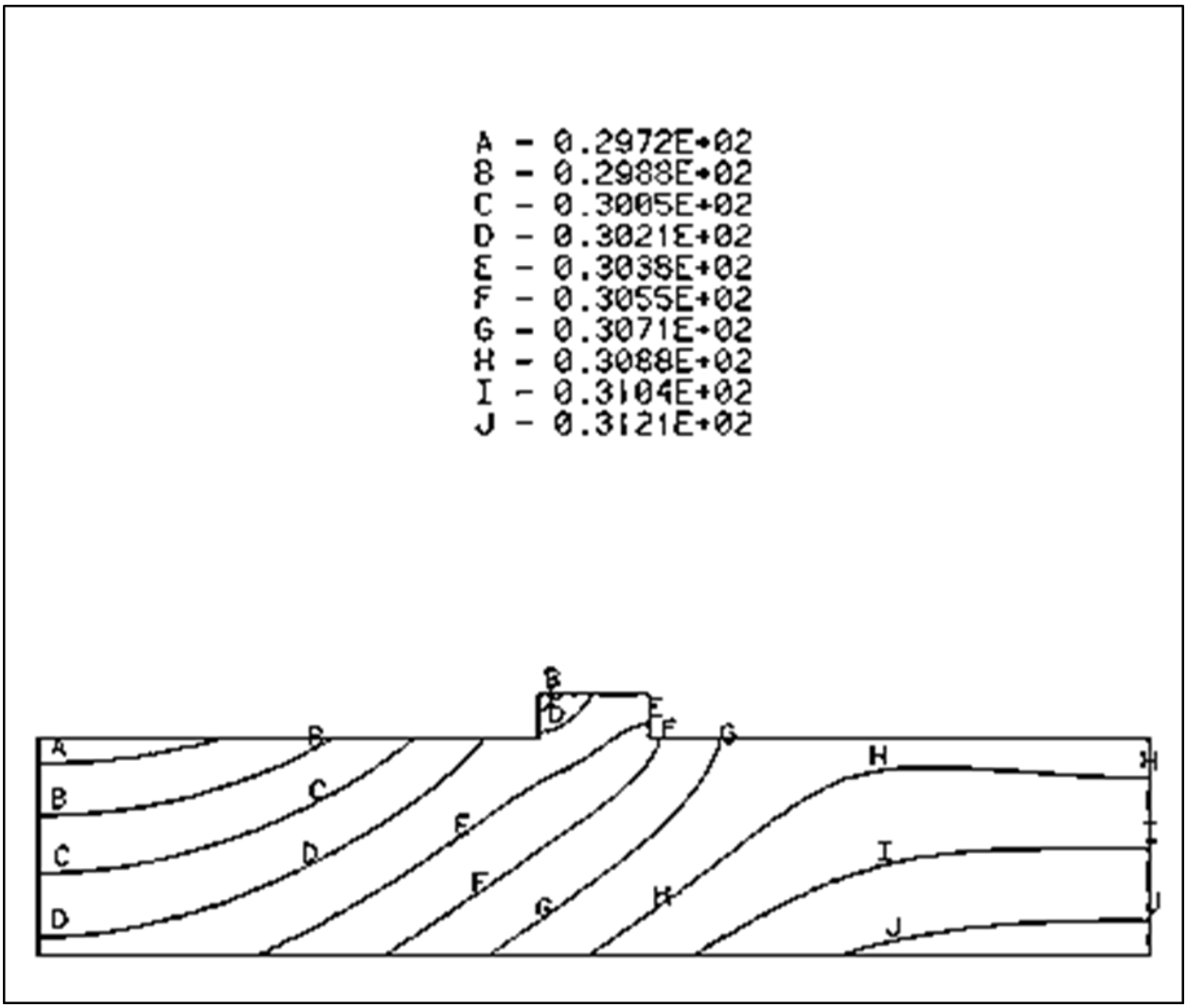

Figure 10: Isothermal Lines of Case B in Degrees Celsius

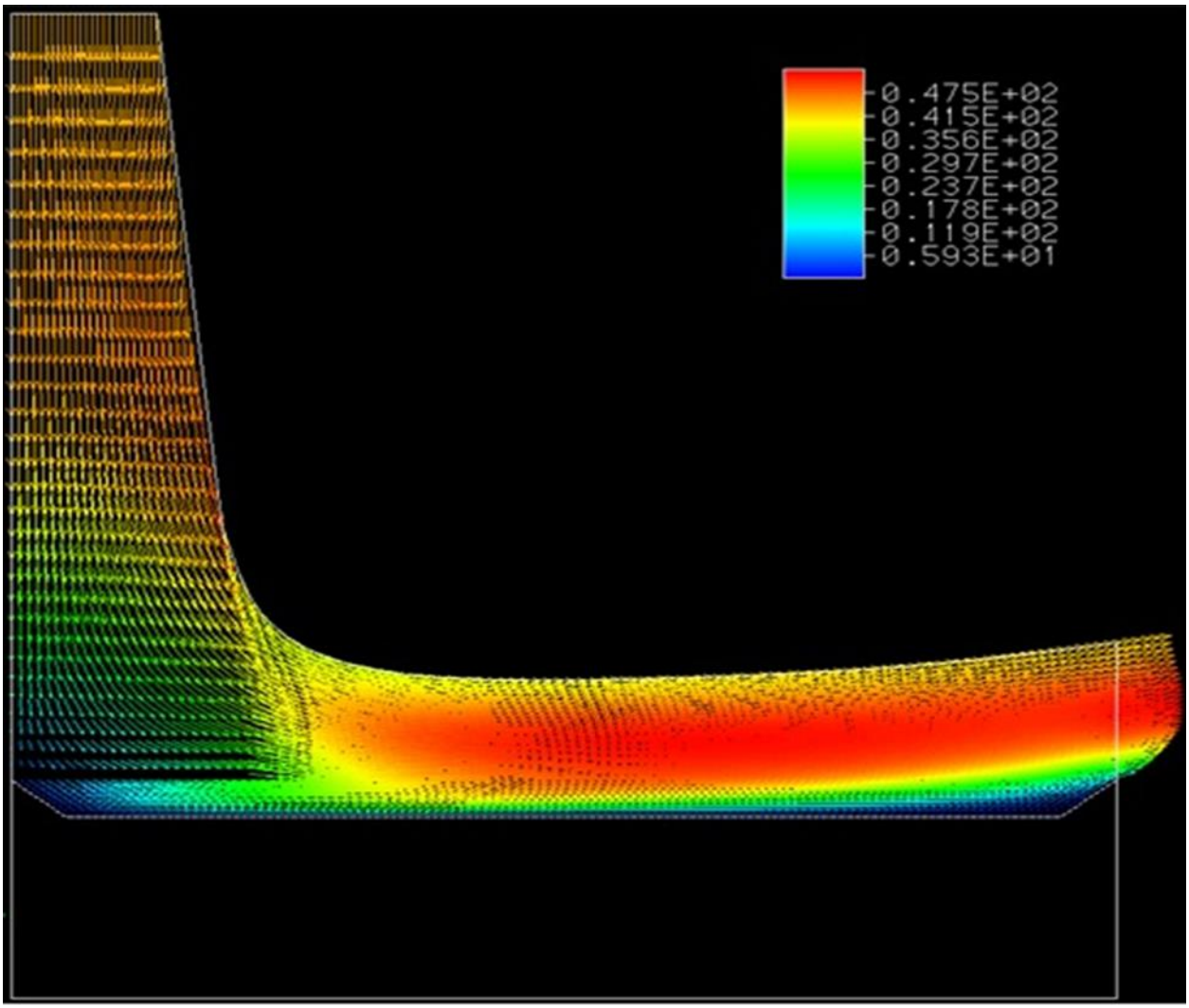

Figure 11: Velocity Vector of Case C

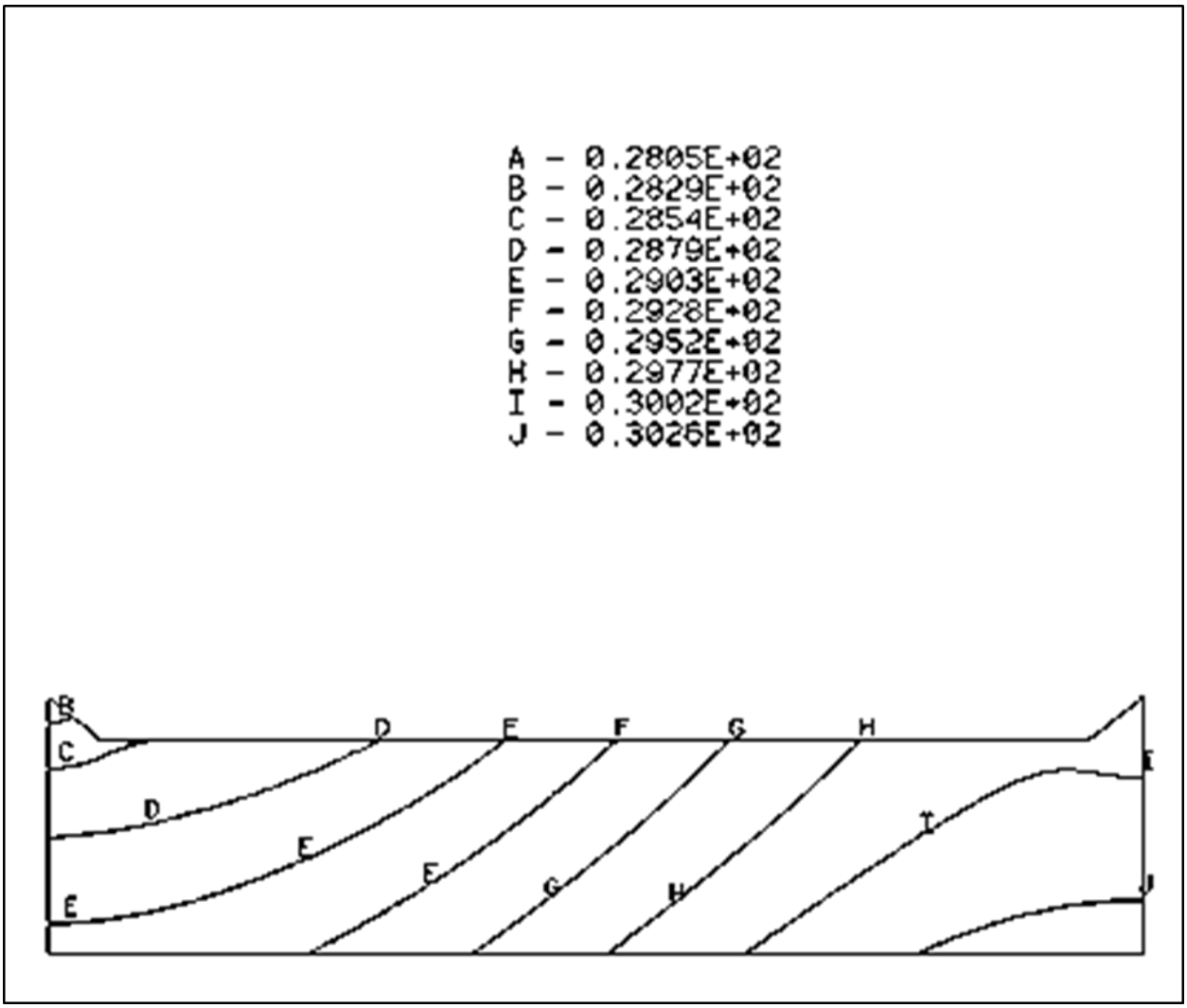

Figure 12: Isothermal Lines of Case C in Degrees Celsius

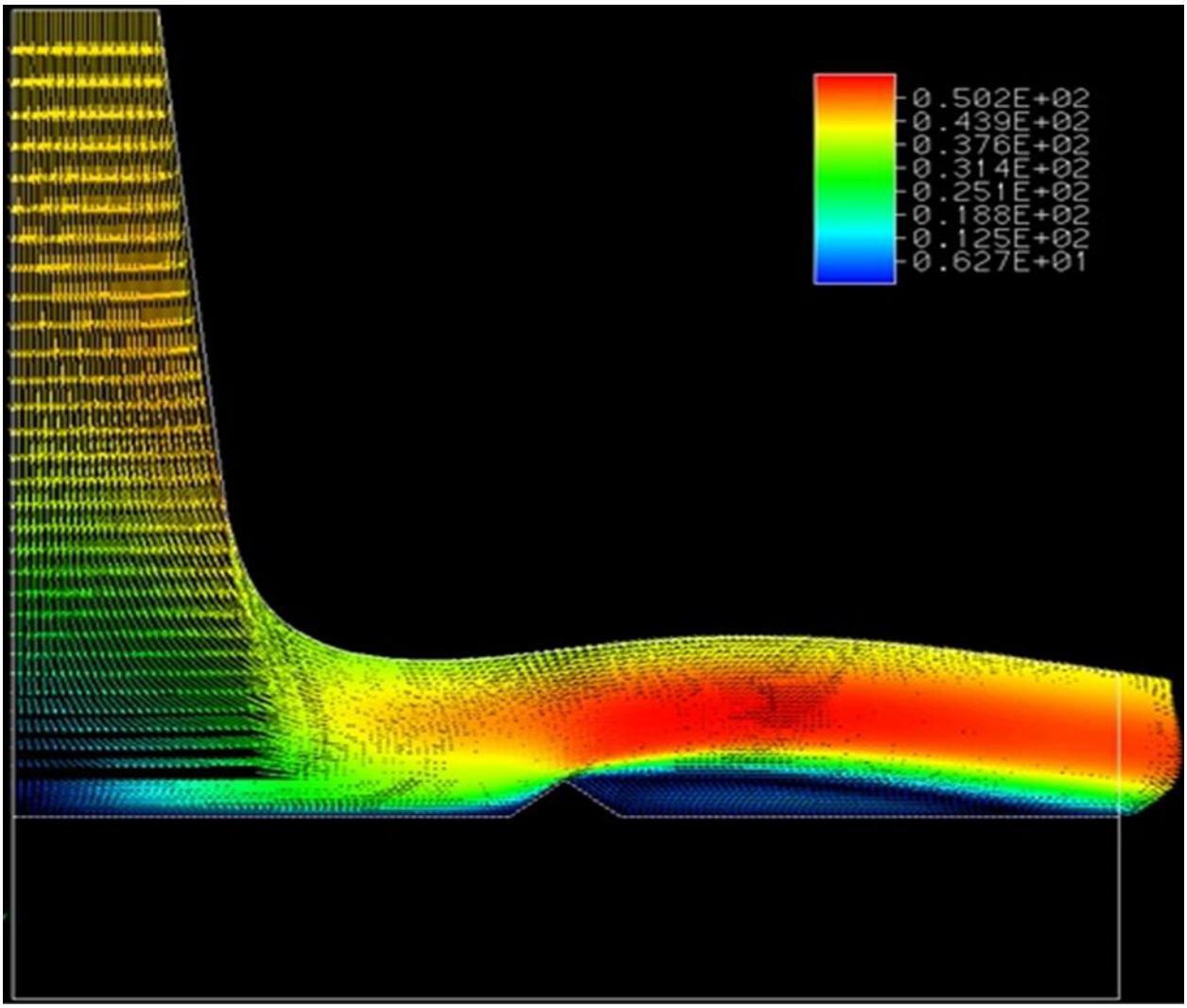

Figure 13: Velocity Vector of Case D

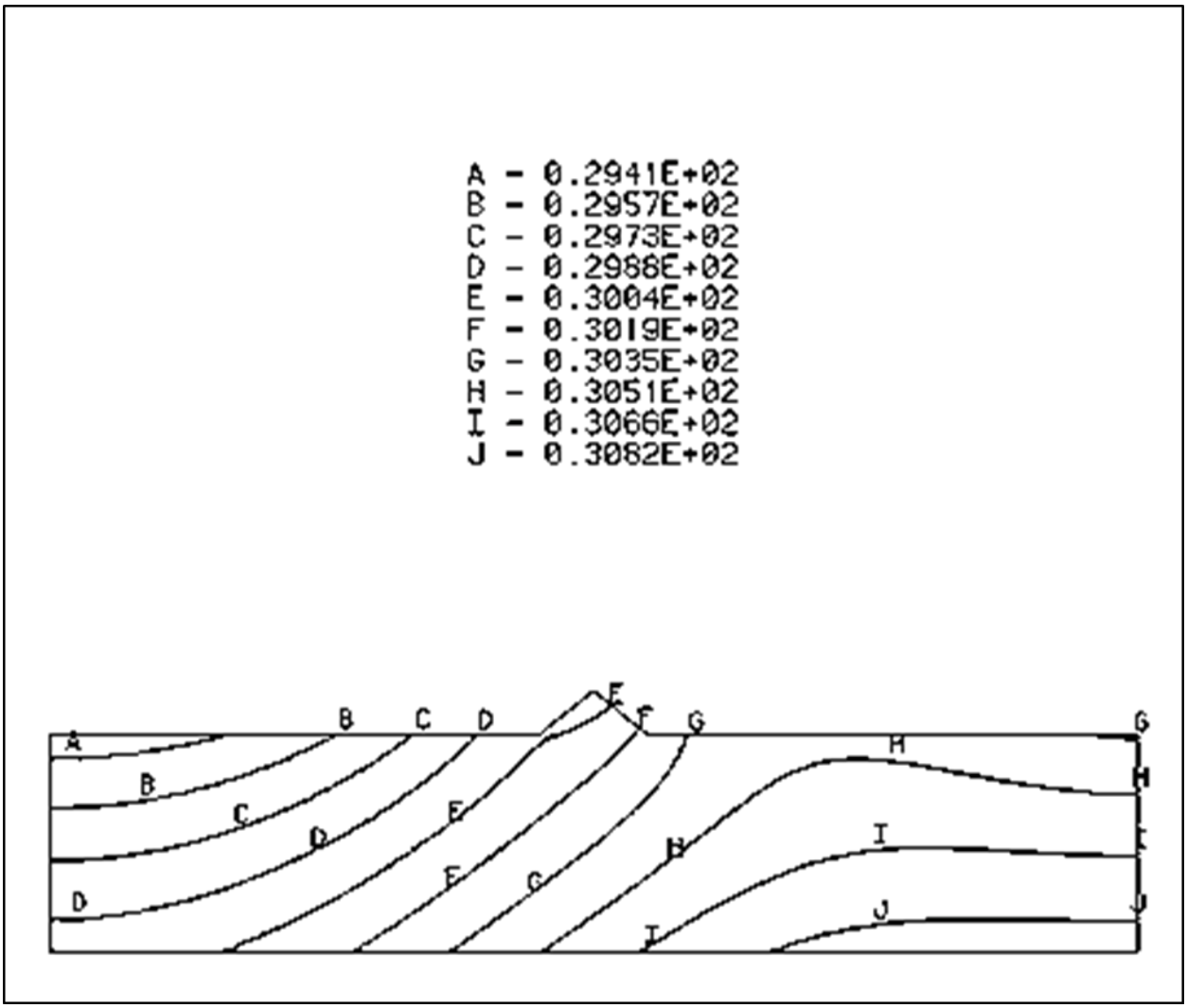

Figure 14: Isothermal Lines of Case D in Degrees Celsius

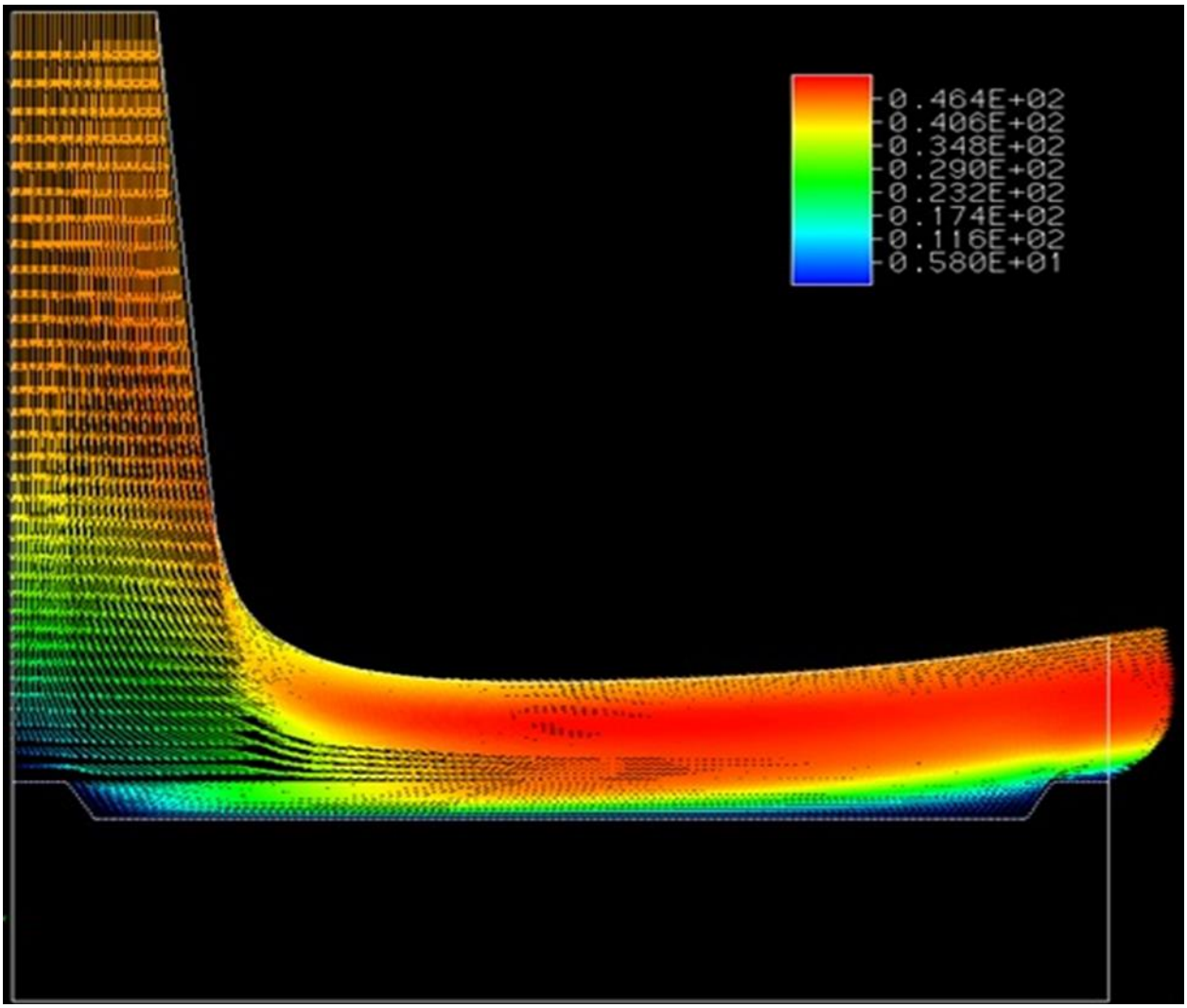

Figure 15: Velocity Vector of Case E

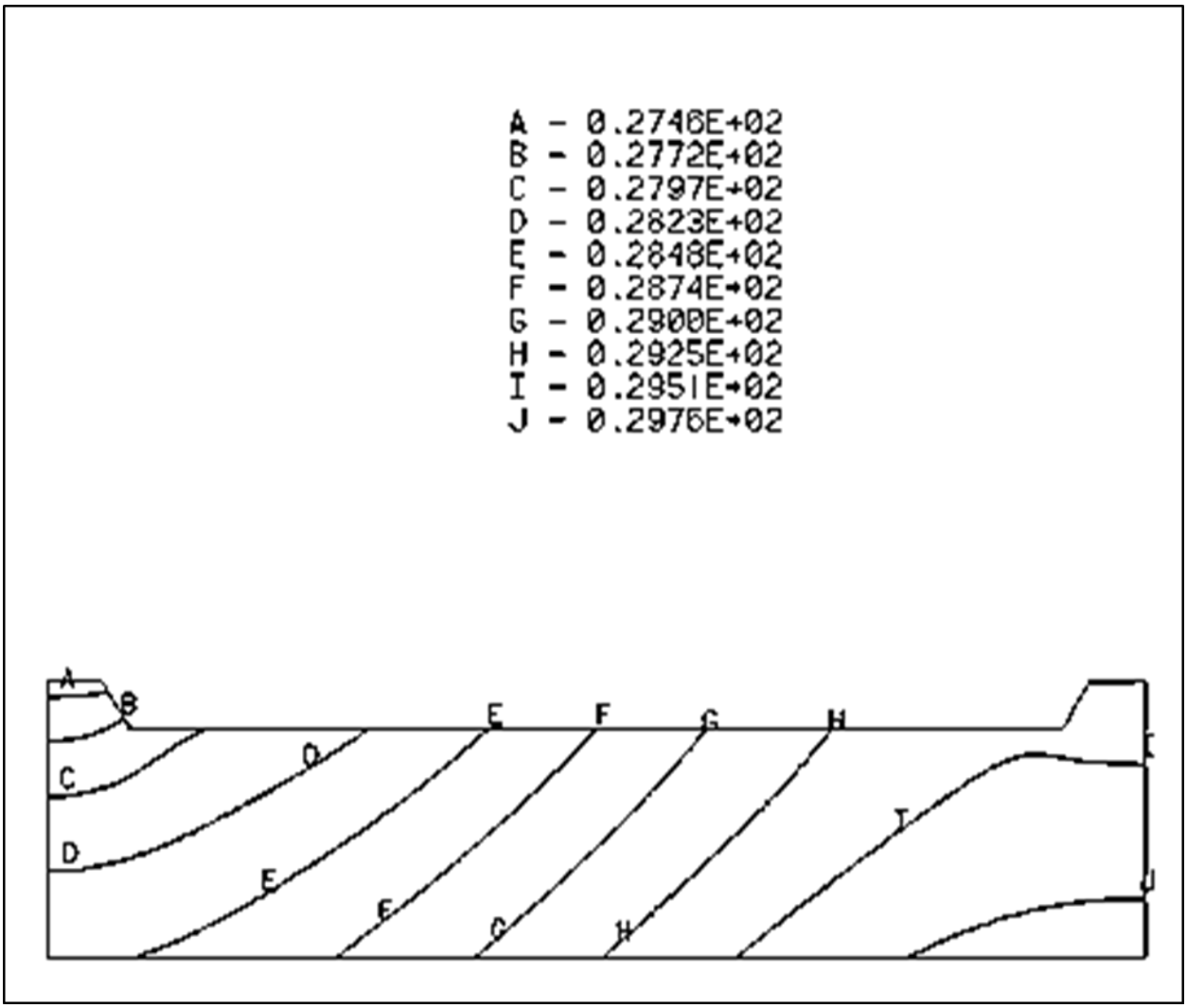

Figure 16: Isothermal Lines of Case E in Degrees Celsius

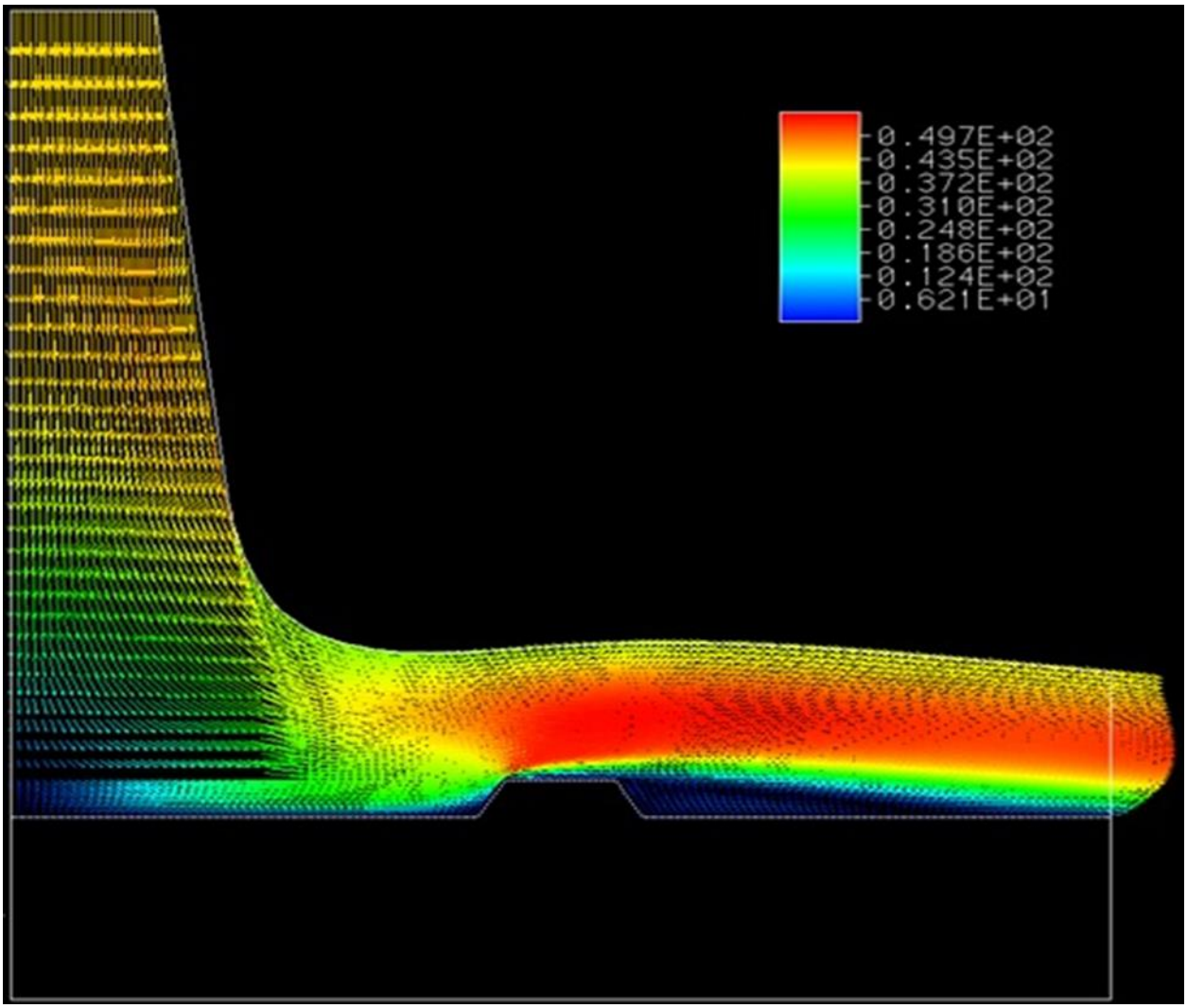

Figure 17: Velocity Vector of Case F

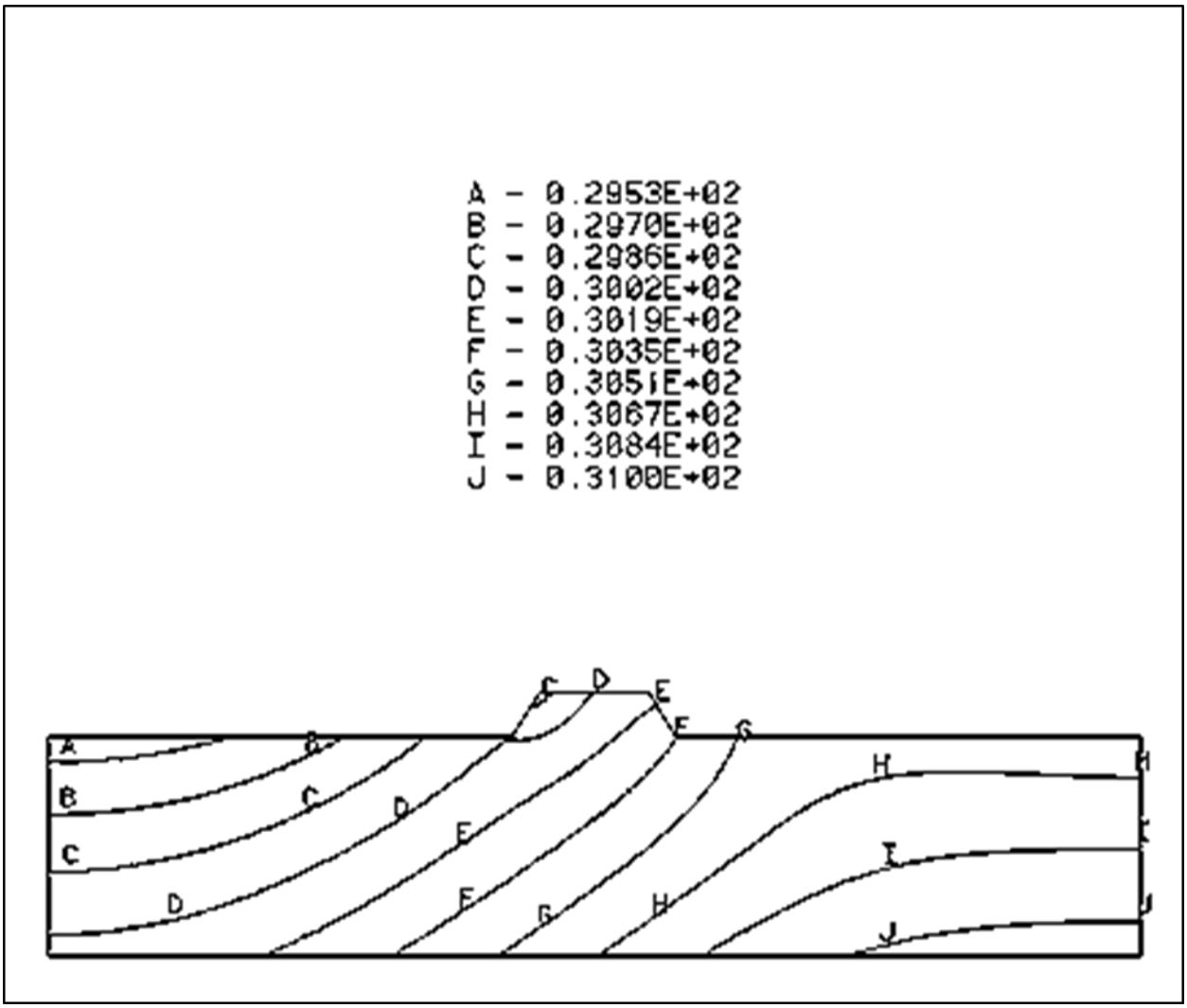

Figure 18: Isothermal Lines of Case F in Degrees Celsius

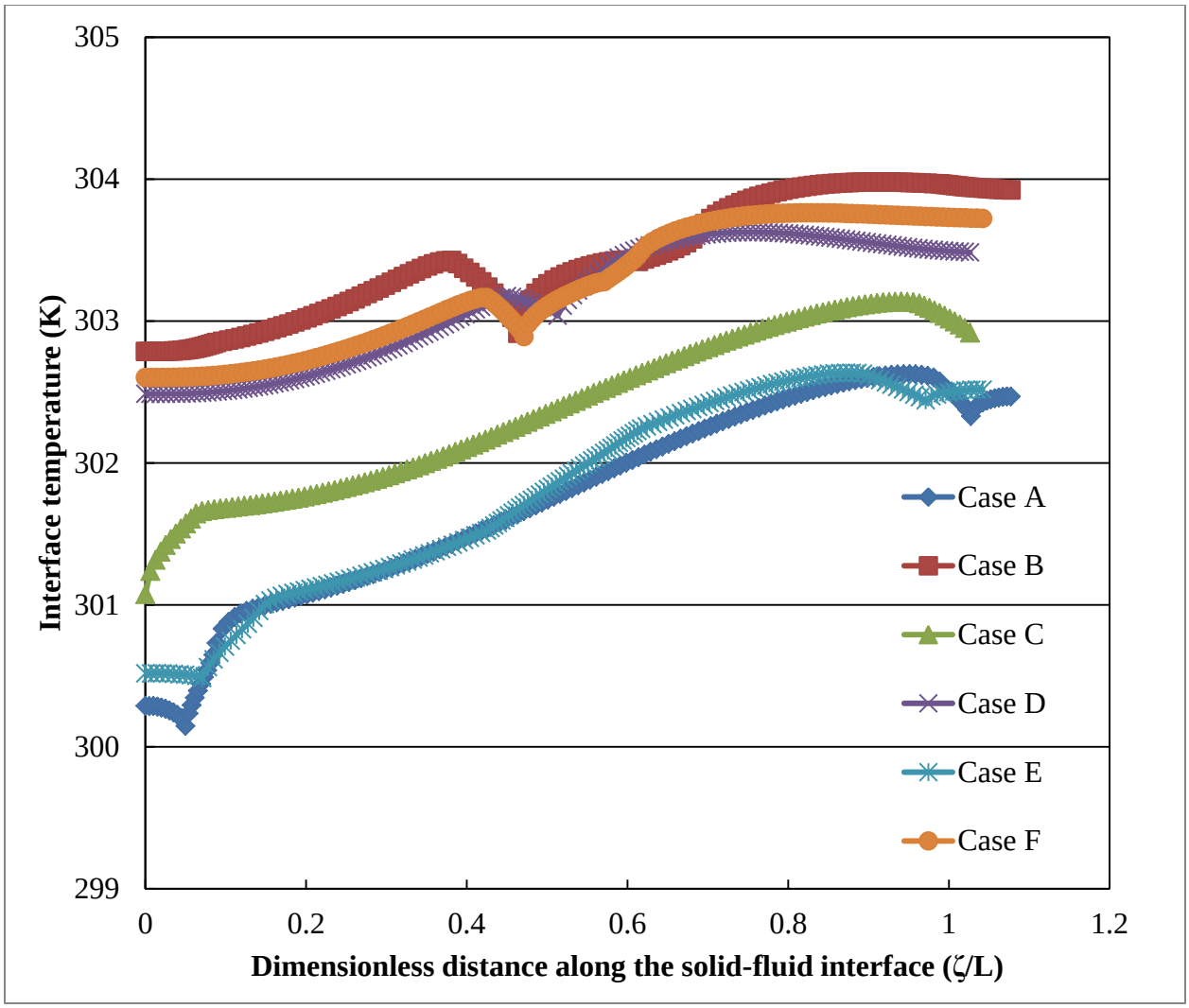

Figure 19: Variations of Interface Temperature of Silicon Plate at Re = 750

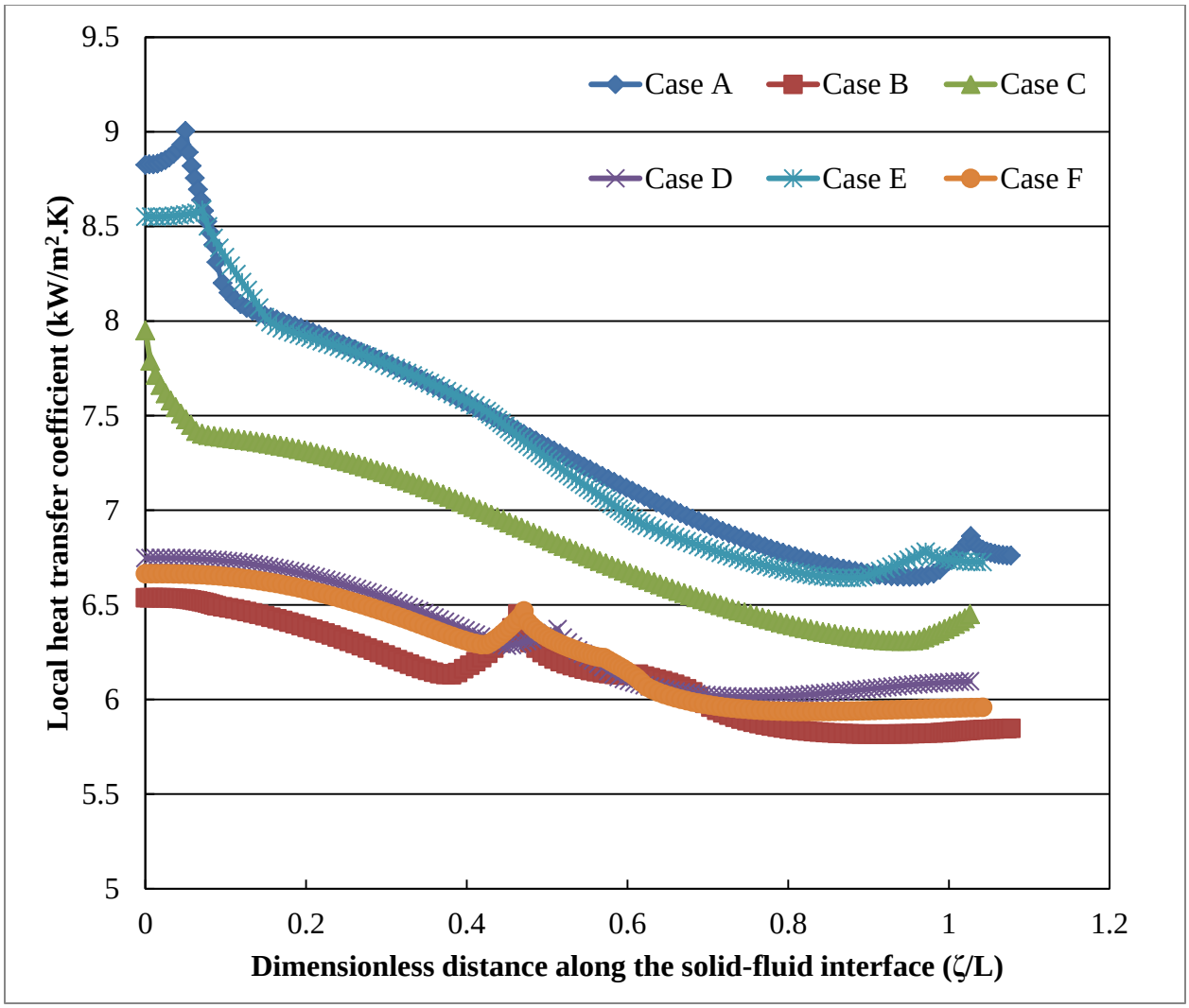

Figure 20: Variations of Local Heat Transfer Coefficient for Silicon Plate at Re = 750

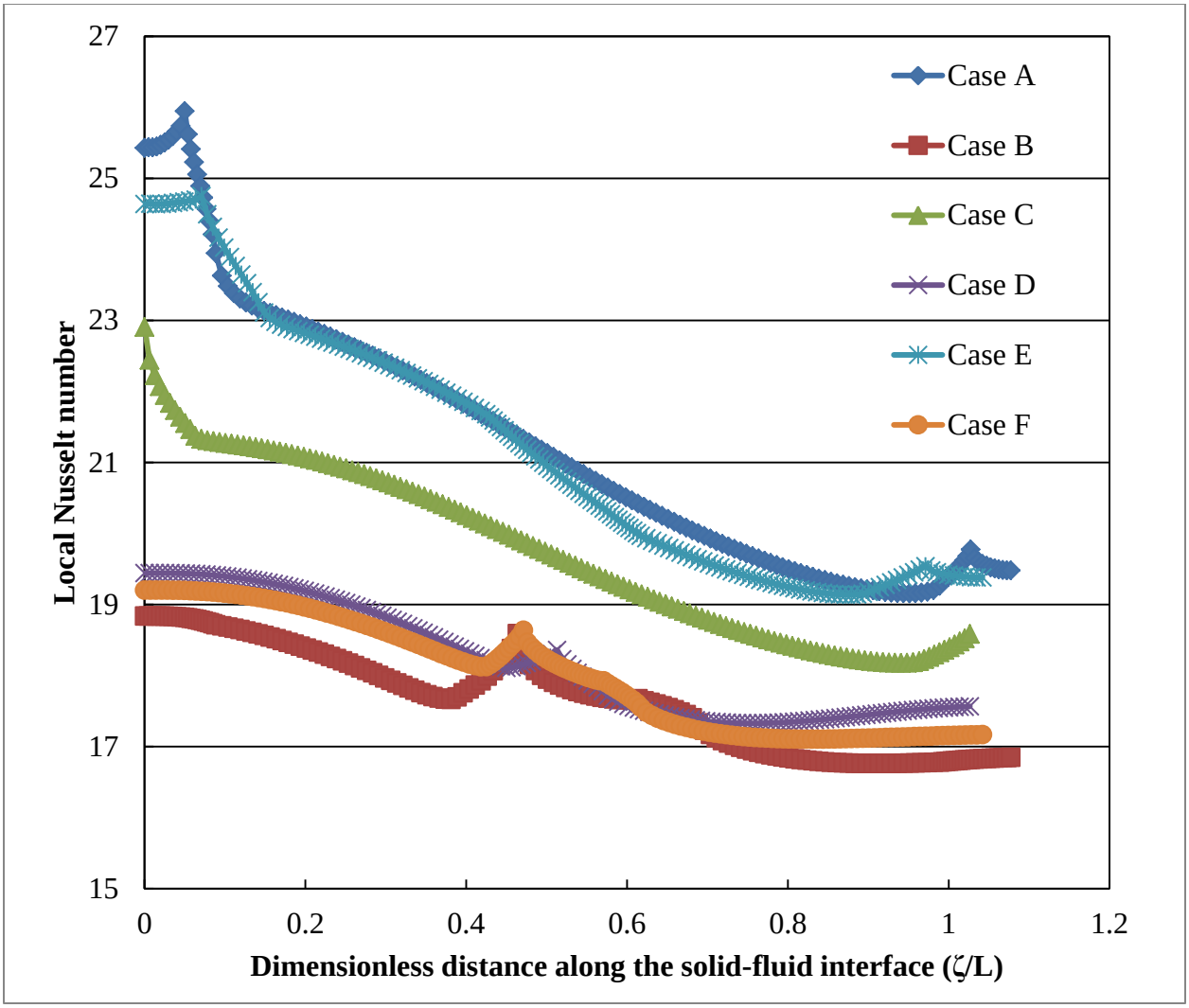

Figure 21: Variations of Local Nusselt Number for Silicon Plate at Re = 750

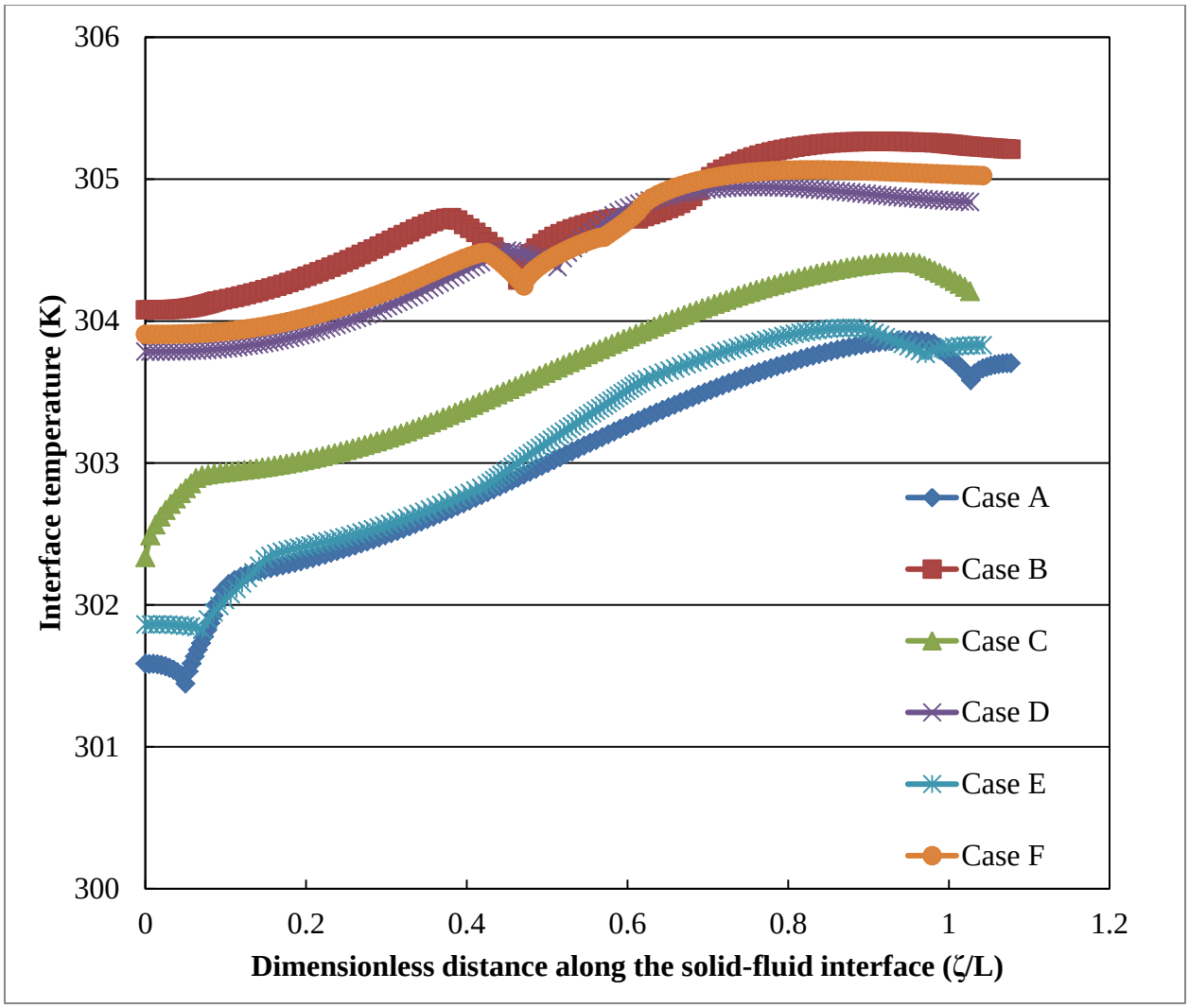

Figure 22: Variations of Interface Temperature of Silicon Plate at Re = 500

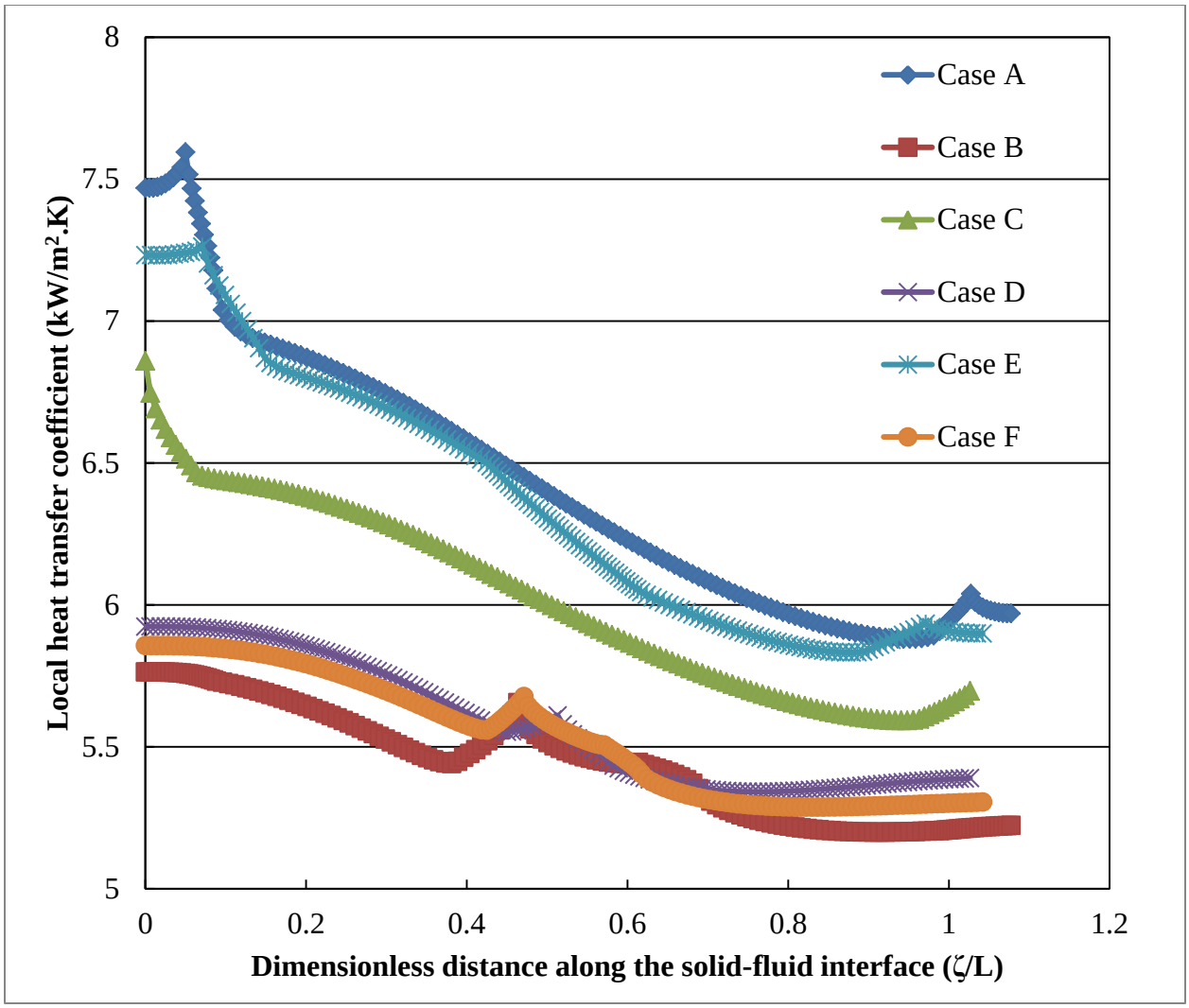

Figure 23: Variations of Local Heat Transfer Coefficient for Silicon Plate at Re = 500

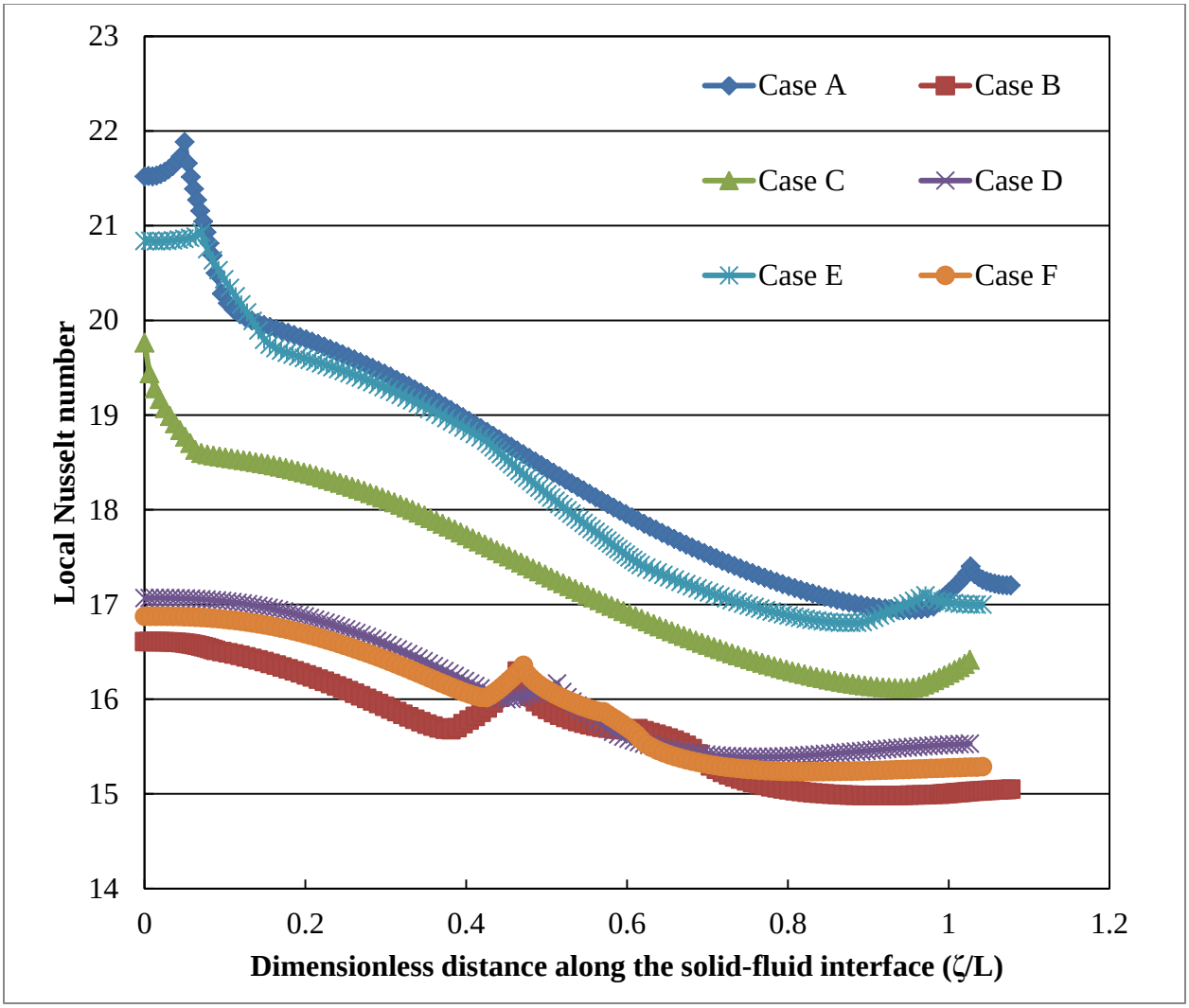

Figure 24: Variations of Local Nusselt Number for Silicon Plate at Re = 500

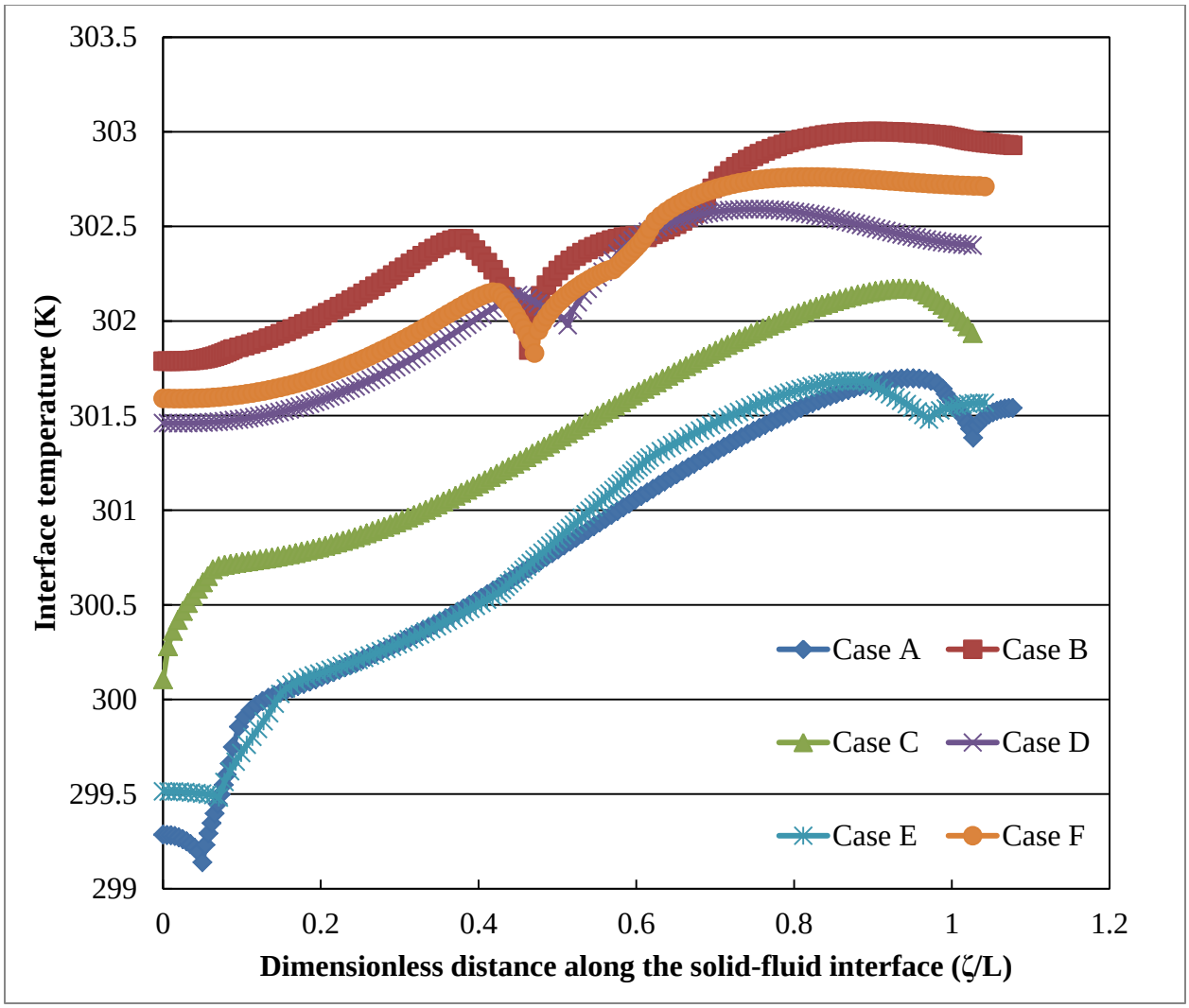

Figure 25: Variations of Interface Temperature of Silicon Plate at Re = 1000

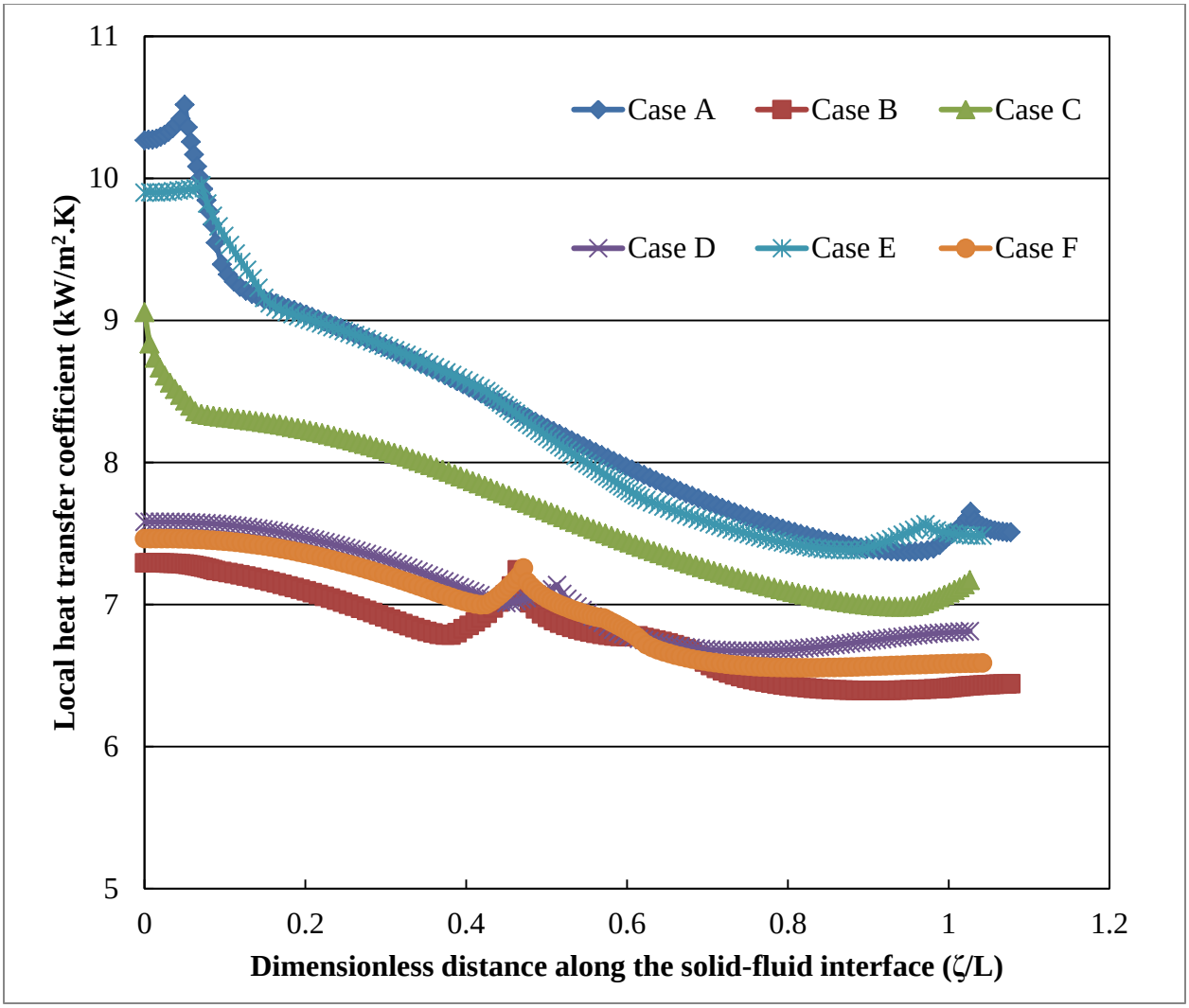

Figure 26: Variations of Local Heat Transfer Coefficient for Silicon Plate at Re = 1000

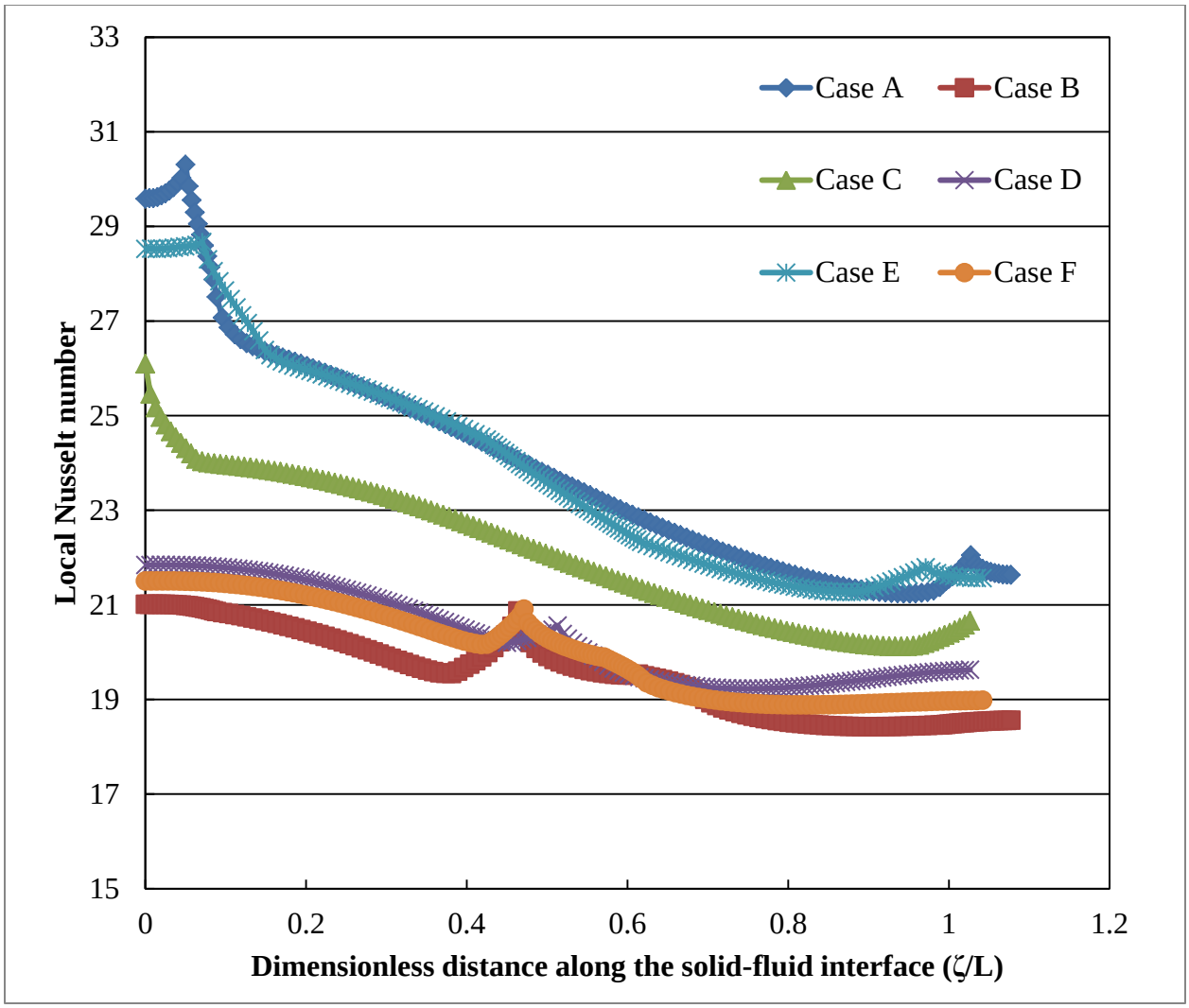

Figure 27: Variations of Local Nusselt Number for Silicon Plate at Re = 1000

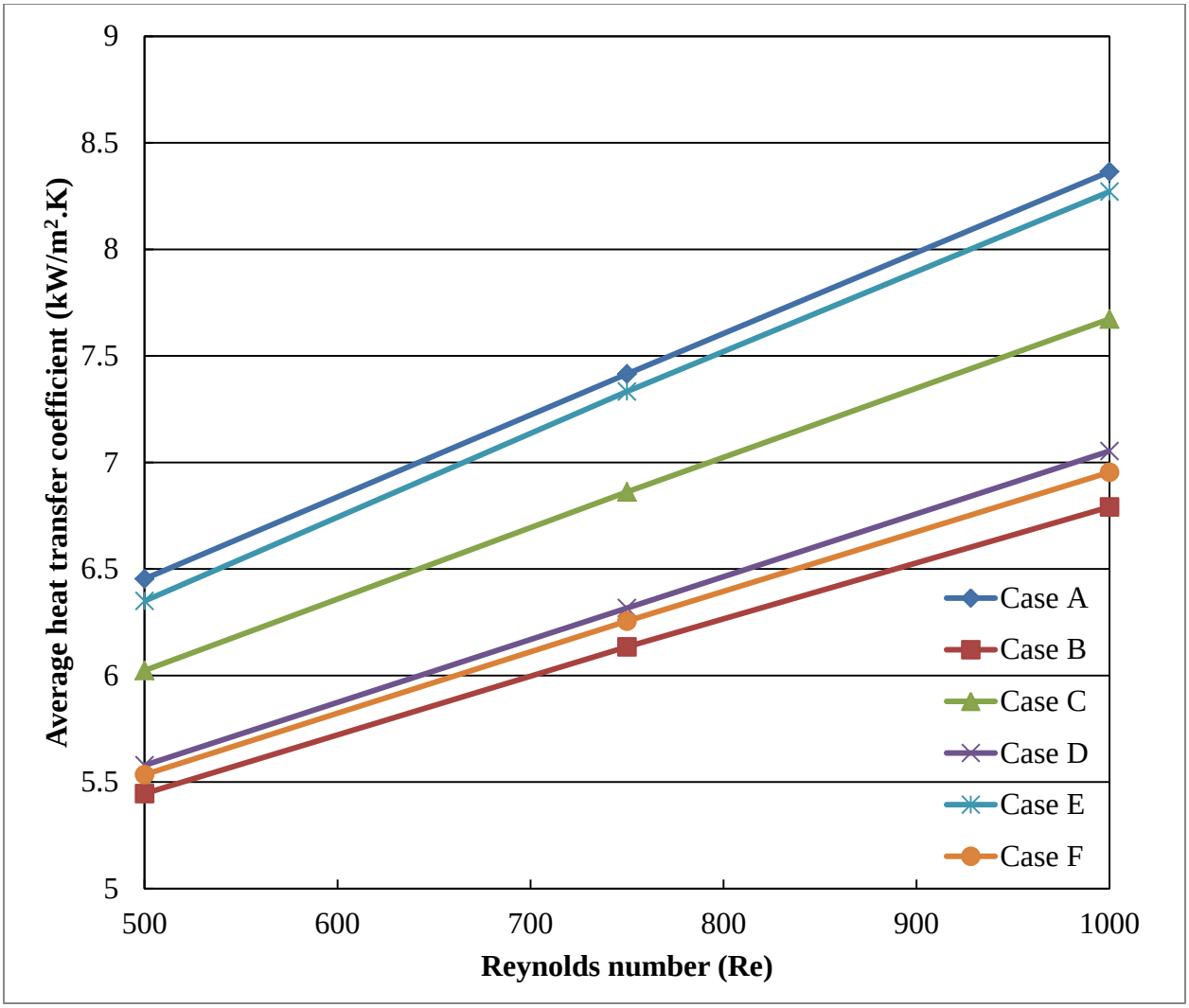

Figure 28: Variations of Average Heat Transfer Coefficient for Silicon Plate

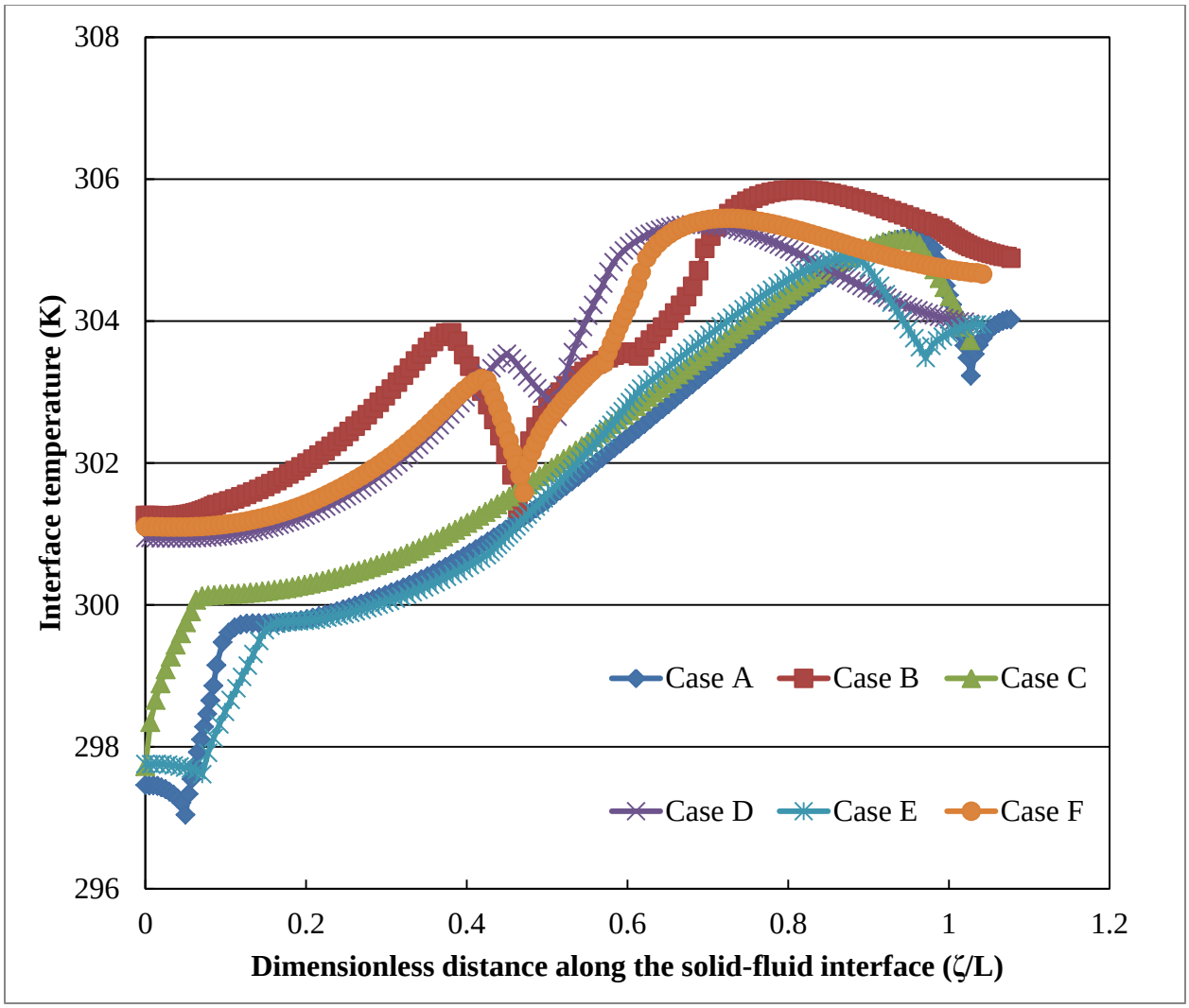

Figure 29: Variations of Interface Temperature of Constantan Plate at Re = 750

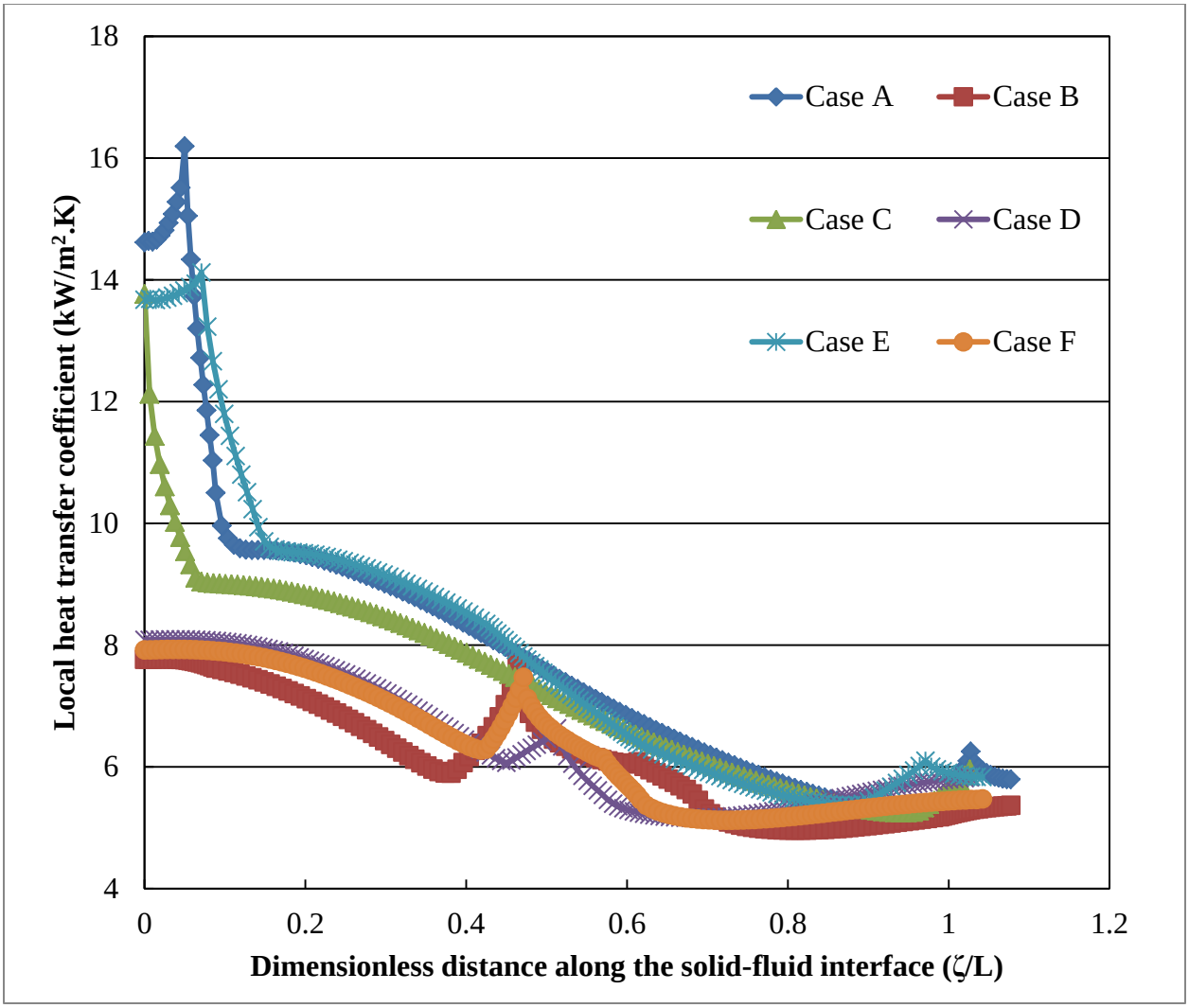

Figure 30: Variations of Local Heat Transfer Coefficient for Constantan Plate at Re = 750

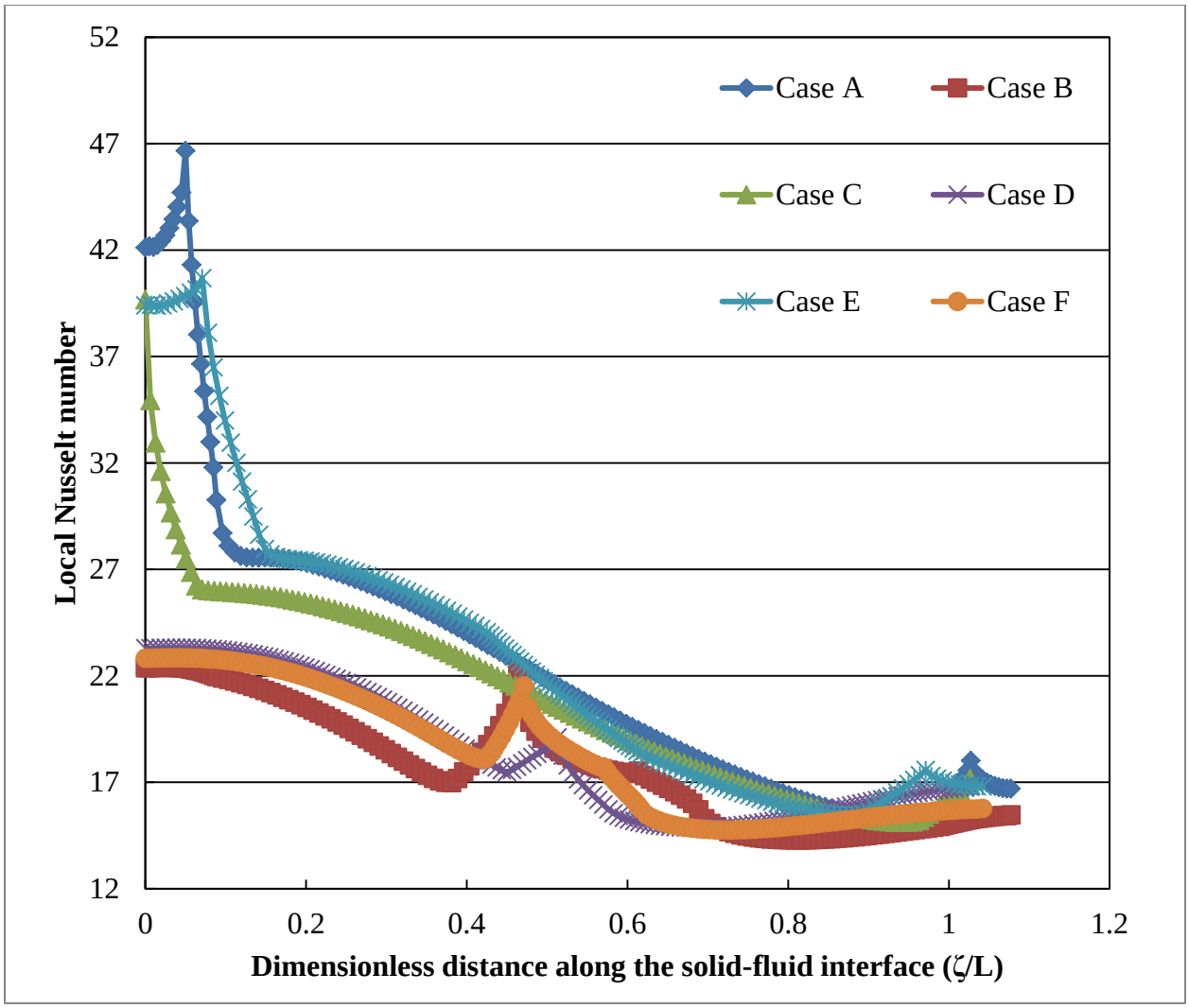

Figure 31: Variations of Local Nusselt Number for Constantan Plate at Re = 750

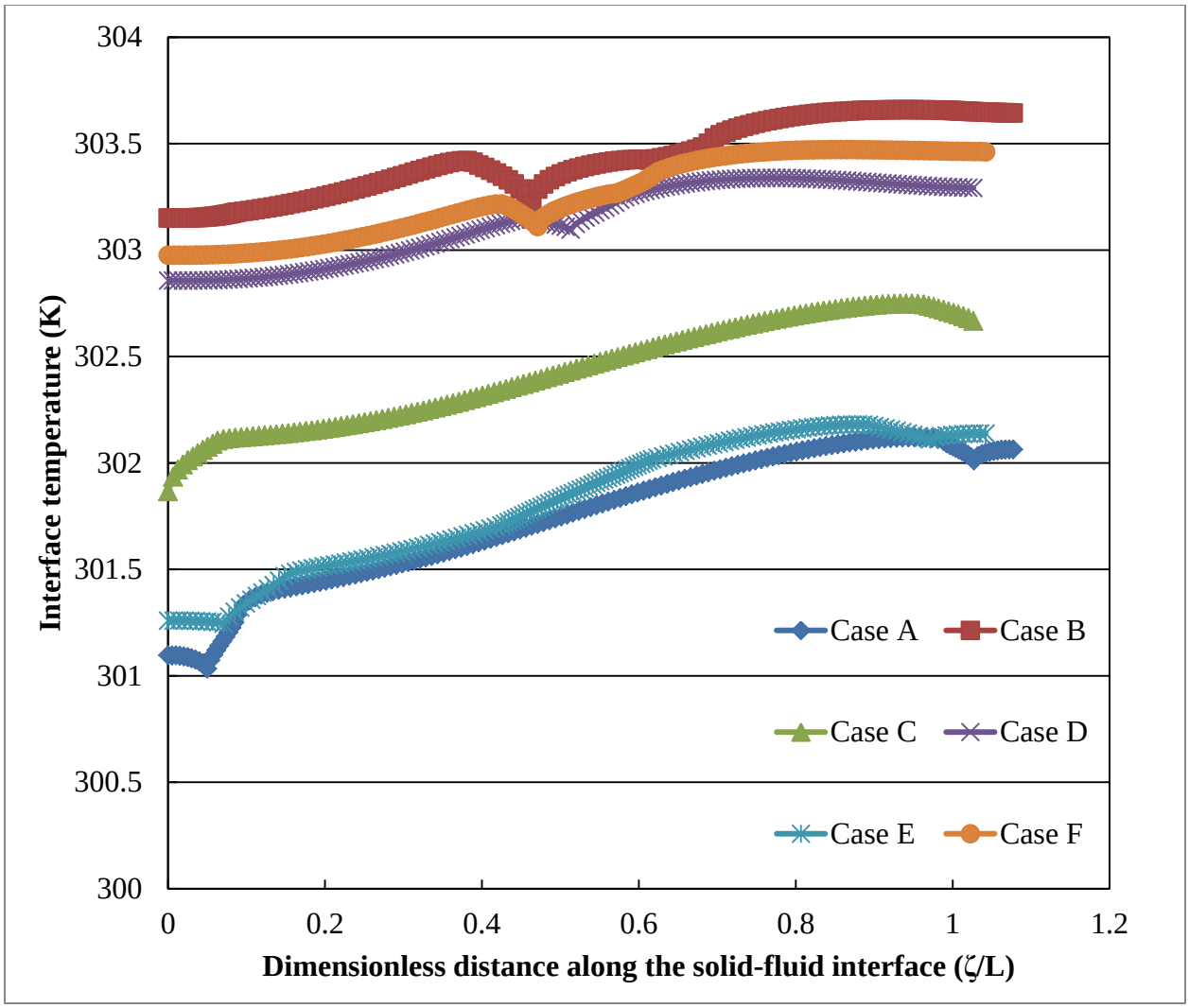

Figure 32: Variations of Interface Temperature of Copper Plate Re = 750

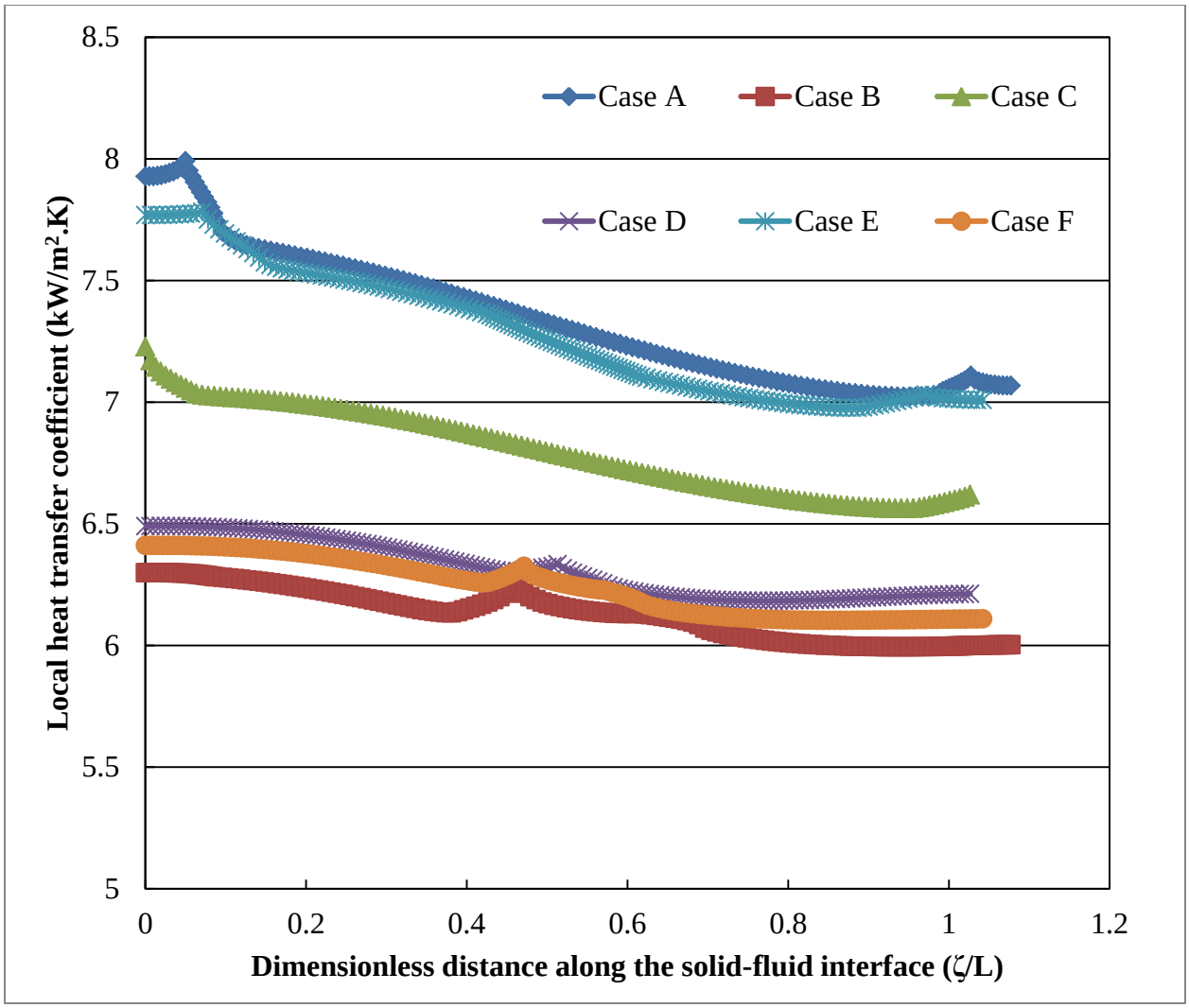

Figure 33: Variations of Local Heat Transfer Coefficient for Copper Plate at Re = 750

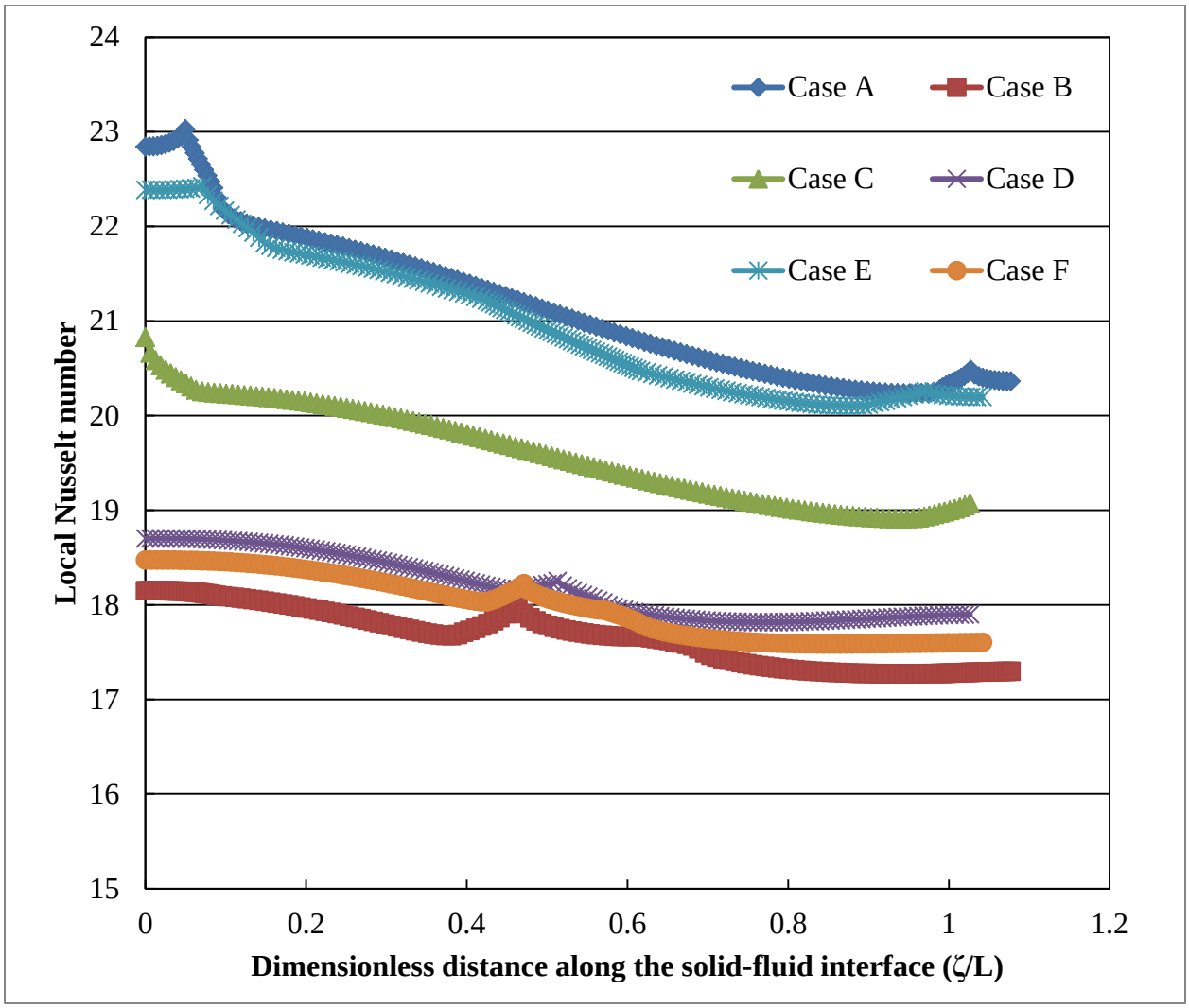

Figure 34: Variations of Local Nusselt Number for Copper Plate at Re = 750

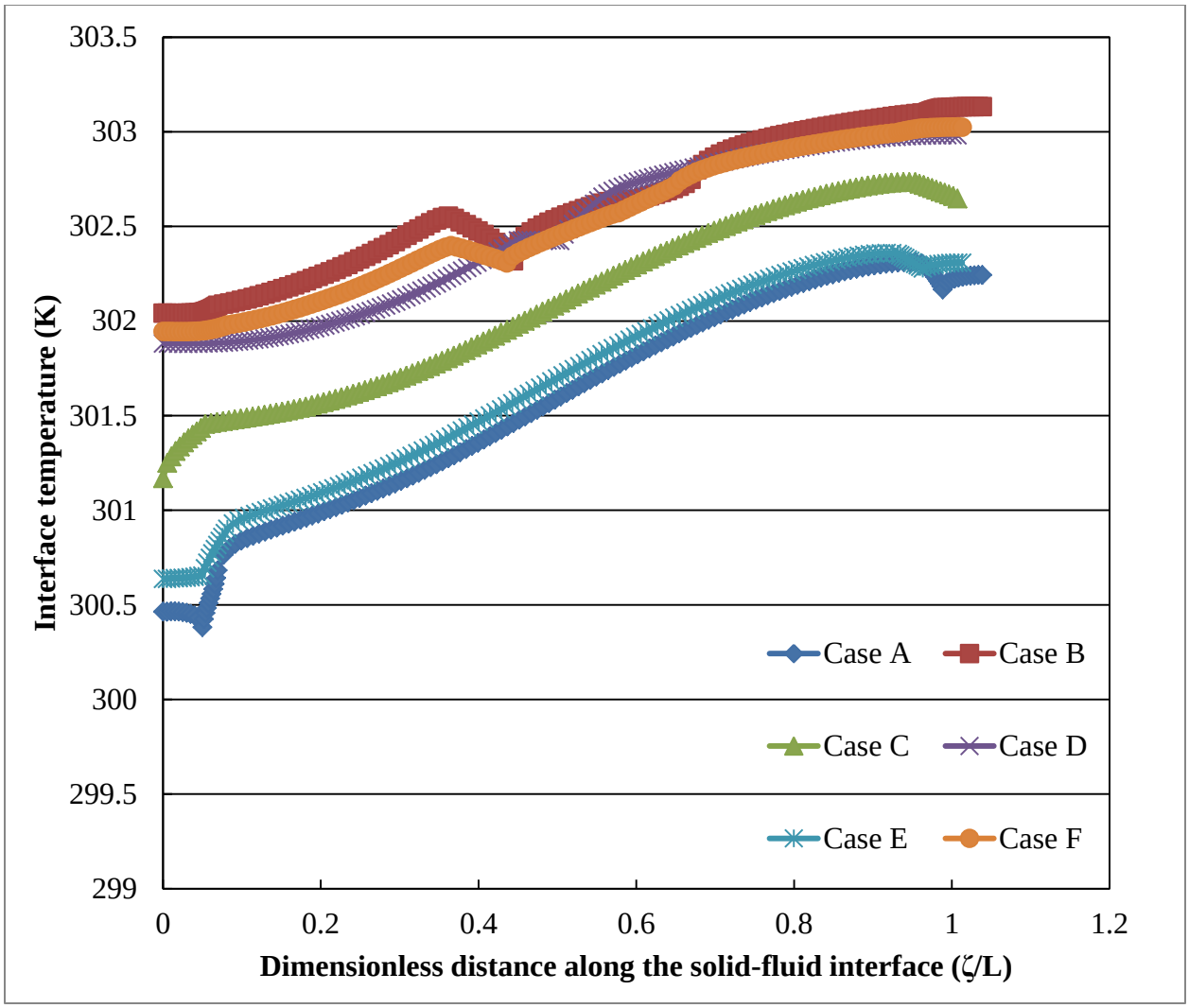

Figure 35: Variations of Interface Temperature of Silicon Plate at Re = 750 with a = 0.000125 m

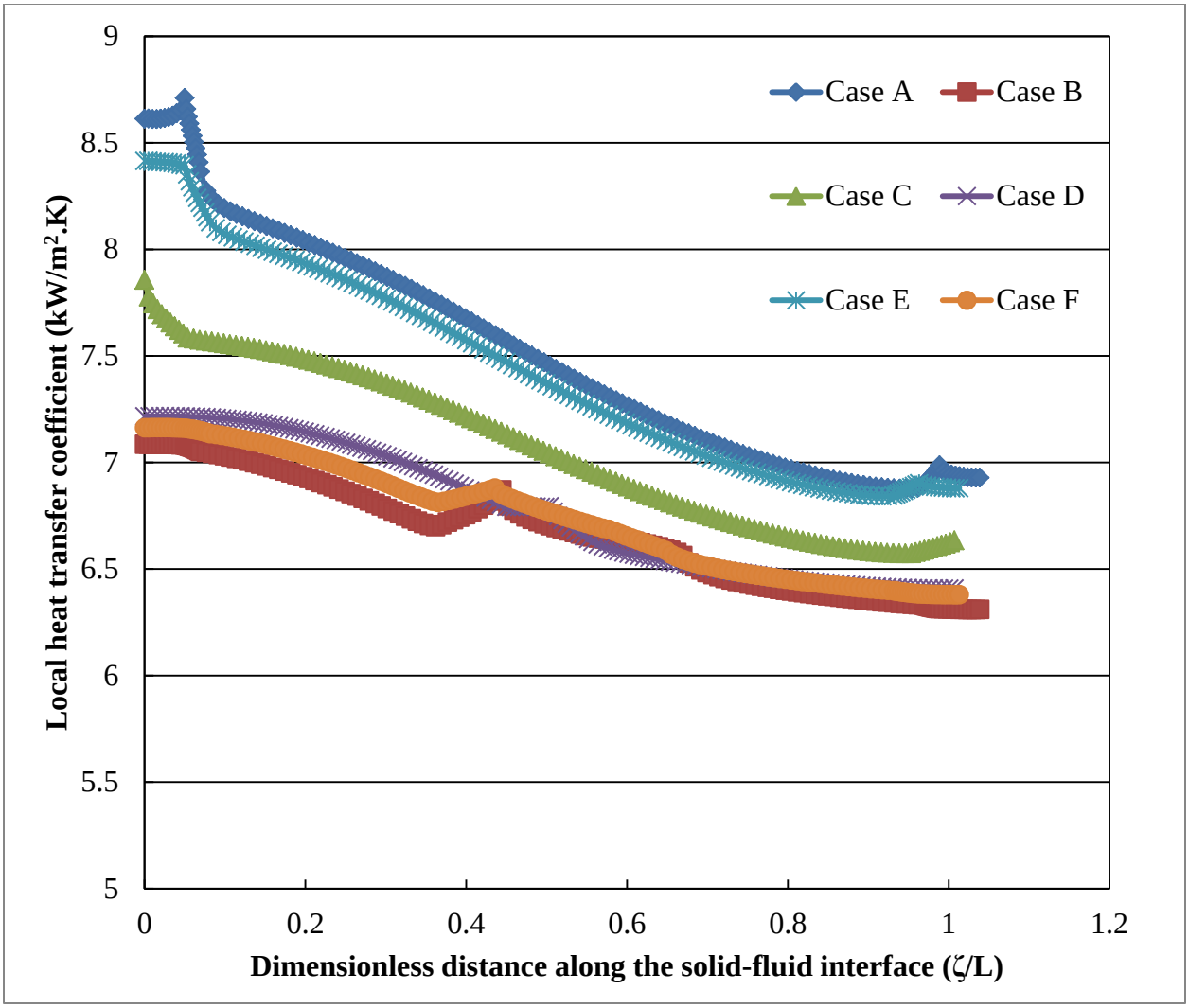

Figure 36: Variations of Local Heat Transfer Coefficient for Silicon Plate at Re = 750 with a = 0.000125 m

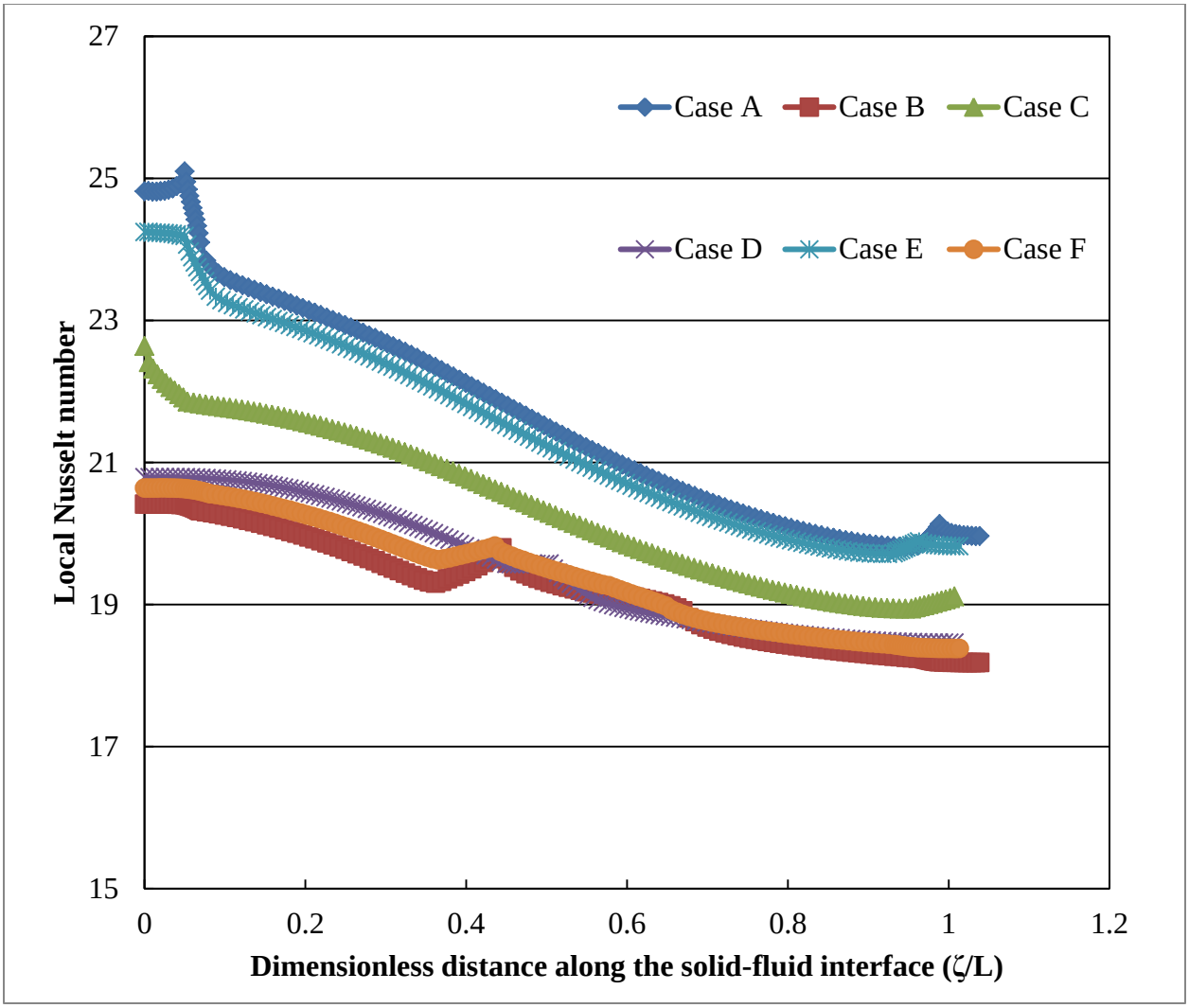

Figure 37: Variations of Local Nusselt Number for Silicon Plate at Re = 750 with a = 0.000125 m

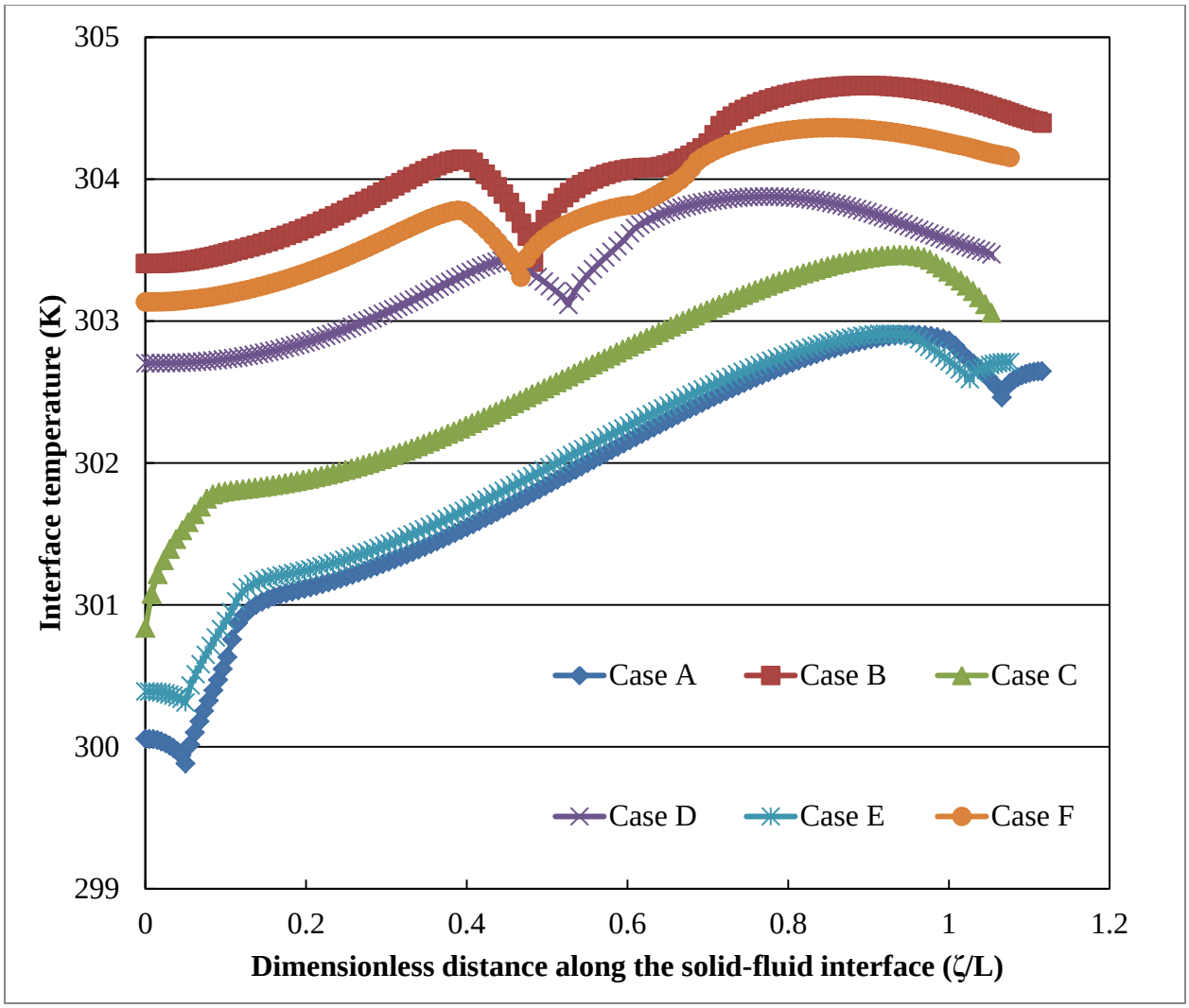

Figure 38: Variations of Interface Temperature of Silicon Plate at Re= 750 with a = 0.000375 m

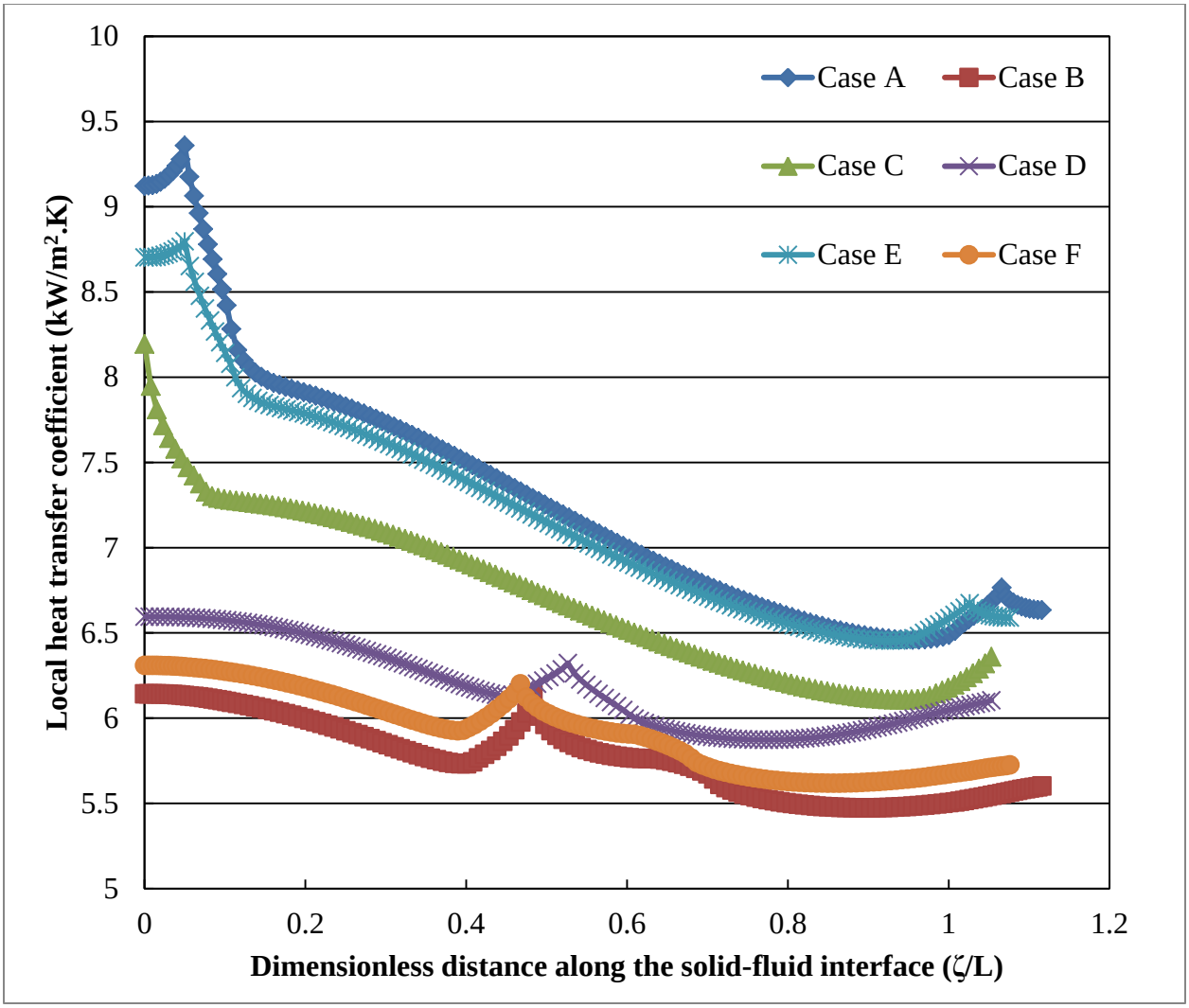

Figure 39: Variations of Local Heat Transfer Coefficient for Silicon Plate at Re = 750 with a = 0.000375 m

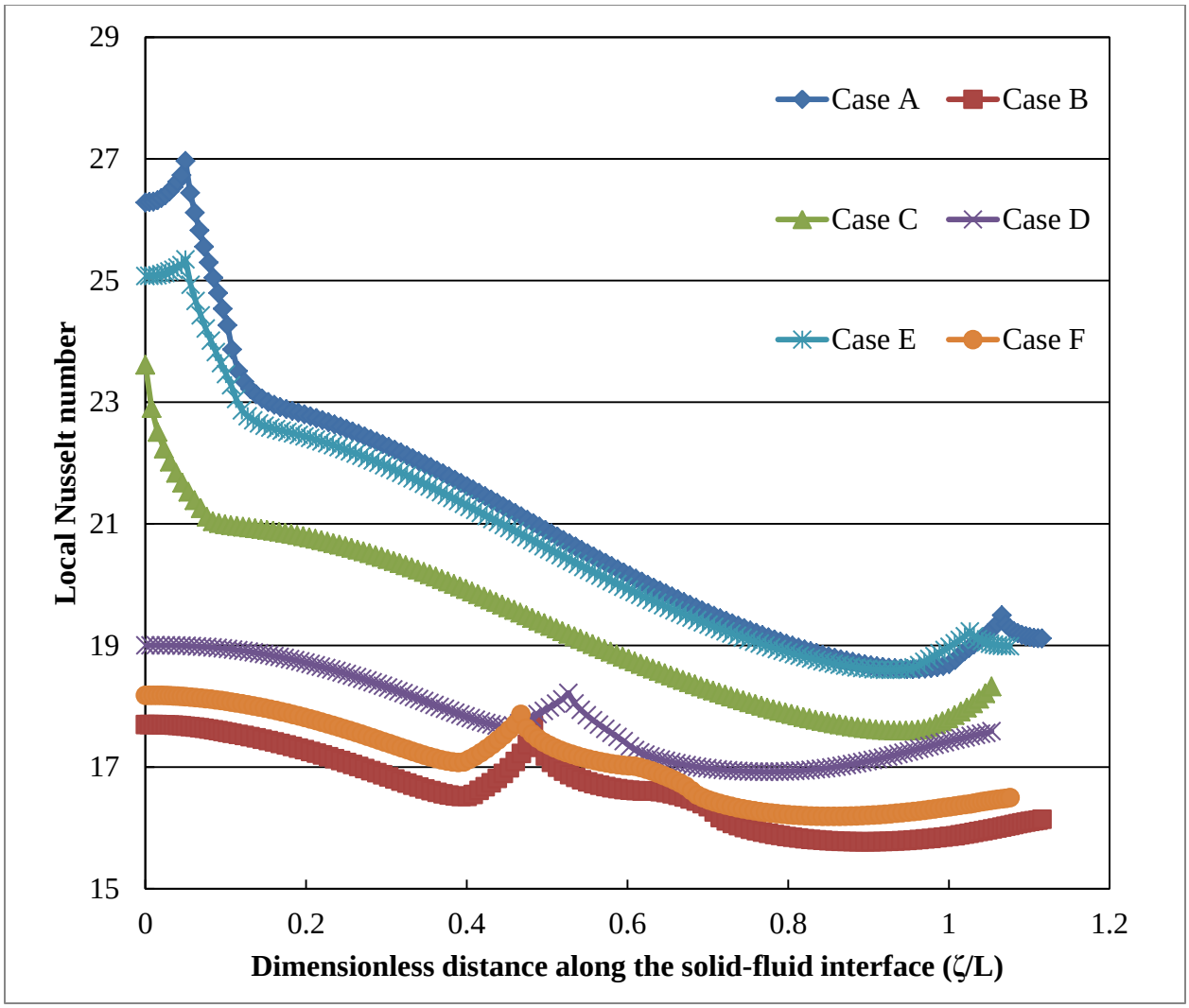

Figure 40: Variations of Local Nusselt Number for Silicon Plate at Re = 750 with a = 0.000375 m

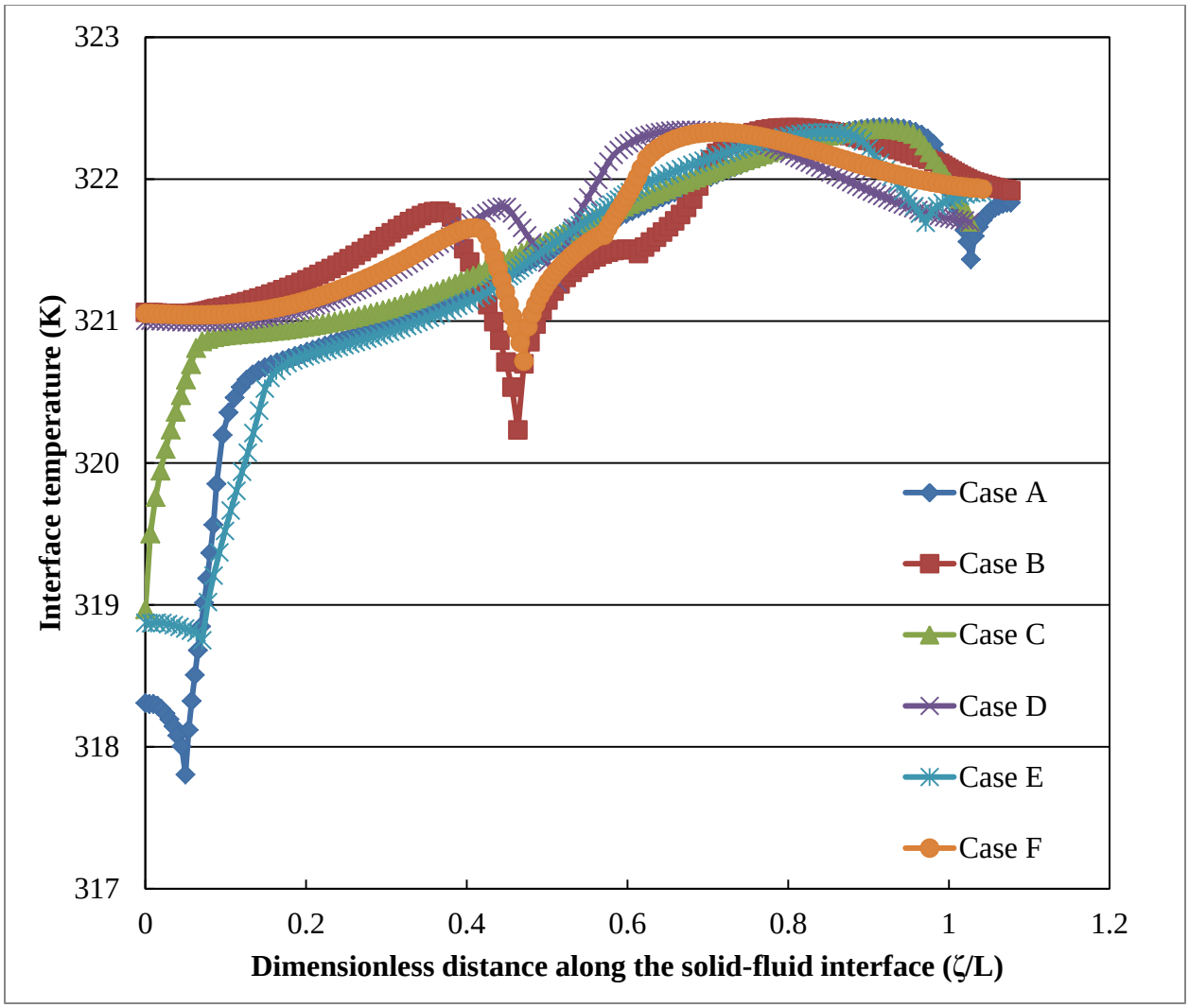

Figure 41: Variations of Interface Temperature of Silicon Plate at Re = 750 with Isothermal Boundary Condition

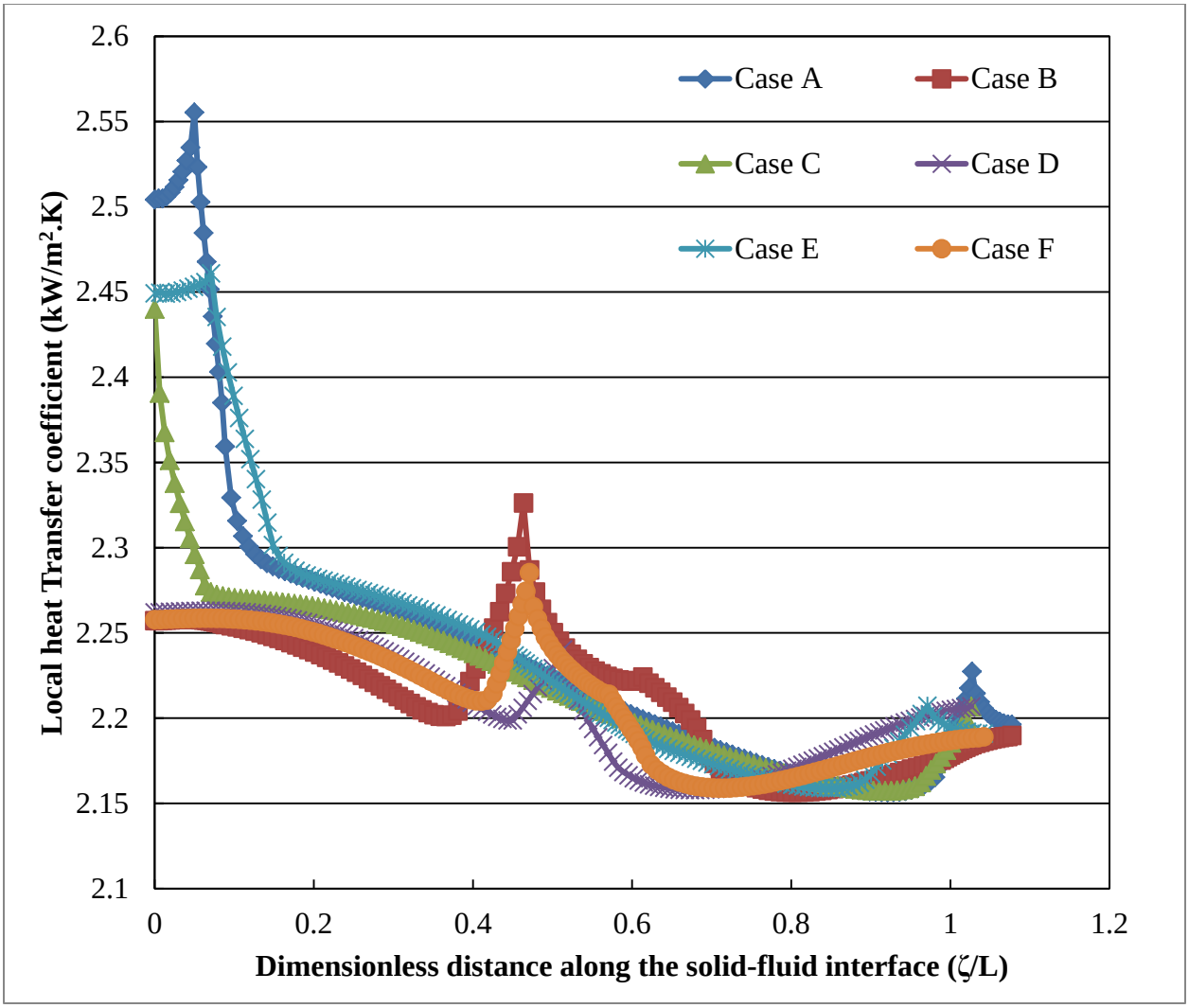

Figure 42: Variations of Local Heat Transfer Coefficient for Silicon Plate at Re = 750 with Isothermal Boundary Condition

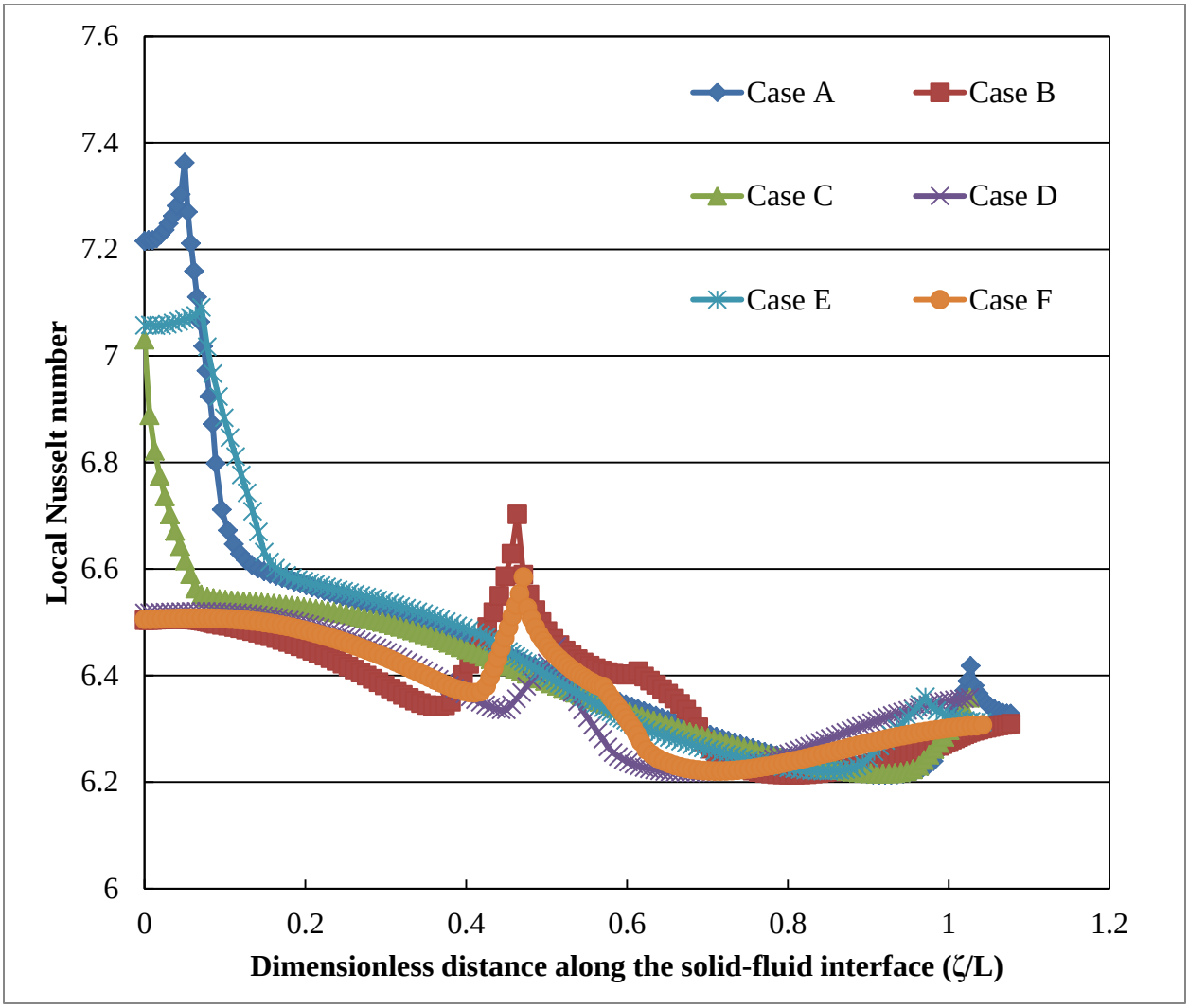

Figure 43: Variations of Local Nusselt Number for Silicon Plate at Re = 750 with Isothermal Boundary Condition

CHAPTER 3: TRANSIENT HEAT TRANSFER

3.1 Mathematical Model

The following mathematical analysis is presented for two-dimensional slot jet impinging normally onto a solid plate with surface roughness as shown in Figures (1-6). The bottom of the solid plate was uniformly heated for the base model; as a variation from the base model, the bottom of the plate was kept at constant temperature. The fluid used in this problem was water and assumed to be incompressible. The heat source was turned on at t= 0 s. The following equations for conservation of mass, momentum, and energy are written in the Cartesian coordinate system [32, 33]:

$$\nabla \cdot \vec{V} = 0 \tag{19}$$

$$\rho_f \frac{\partial \upsilon_x}{\partial t} + \left(\rho_f \vec{V} \cdot \nabla\right) \cdot \upsilon_x = -\frac{\partial p}{\partial x} + \mu \nabla^2 \upsilon_x \tag{20}$$

$$\rho_f \frac{\partial \upsilon_y}{\partial t} + \left(\rho_f \vec{V} \cdot \nabla\right) \cdot \upsilon_y = -\rho_f g - \frac{\partial p}{\partial y} + \mu \nabla^2 \upsilon_y \tag{21}$$

$$\rho_f c_{p_f} \frac{\partial T_f}{\partial t} + \left(\rho_f c_{p_f} \vec{V} \cdot \nabla\right) \cdot T_f = k_f \nabla^2 T_f \tag{22}$$

The heat conduction inside the solid plate can be written as:

$$\rho_s c_{p_s} \frac{\partial T_s}{\partial t} = k_s \nabla^2 T_s \tag{23}$$

The previous equations can be solved using boundary conditions found in equations (6-14).

The beginning of the transient condition can be expressed as:

At $t = 0$:

$$T_s = T_f = T_j, \upsilon = \upsilon_i(x, y) \tag{24}$$

3.2 Numerical Computation

The governing equations along with the boundary conditions in section 2.1 and section 3.1 were solved using the same numerical methods used in section 2.2. Once the initial free surface height and velocity field established, the heat source at the bottom surface of the plate was turned on at t = 0 s. The fluid and the solid plate were at isothermal equilibrium condition at the beginning of the transient process. When the sum of the residuals for each degree of freedom was less than 1E-6, the solution was assumed to converge. Therefore, the solution was obtained for each time step until steady state condition was met. Due to larger variations at the beginning of the transient process and smaller variations when the solution approached the steady state condition, a variable time step used to obtain the results.

All fluid and materials properties were obtained from Bejan [37]. The working fluid used in this research was water. Three different plate materials, which are silicon, copper, and constantan, were considered. The jet nozzle width (W), nozzle height (H_n), plate length (L), and plate thickness (b) were kept at 0.0017 m, 0.0055 m, 0.006475 m, and 0.00125 m, respectively, for all cases. Also, the temperature of the jet (T_j), the temperature of the bottom surface of the plate for the isothermal boundary condition (T_w), and heat flux for the constant heat flux boundary condition (q_w) were kept at 20°C, 50°C and 63 kW/m^2, respectively, for all cases as well. The range of the Reynolds number (Re) studied was from 500 to 1000. The height of the step (a) is 0.00025 m for the base model and the range studied was from 0.000125 m to 0.000375 m.

3.3 Results and Discussion

Transient heat transfer analysis was conducted for the base model. The base model considered in the analysis is the same used for the steady state heat transfer analysis. Figure 44 shows the isothermal lines of the silicon plate for case A. The lowest temperature of the plate can be found at the stagnation region. The temperature of the plate increases towards the outlet of the liquid at the end of the plate and towards the heat source. Locations with sudden geometry change exhibit the lowest temperatures compared to the neighboring points. As time progresses towards steady state condition, the trend remains the same with an overall increase in temperature. The interface temperature for case A is shown in Figure 45. At the beginning of the transient process, the temperature is more uniform across the plate length. As time progresses towards steady state condition, the difference between maximum to minimum interface temperature becomes higher. The reason behind this trend is due to the transient thermal storage that is required to develop the thermal boundary layer of the fluid. The local heat transfer coefficient for case A is shown in Figure 46. The local heat transfer coefficient decreases with time due to the increase in interface temperature. The largest drop in local heat transfer coefficient values during the first 0.5 s of the transient process. The local Nusselt number for case A is shown in Figure 47. The peaks along each line show the top edges of the steps where higher rates of heat transfer can be removed. Higher removal rates of heat transfer are due to more renewal and less recirculation of the fluid around those points.

Figure 48 shows the isothermal lines of the silicon plate for case B. At the beginning of the transient process, the lowest temperature point can be found at the top first corner of the step. As time progress towards steady state condition, the location of the lowest temperature can be found at the stagnation region. The interface temperature for case B is shown in Figure 49. A

smaller maximum to minimum temperature difference exists compared to case A. The local heat transfer coefficient for case B is shown in Figure 50. As time progresses toward steady state condition, the distribution of local heat transfer coefficient becomes more uniform due to the increase in interface temperature. The local Nusselt number for case B is shown in Figure 51. As time proceeds towards steady state condition, the stagnation region becomes the location where large removal of heat fluxes occurs. The local Nusselt number peak at the middle of the plot occurs at the location of top corner of the step. The reason behind this behavior is due to the sudden geometry change. The change in geometry leads to the break of the thermal boundary layer.

Figure 52 shows the isothermal lines of the silicon plate for case C. There is a gradual increase across the plate length with a sudden decrease at the end of the plate where the second step located. The interface temperature for case C is shown in Figure 53. The interface temperature is more uniform due to the shape of the geometry. Also, the difference between maximum to minimum temperature is less than case A as shown in Figure 45. The local heat transfer coefficient for case C is shown in Figure 54. The local heat transfer coefficient is lower in values but more uniform than case A. The local Nusselt number for case C is shown in Figure 55. The local Nusselt number follows the same trend seen in the local heat transfer coefficient due to the temperature dependence.

Figure 56 shows the isothermal lines of the silicon plate for case D. The lowest temperature of the plate can be found at the stagnation region. At the beginning of the transient process, the maximum to minimum temperature difference of case D is less than case B. As time progresses towards steady state condition, the temperature of the plate for case D is less than case B. The interface temperature for case D is shown in Figure 57. By comparing Figure 57 to

Figure 49, there is an advantage when using a triangular shaped step compared to a rectangular shaped step. The overall interface temperature is less compared to Figure 49 due to smoother flow of the fluid. The local heat transfer coefficient for case D is shown in Figure 58. The local heat transfer coefficient is higher than case B as shown in Figure 50. The local Nusselt number for case D is shown in Figure 59. There is an advantage for heat transfer when using case D compared to case B. The triangular shaped step prevents some of the fluid recirculation that happens before and after the step compared to case B.

Figure 60 shows the isothermal lines of the silicon plate for case E. The lowest temperature of the plate occurs at the stagnation region. There is a slight advantage for case E to case C, but there is a disadvantage for case E compared to case A. The interface temperature for case E is shown in Figure 61. The difference between maximum to minimum interface temperature is less than case A, which is due to less recirculation that occurs before and after the sharp edges of the step found in case A. The local heat transfer coefficient for case E is shown in Figure 62. There is a slight decrease in local heat transfer coefficient compared to case A. The local Nusselt number for case E is shown in Figure 63. The behavior is somewhat similar to that found in Figure 47 with a slight decrease in values.

Figure 64 shows the isothermal lines of the silicon plate for case F. The overall temperature of the plate for case F is better than case B, but it is worse than case D. The interface temperature for case F is shown in Figure 65. Case F has a slight advantage compared to case B. The interface temperature along the interface for case F is slightly less than case B. The local heat transfer coefficient for case F is shown in Figure 66. There is a slight increase in local heat transfer coefficient compared to case B. The local Nusselt number for case F is shown in Figure 67. The results are very comparable to case B with a slight advantage to case F.

The variations in time for the average heat transfer coefficient and the average Nusselt number are shown in Figure 68. The highest values of the average heat transfer coefficient and the average Nusselt number are at the beginning of the transient process. The values of the average heat transfer and average Nusselt number decrease rapidly until reaching steady state condition.

The variations in time for the average heat transfer coefficient and the average Nusselt number is shown in Figure 69. The calculations were conducted for the base model with Reynolds number of 500. The decrease in Reynolds number increases the time required to reach steady state condition compared to Figure 68.

The variations in time for the average heat transfer coefficient and the average Nusselt number are shown in Figure 70. The calculations were conducted for the base model with Reynolds number of 1000. The increase in Reynolds number decreases the time required to reach steady state condition.

The variations in time for the average heat transfer coefficient and the average Nusselt number are shown in Figure 71. The calculations were conducted for the base model with constantan as a plate material. In comparison to Figure 68, the constantan plate takes more time than the silicon plate to reach steady state due to the low thermal diffusivity of constantan.

The variations in time for the average heat transfer coefficient and the average Nusselt number are shown in Figure 72. The calculations were conducted for the base model with copper as a plate material. It takes the copper plate slightly less time to reach steady state condition compared to the silicon plate due to the increase in thermal diffusivity of copper.

The variations in time for the average heat transfer coefficient and the average Nusselt number are shown in Figure 73. The calculations were conducted for the base model with a step

height of 0.000125 m. It takes less time to reach steady state condition when decreasing the step size compared to the base model in Figure 68 due to better recirculation of the fluid when decreasing the step height.

The variations in time for the average heat transfer coefficient and the average Nusselt number are shown in Figure 74. The calculations were conducted for the base model with a step height of 0.000375 m. There is a slight increase in time to reach steady state condition compared to Figure 68 due to the increase in obstructing the fluid flow.

Figure 75 shows the variations of the average heat transfer coefficient and the average Nusselt number with time. The results were obtained for the base model with an isothermal boundary condition at the bottom of the plate. All cases met the steady state condition in a very short period of time compared to the constant heat flux boundary condition.

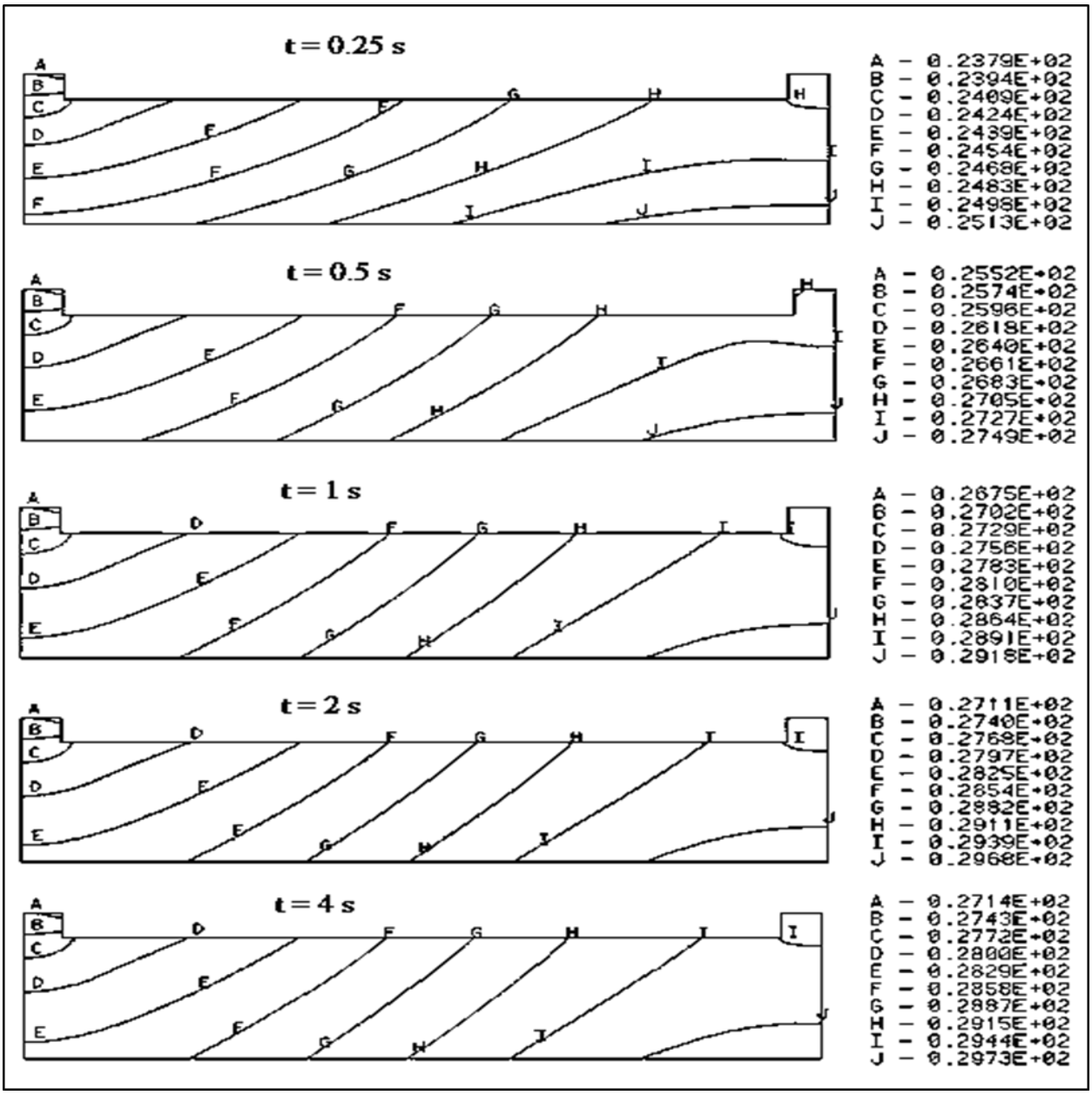

Figure 44: Isothermal Lines of Case A in Degrees Celsius

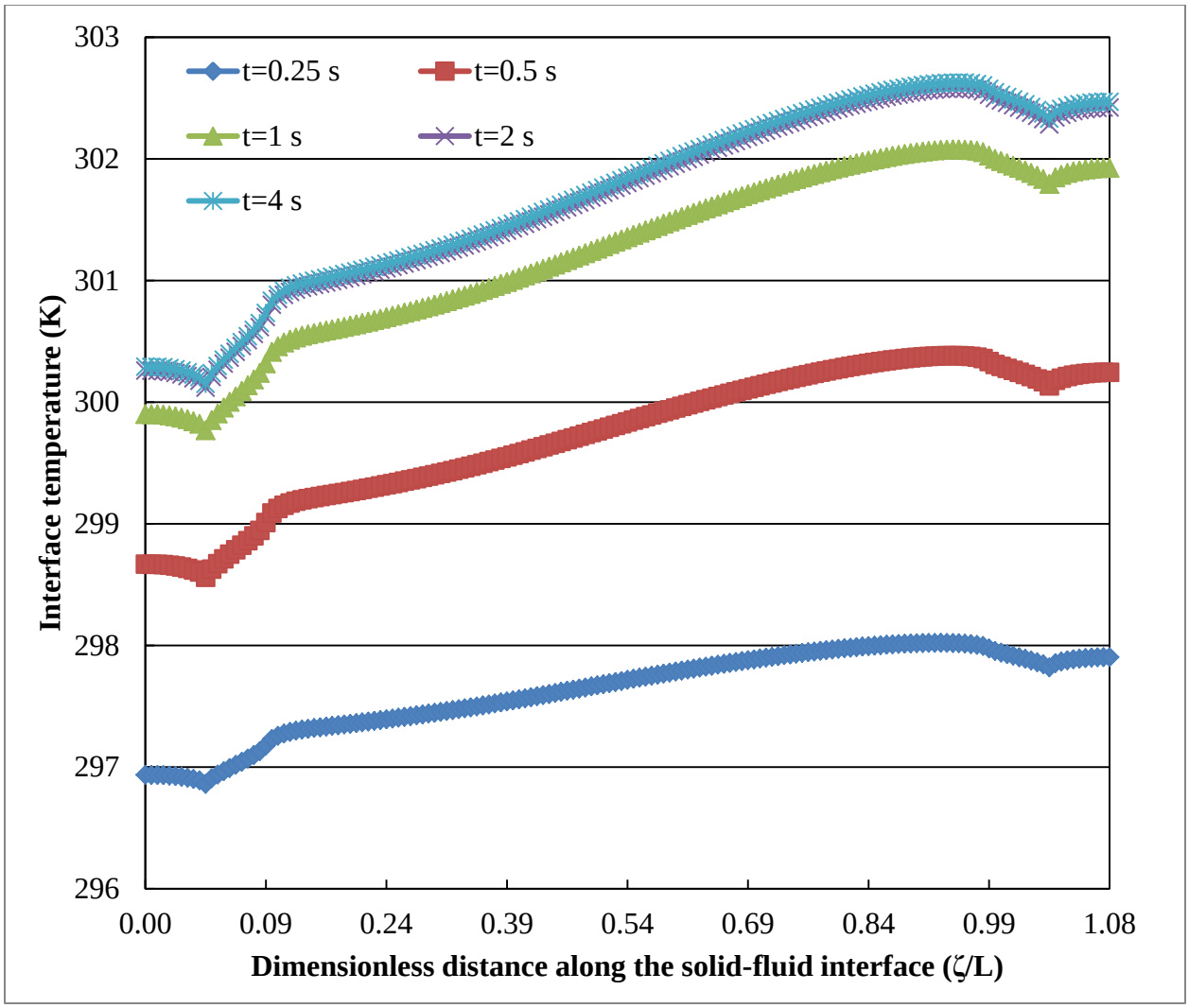

Figure 45: Variations of Interface Temperature of Silicon Plate at Re = 750 for Case A

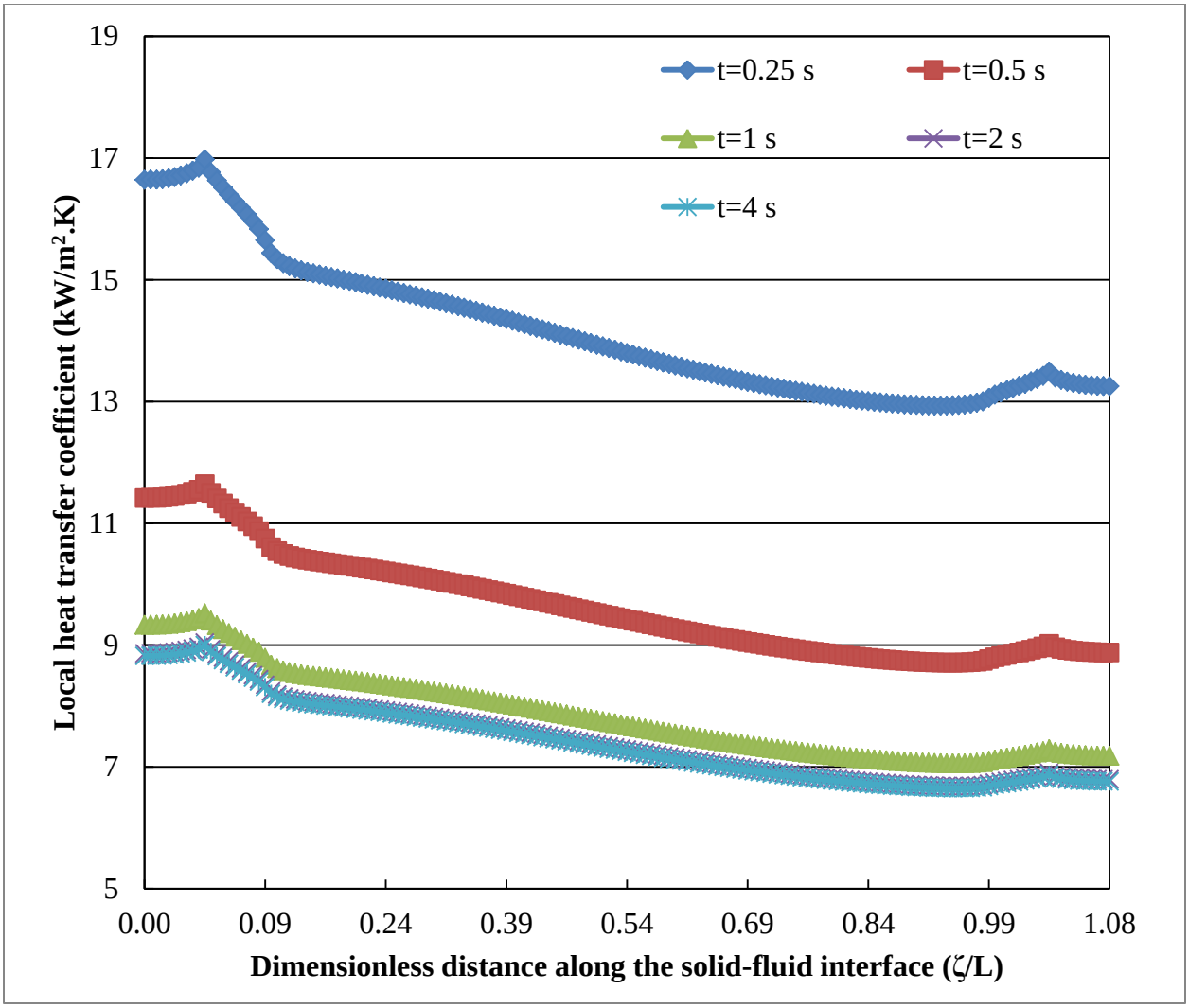

Figure 46: Variations of Local Heat Transfer Coefficient for Silicon Plate at Re = 750 for Case A

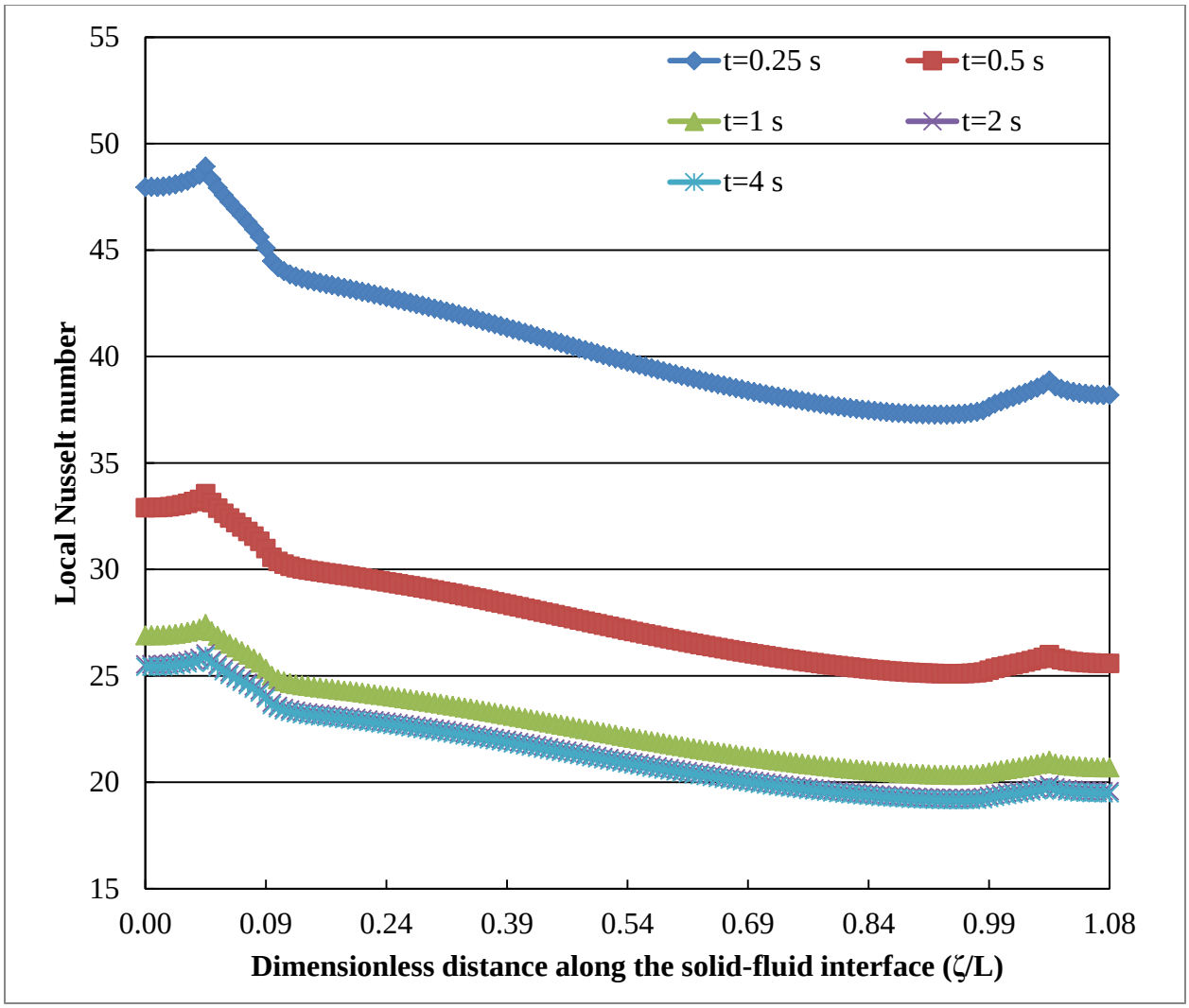

Figure 47: Variations of Local Nusselt Number for Silicon Plate at Re = 750 for Case A

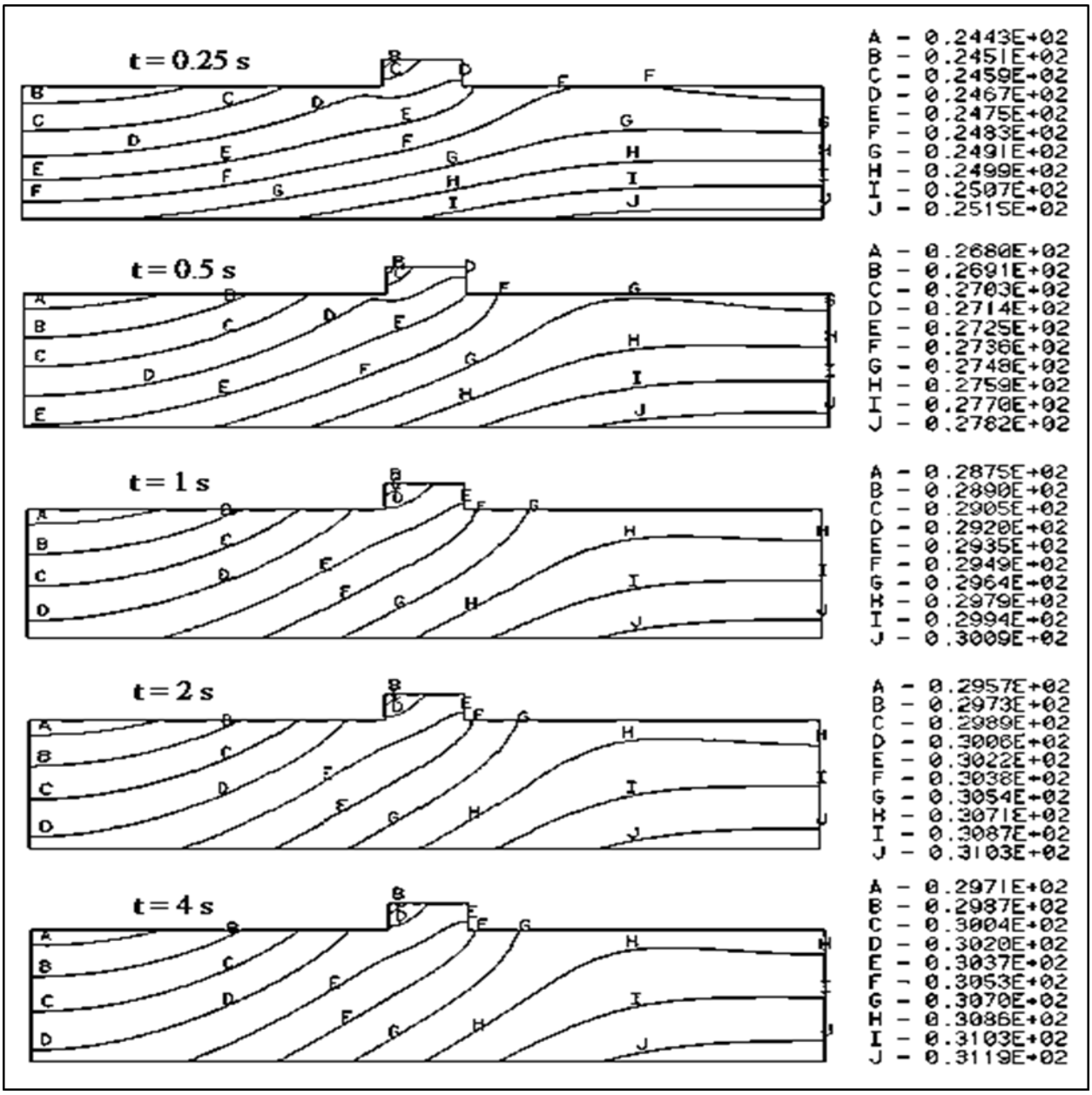

Figure 48: Isothermal Lines of Case B in Degrees Celsius

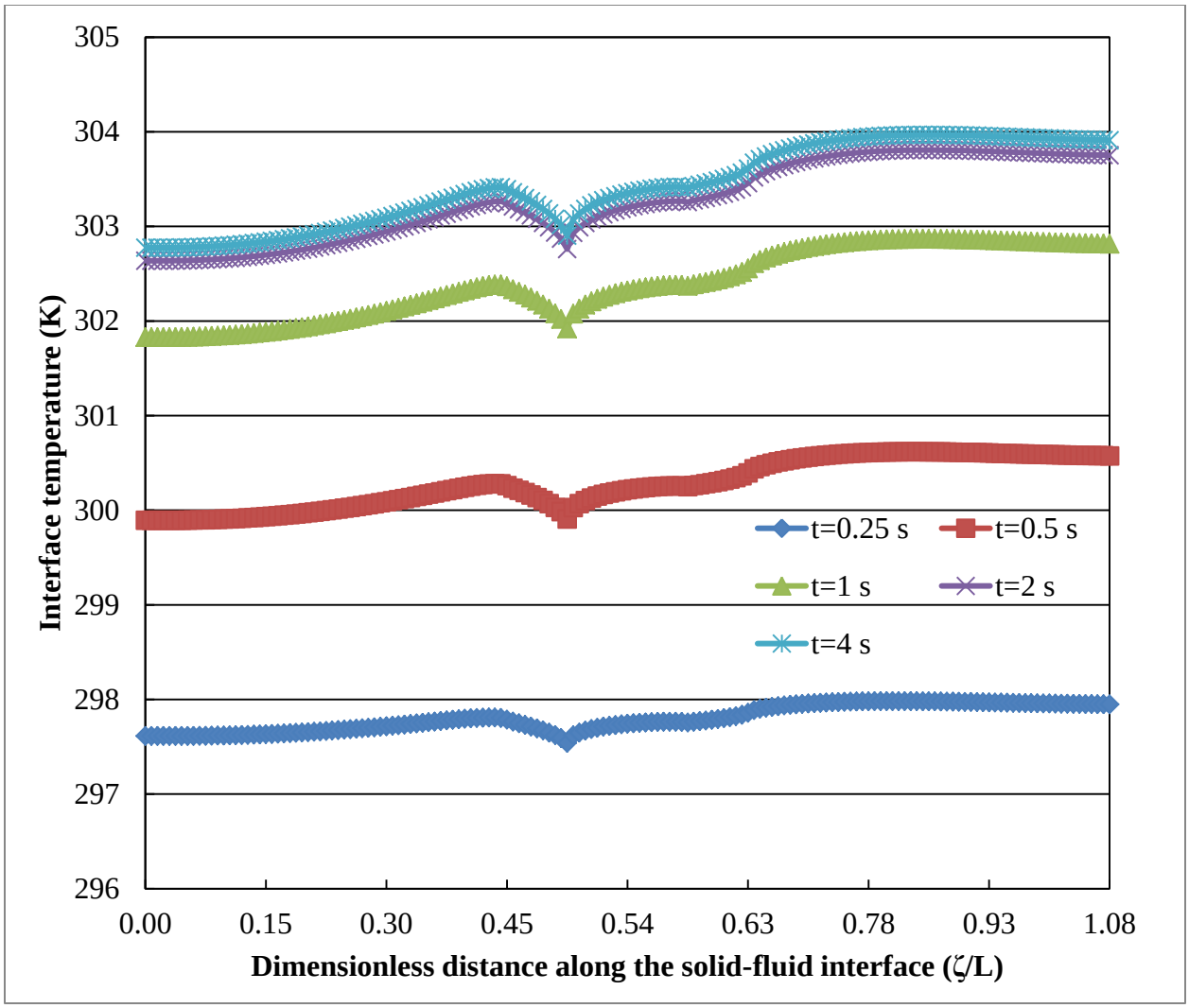

Figure 49: Variations of Interface Temperature of Silicon Plate at Re = 750 for Case B

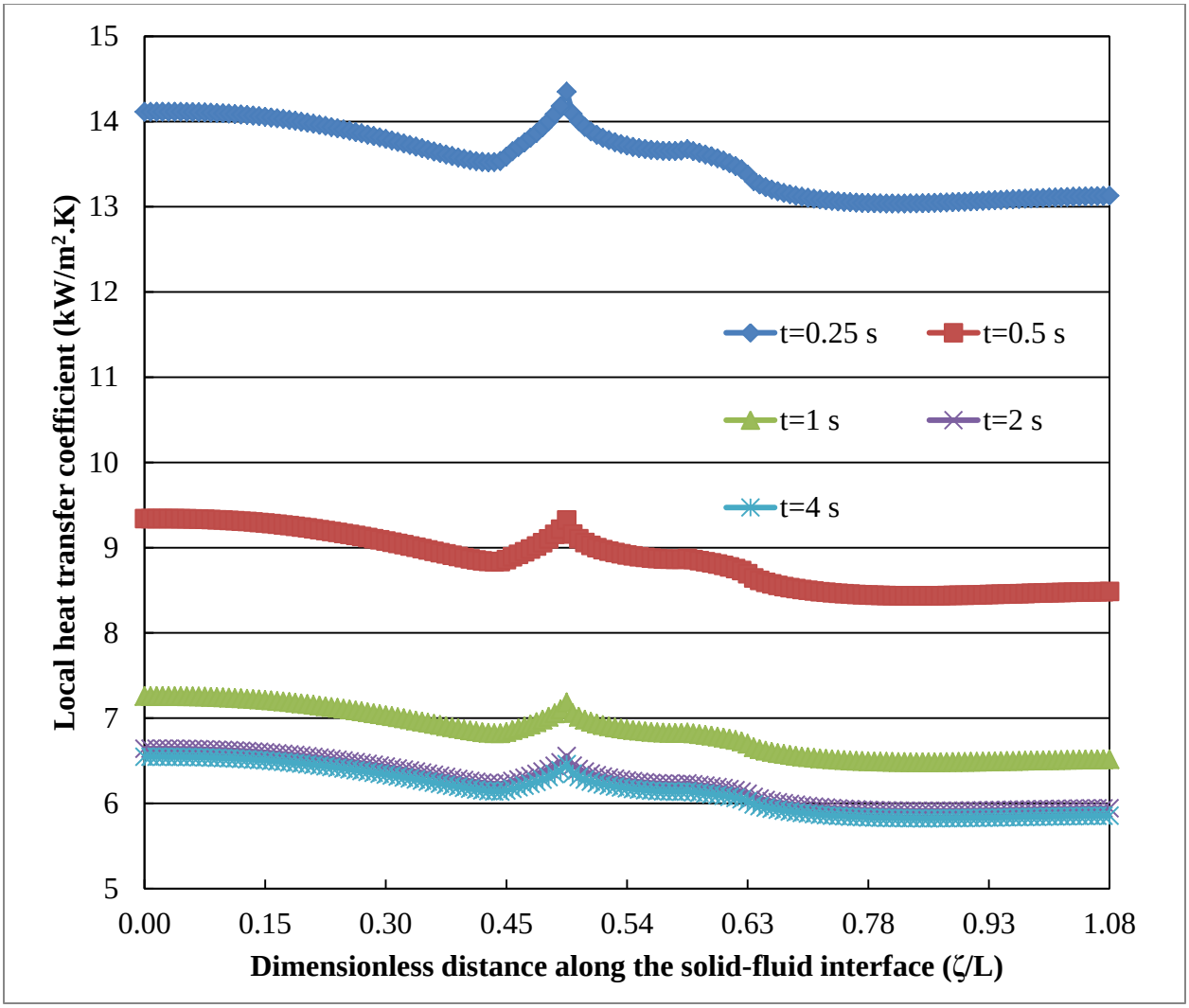

Figure 50: Variations of Local Heat Transfer Coefficient for Silicon Plate at Re = 750 for Case B

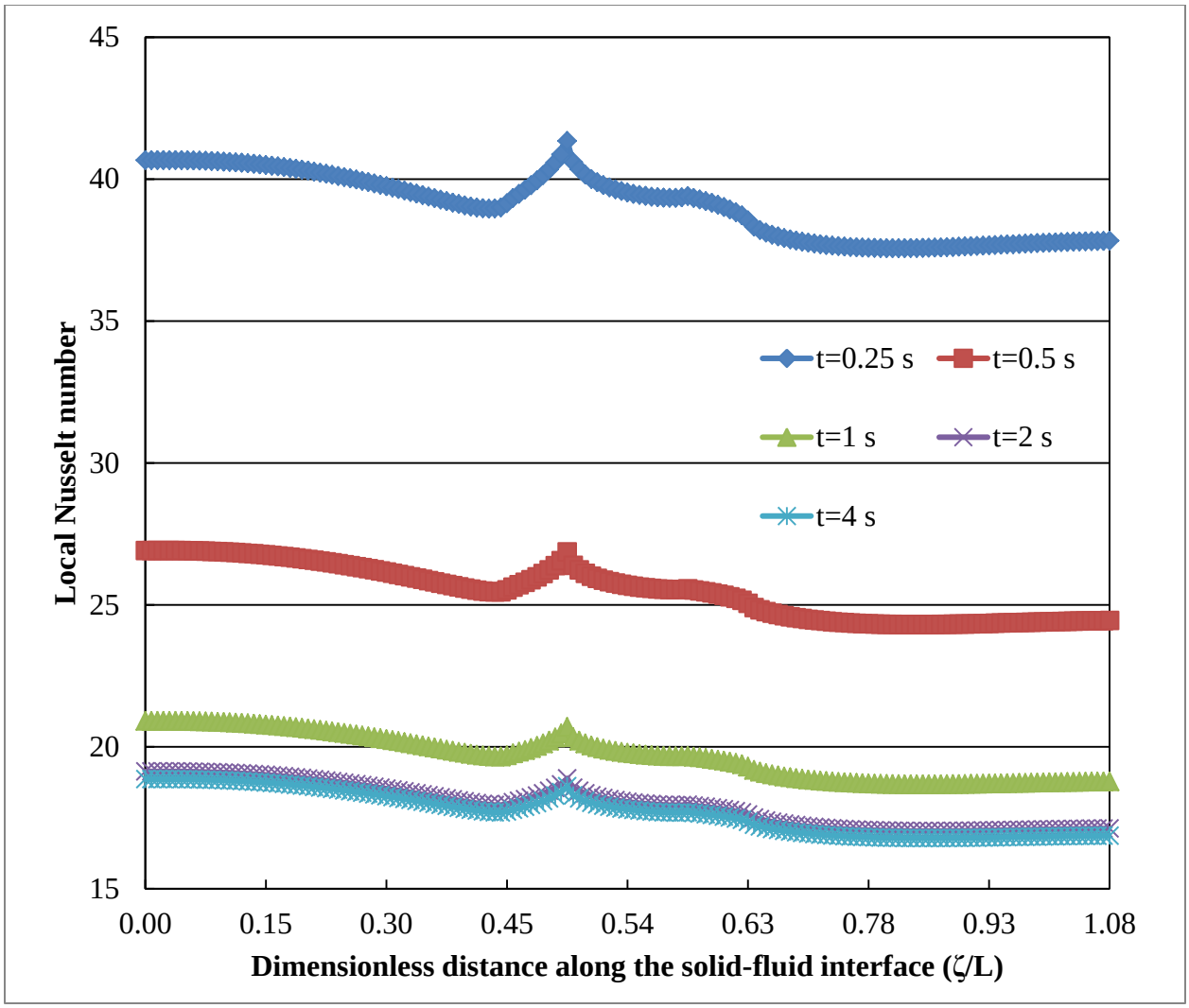

Figure 51: Variations of Local Nusselt Number for Silicon Plate at Re = 750 for Case B

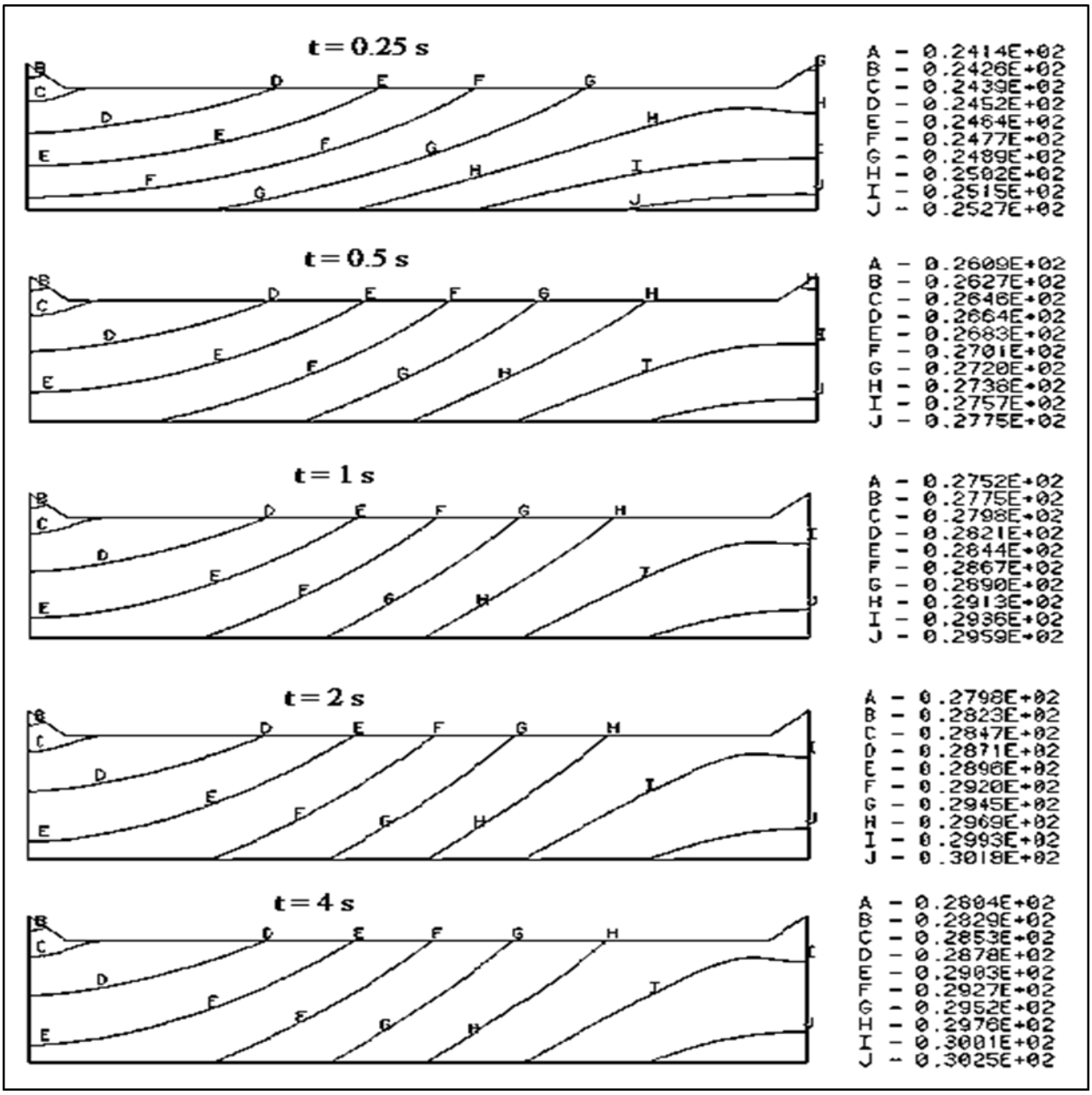

Figure 52: Isothermal Lines of Case C in Degrees Celsius

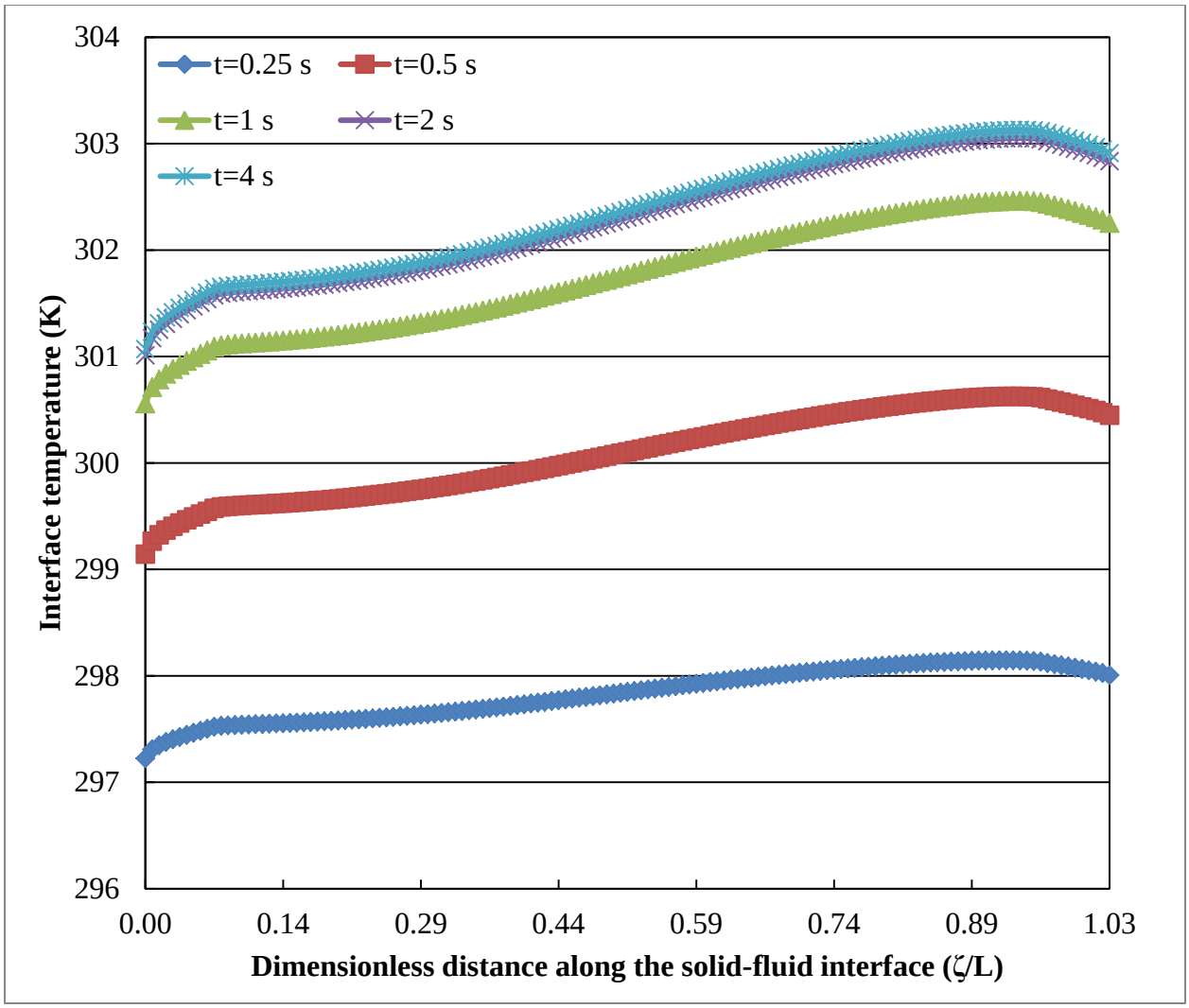

Figure 53: Variations of Interface Temperature of Silicon Plate at Re = 750 for Case C

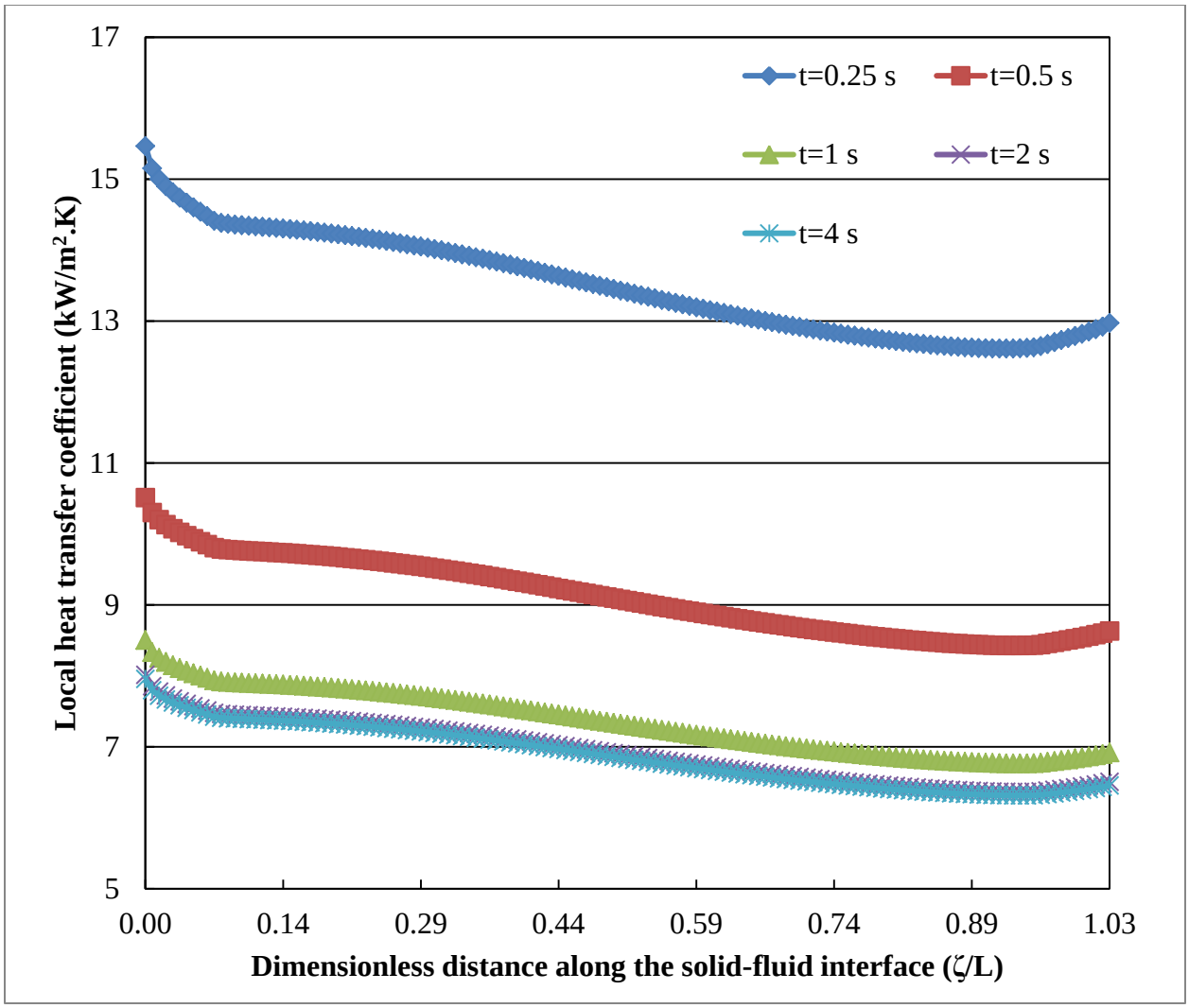

Figure 54: Variations of Local Heat Transfer Coefficient for Silicon Plate at Re = 750 for Case C

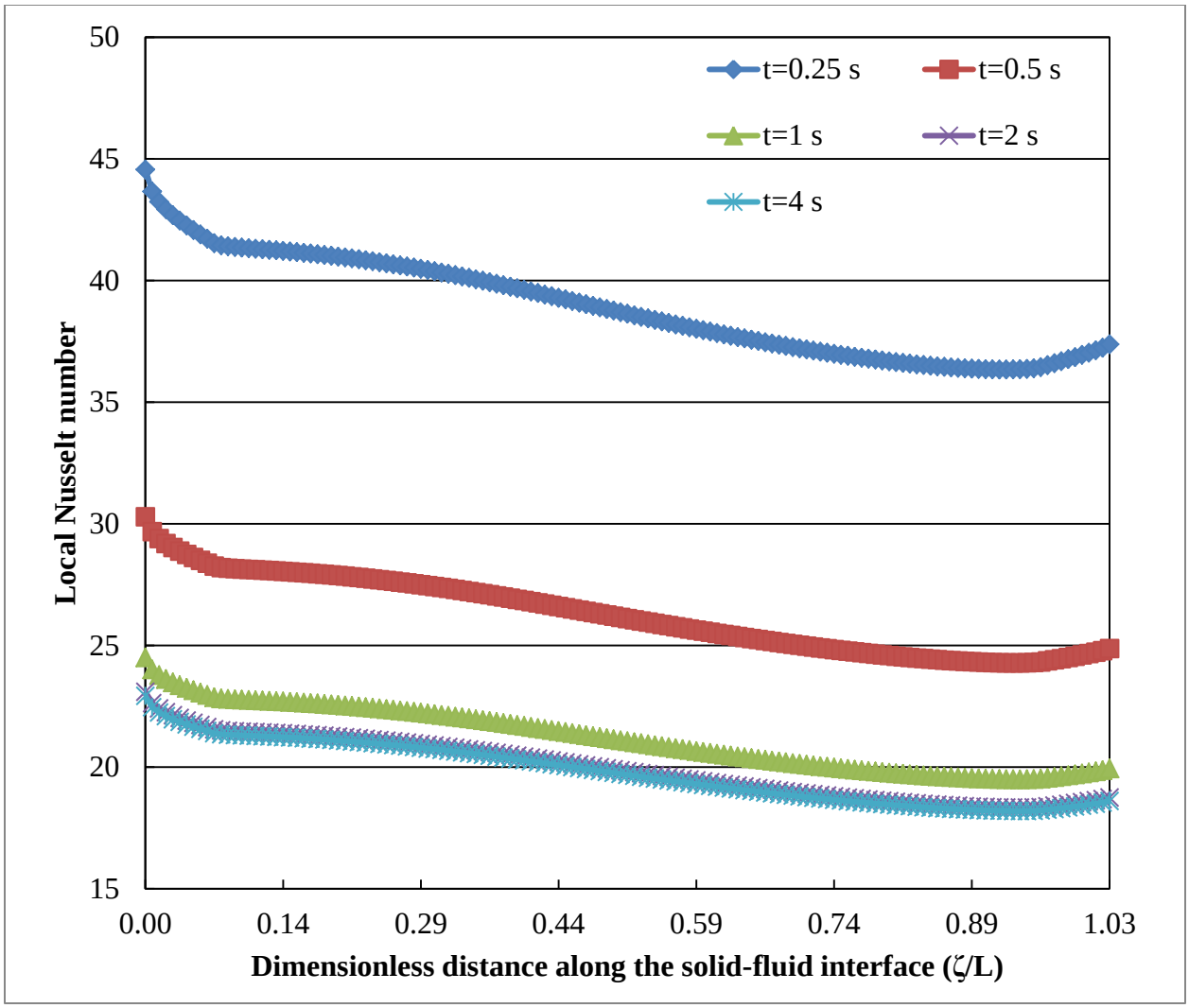

Figure 55: Variations of Local Nusselt Number for Silicon Plate at Re = 750 for Case C

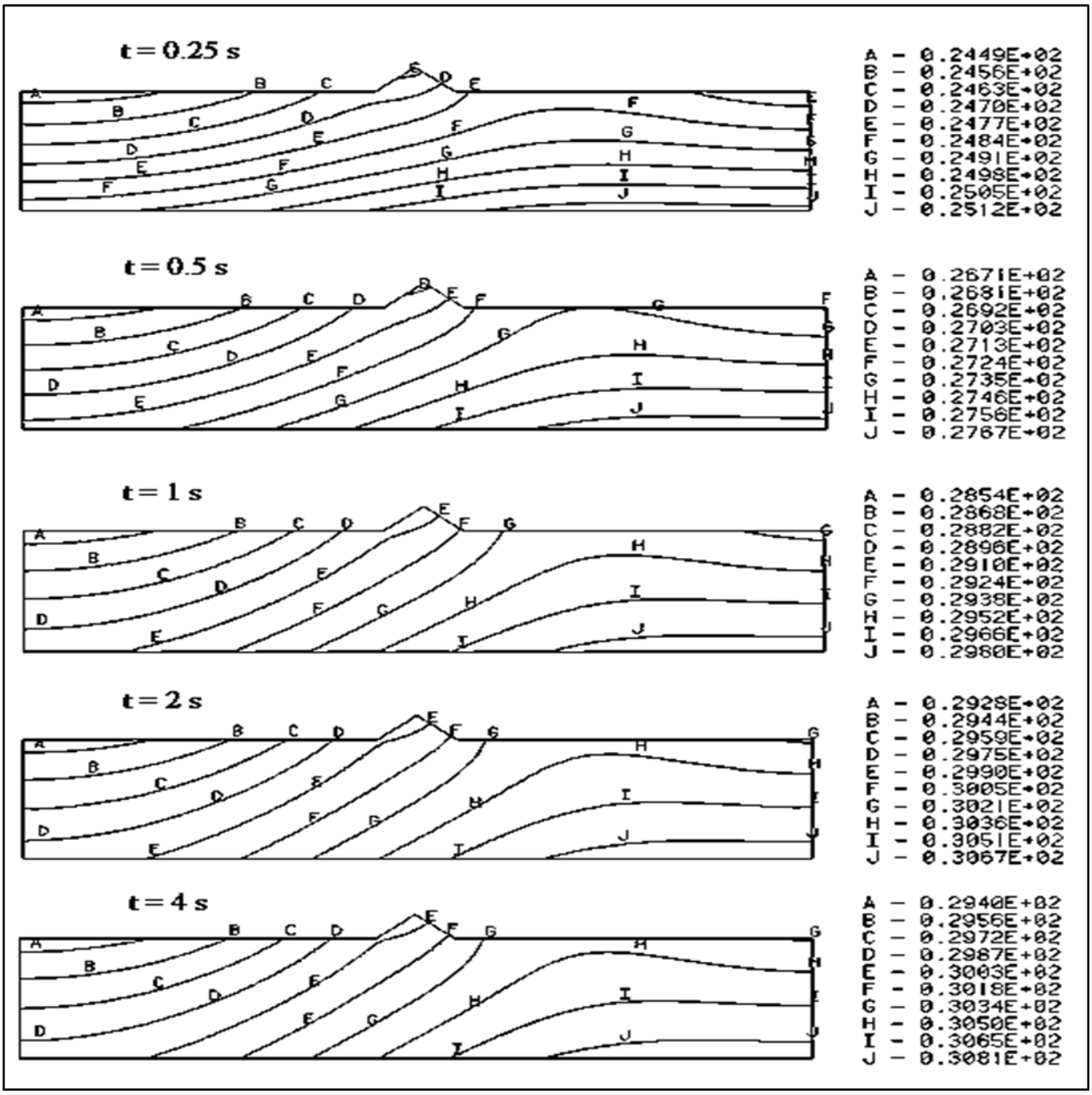

Figure 56: Isothermal Lines of Case D in Degrees Celsius

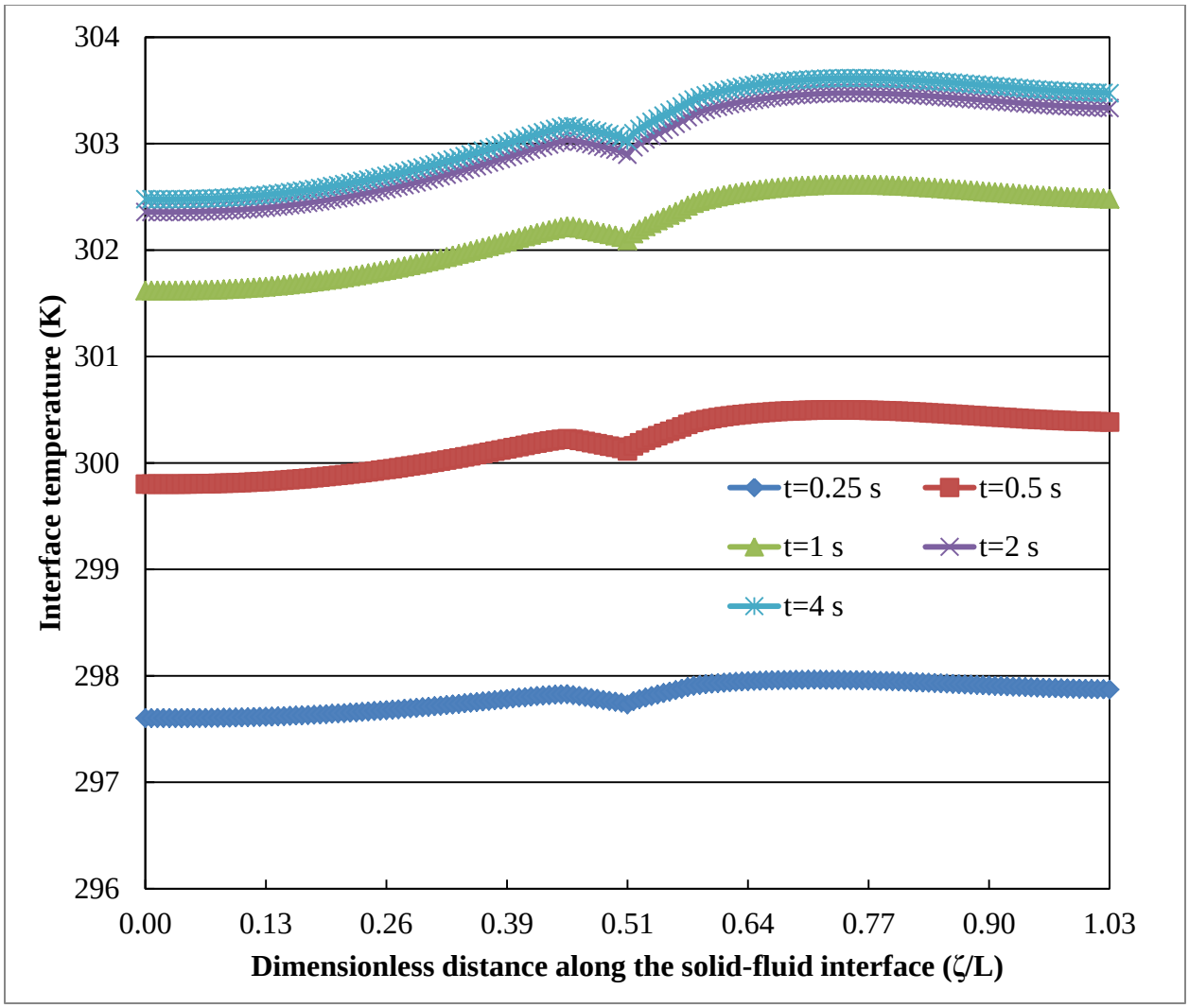

Figure 57: Variations of Interface Temperature of Silicon Plate at Re = 750 for Case D

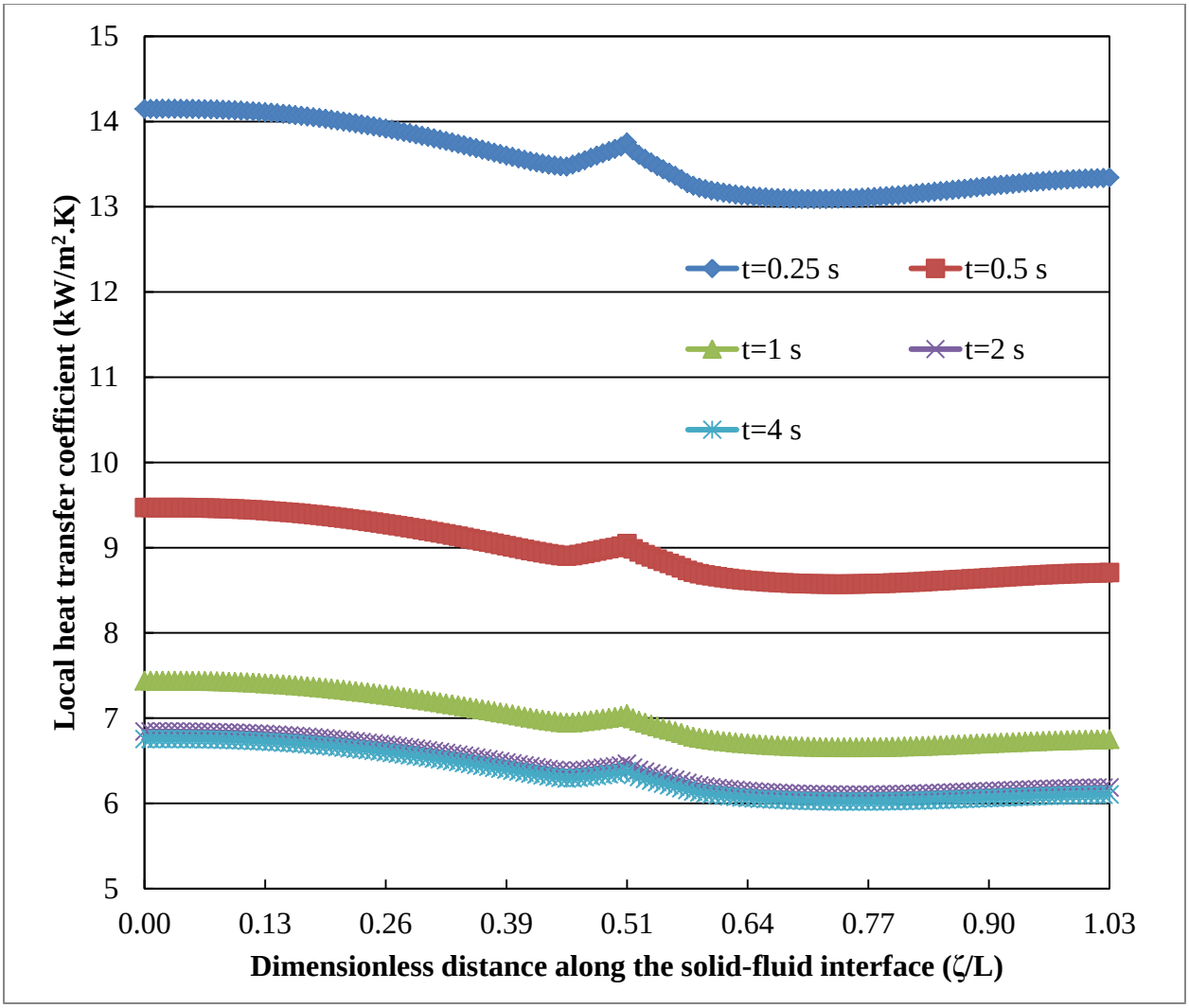

Figure 58: Variations of Local Heat Transfer Coefficient for Silicon Plate at Re = 750 for Case D

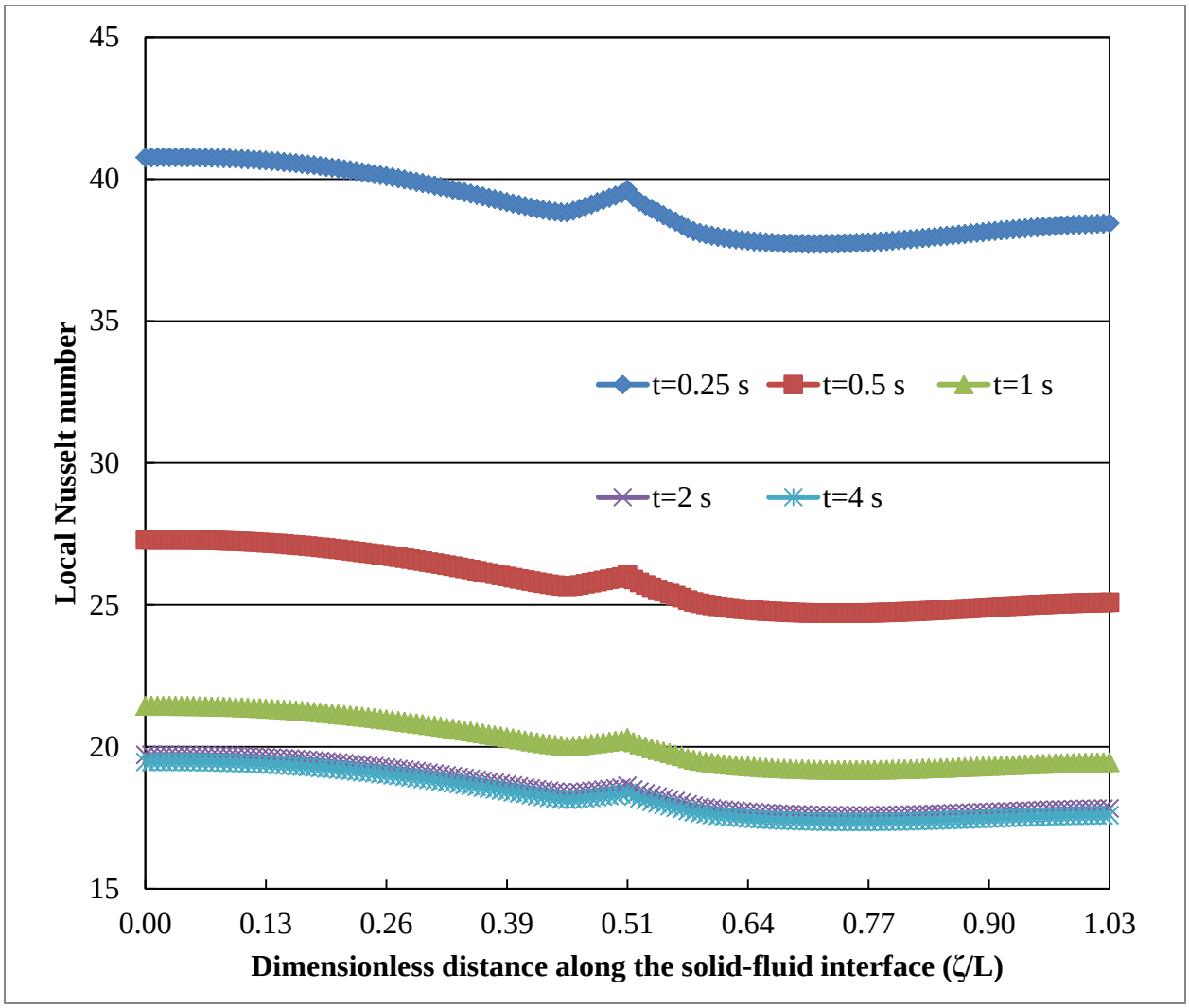

Figure 59: Variations of Local Nusselt Number for Silicon Plate at Re = 750 for Case D

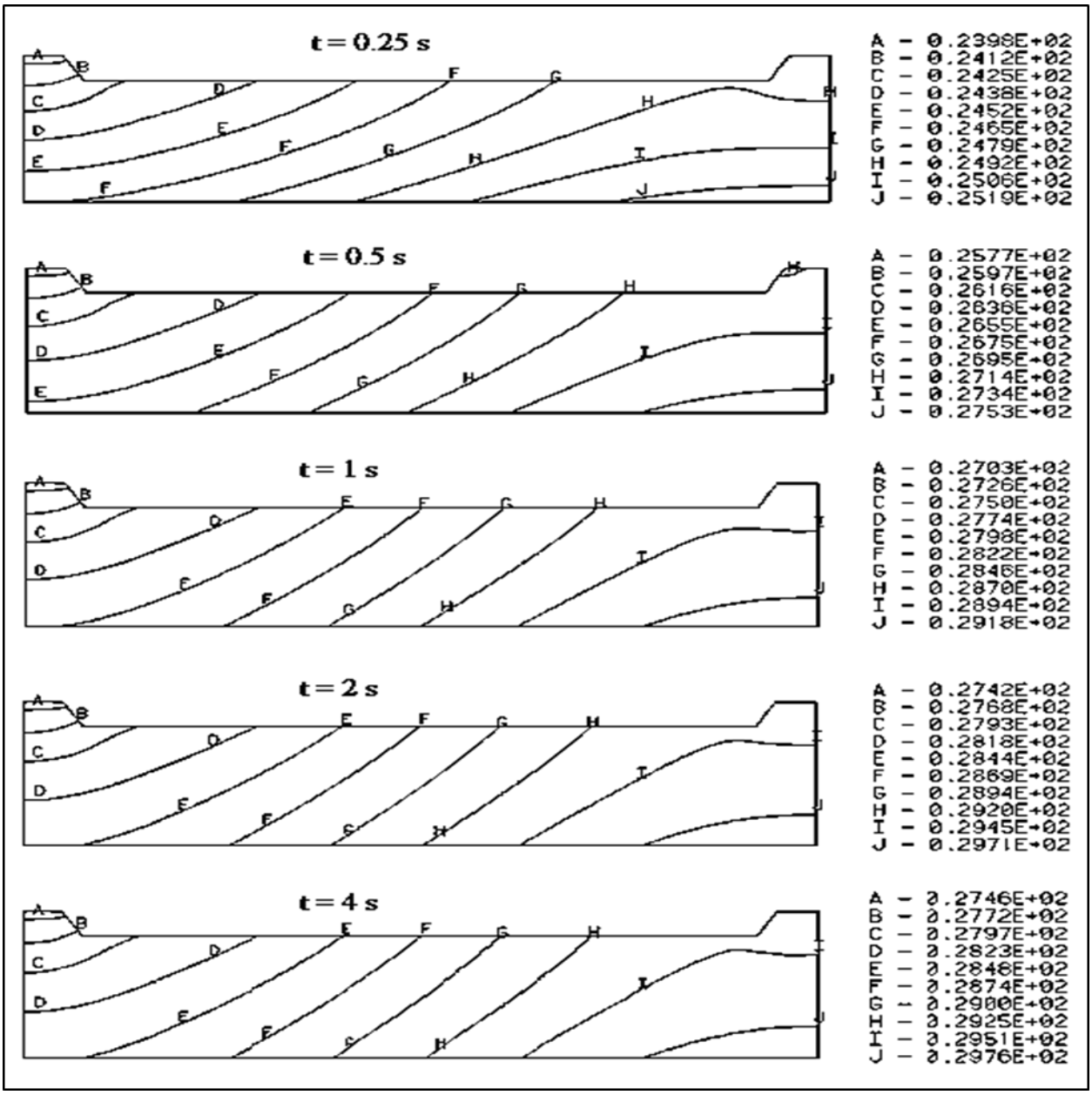

Figure 60: Isothermal Lines of Case E in Degrees Celsius

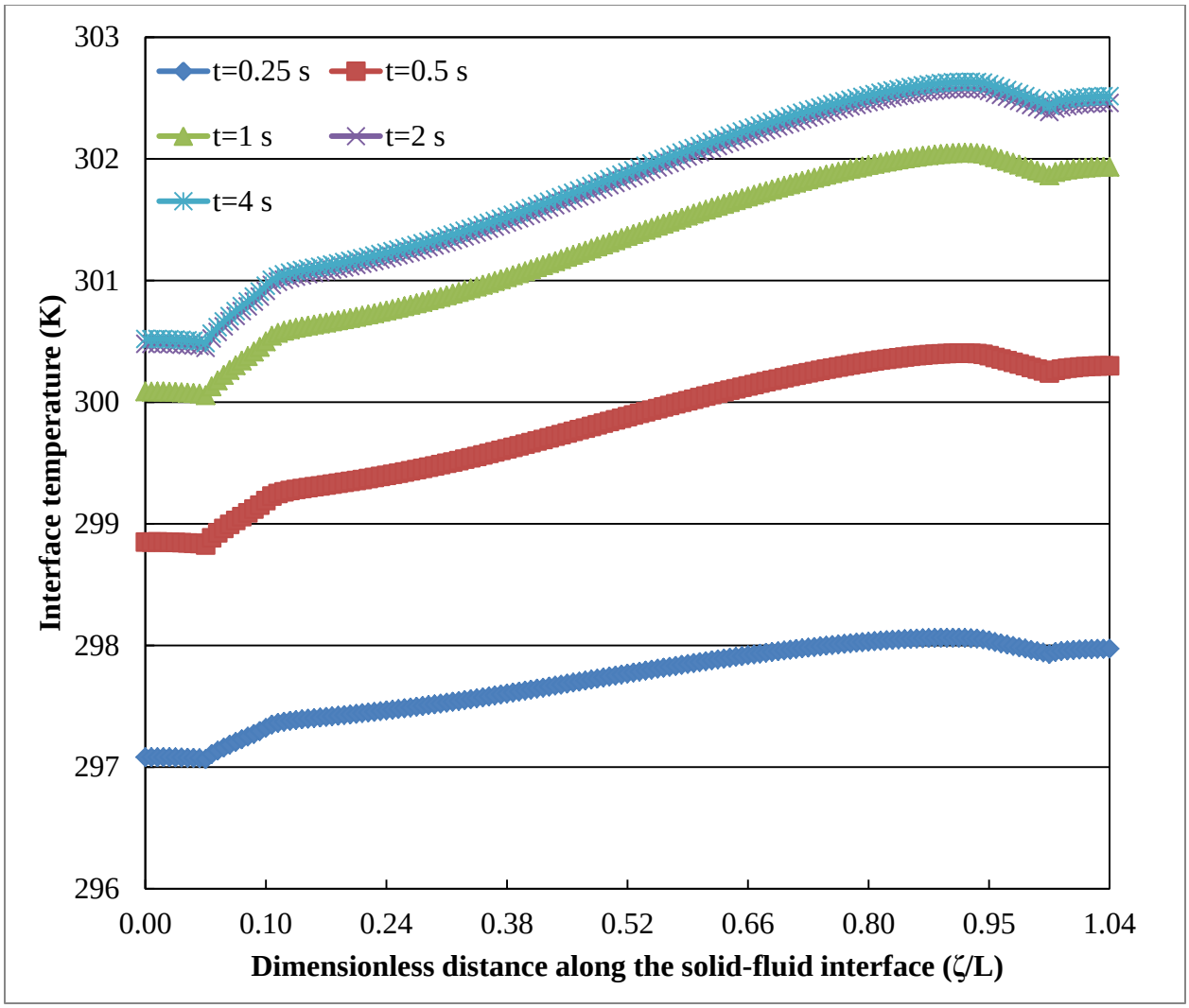

Figure 61: Variations of Interface Temperature of Silicon Plate at Re = 750 for Case E

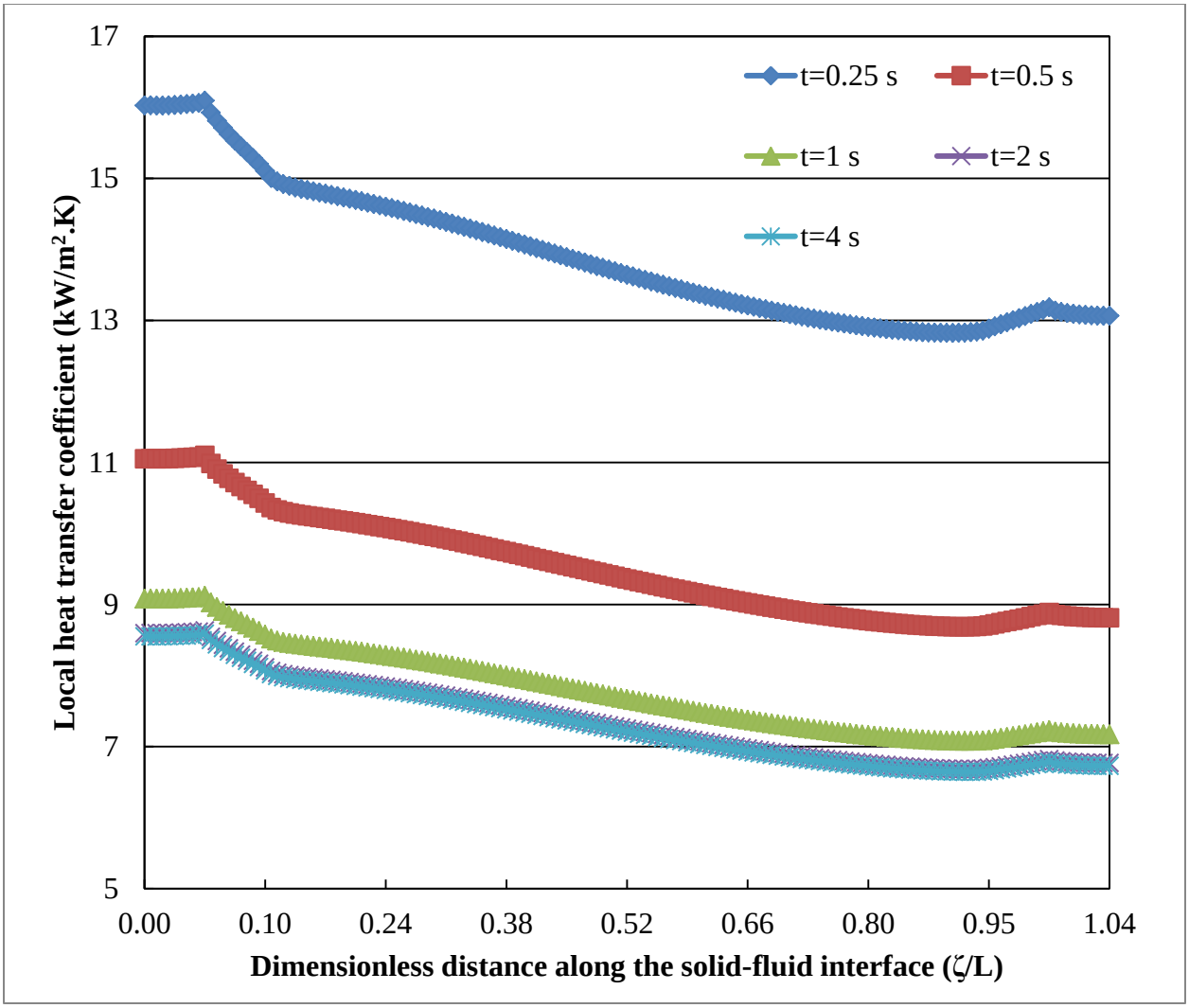

Figure 62: Variations of Local Heat Transfer Coefficient for Silicon Plate at Re = 750 for Case E

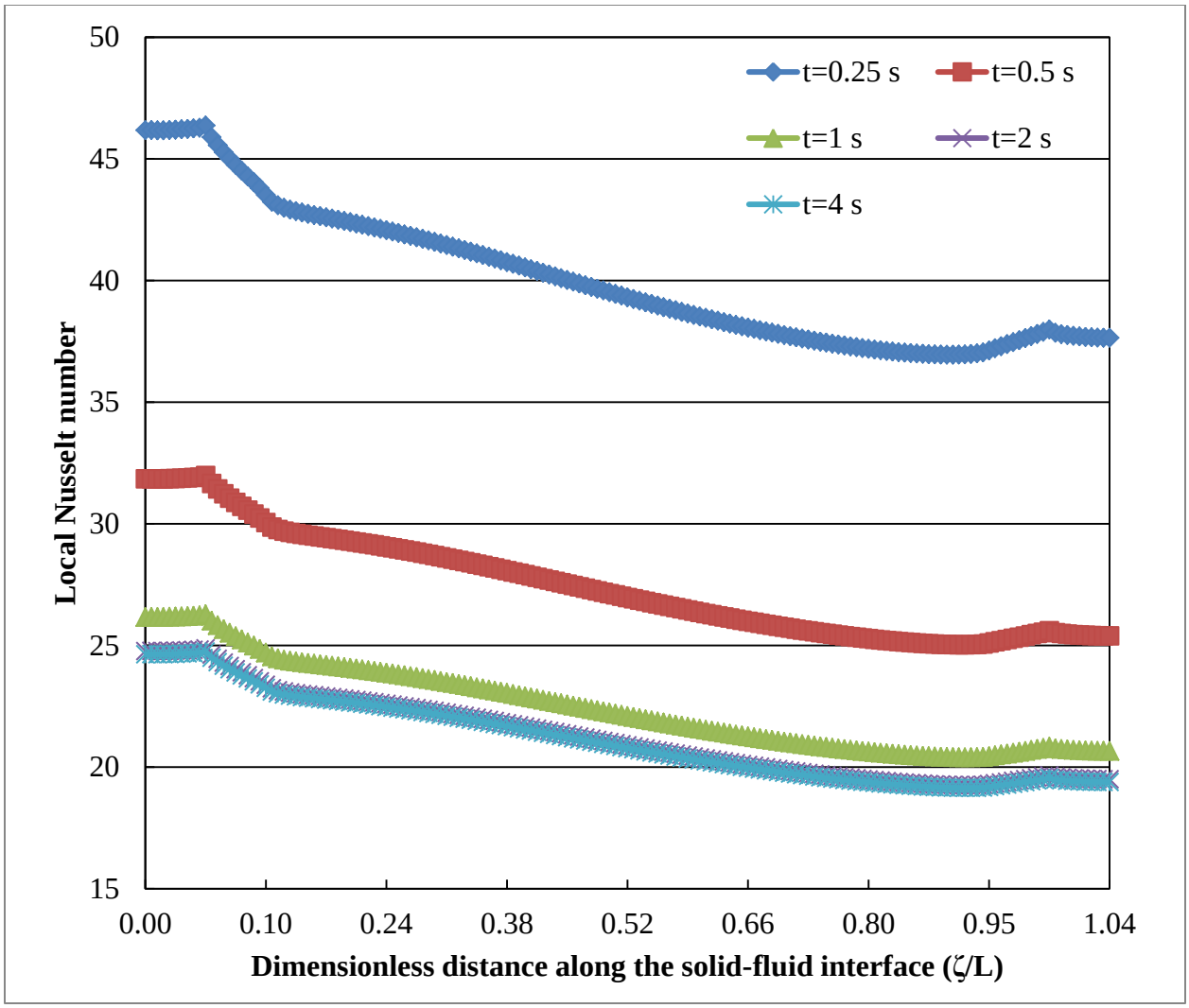

Figure 63: Variations of Local Nusselt Number for Silicon Plate at Re = 750 for Case E

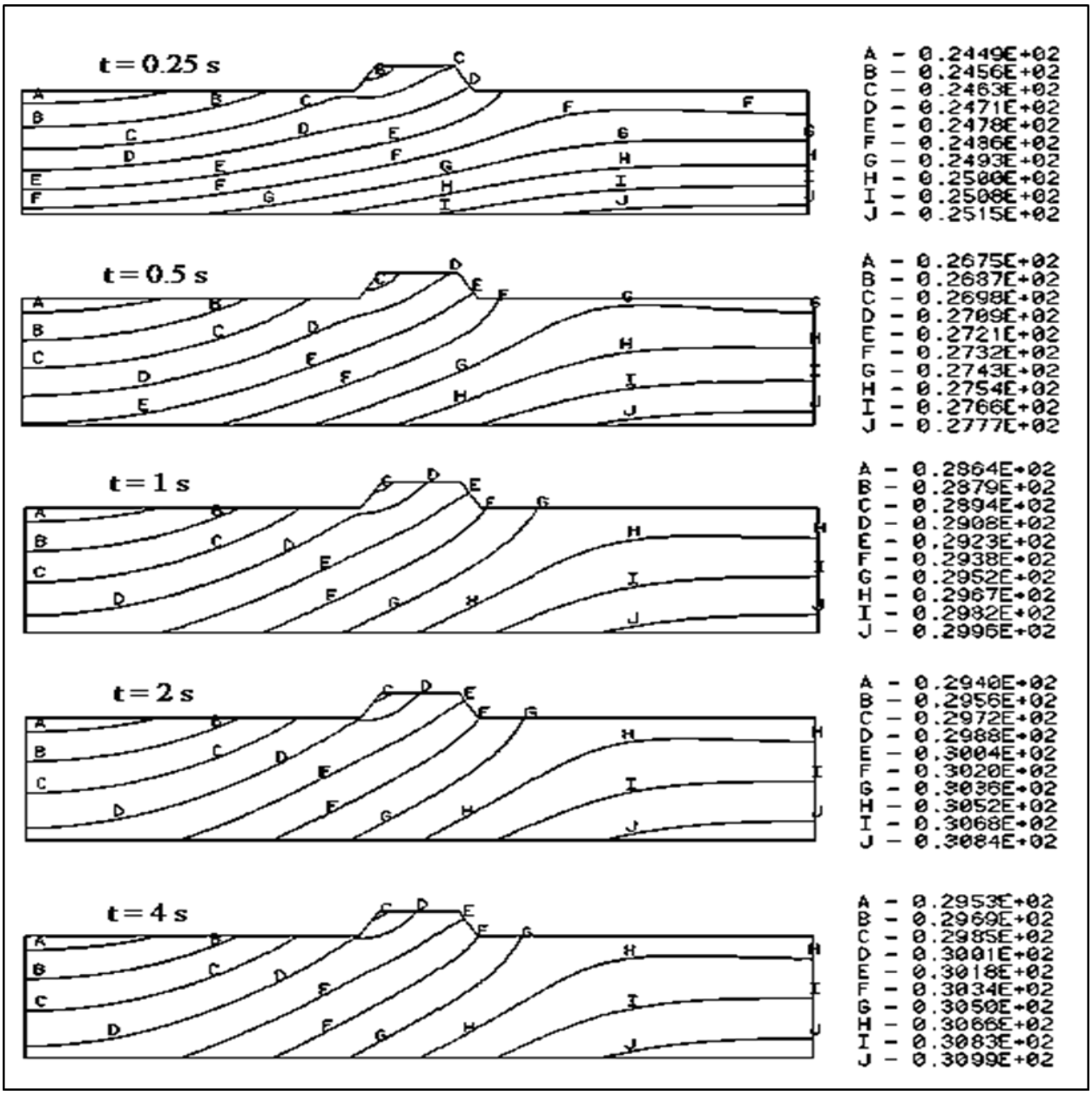

Figure 64: Isothermal Lines of Case F in Degrees Celsius

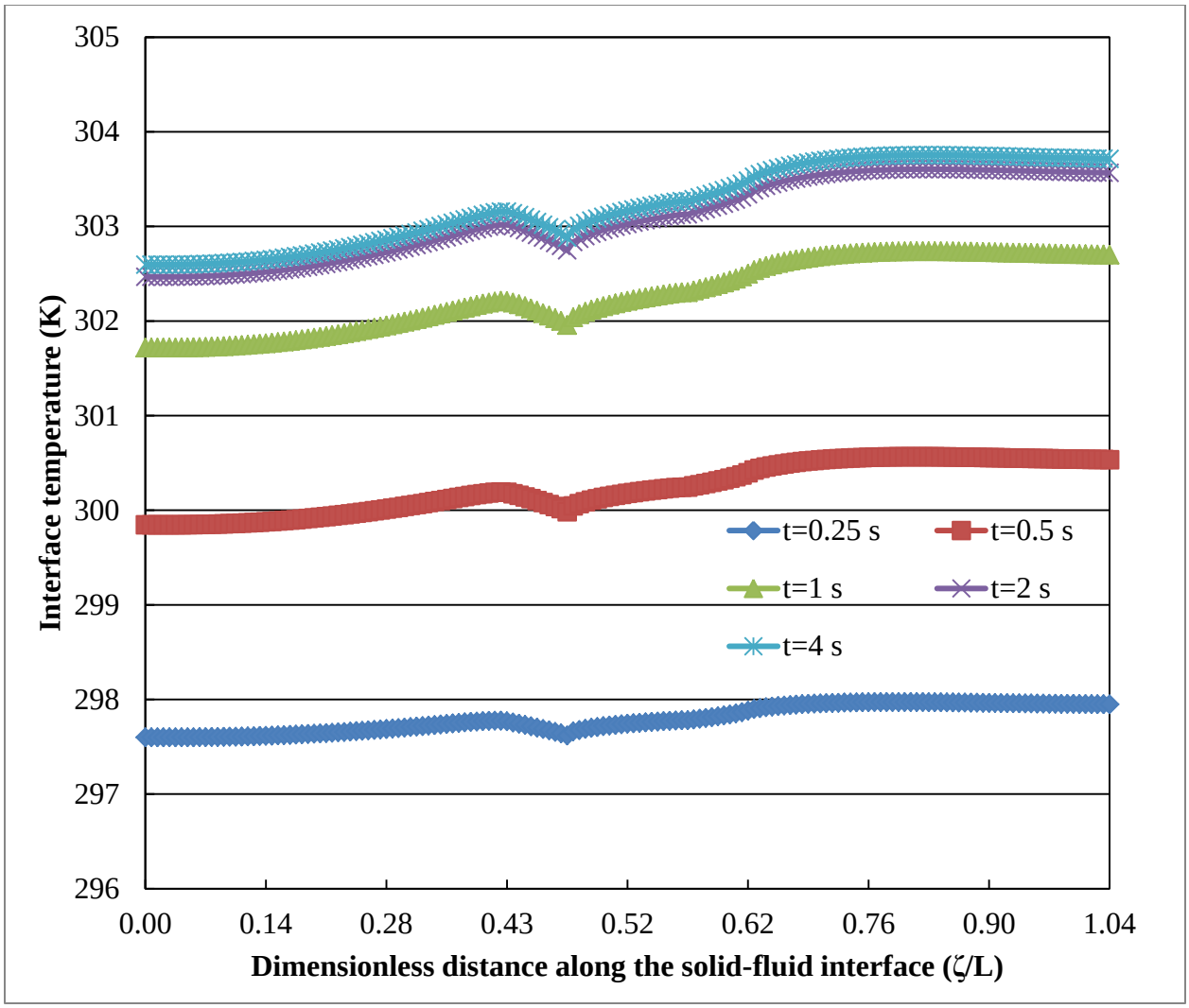

Figure 65: Variations of Interface Temperature of Silicon Plate at Re = 750 for Case F

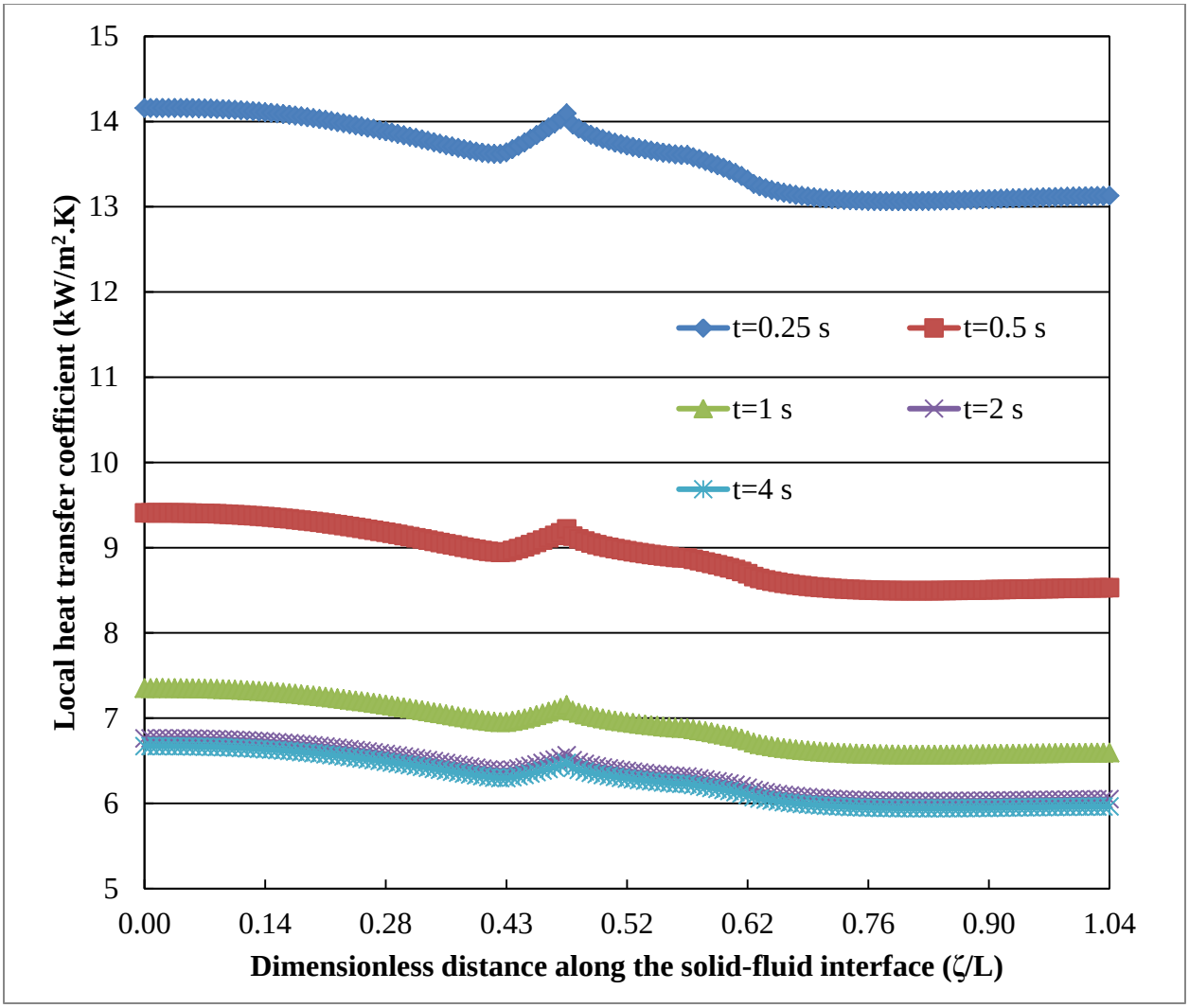

Figure 66: Variations of Local Heat Transfer Coefficient for Silicon Plate at Re = 750 for Case F

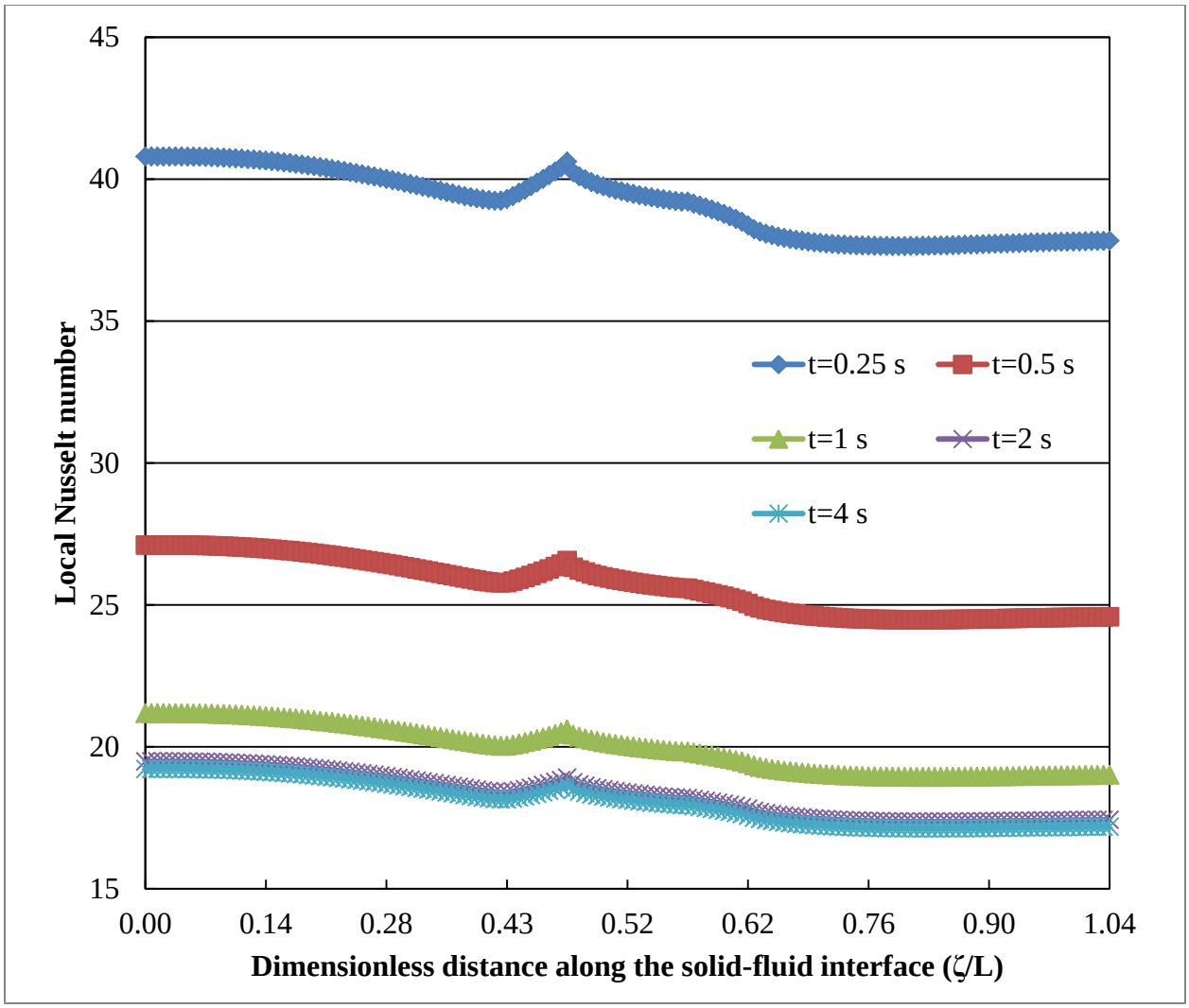

Figure 67: Variations of Local Nusselt Number for Silicon Plate at Re = 750 for Case F

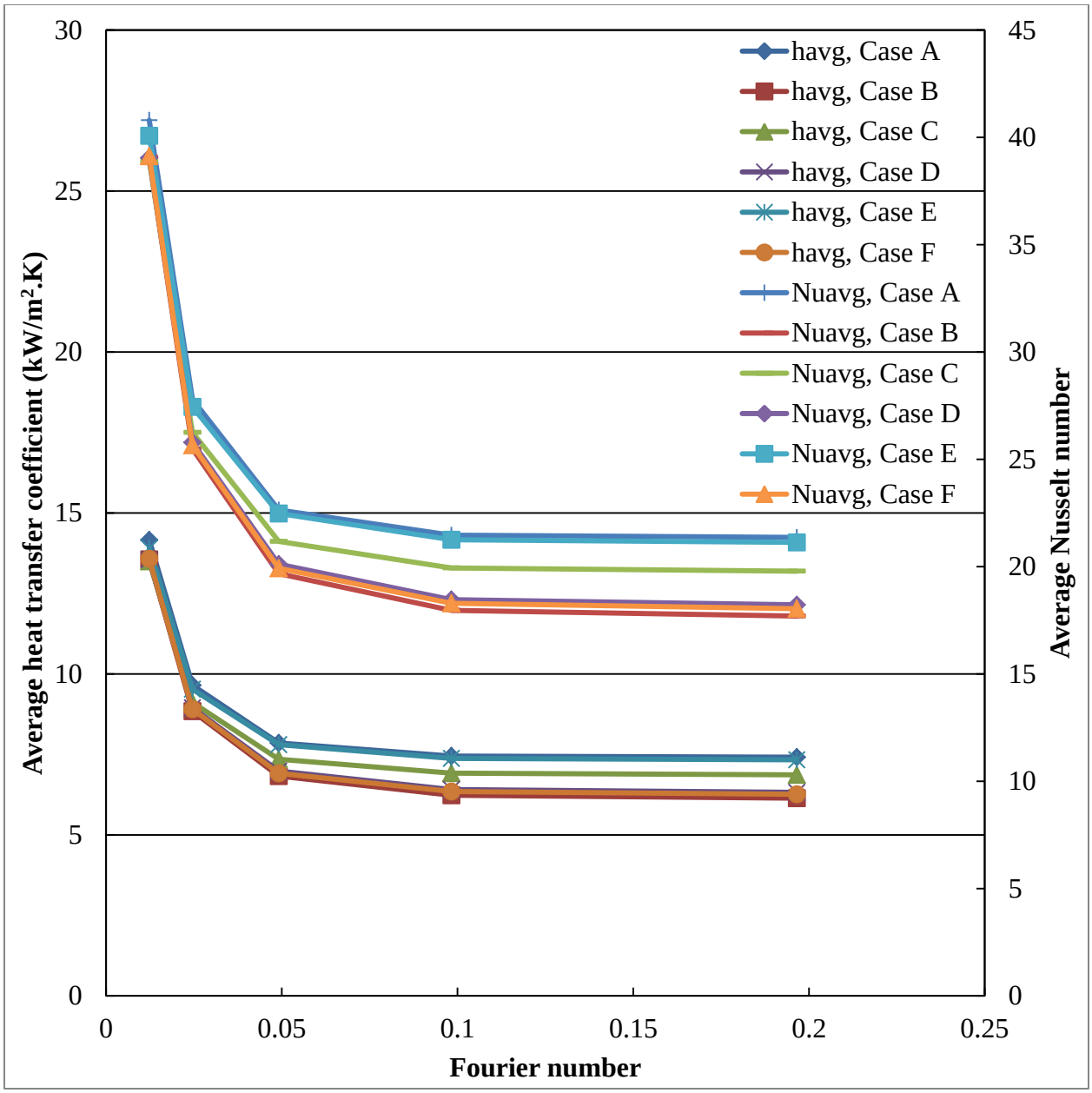

Figure 68: Variations of Average Heat Transfer Coefficient and Average Nusselt Number for Silicon Plate at Re = 750

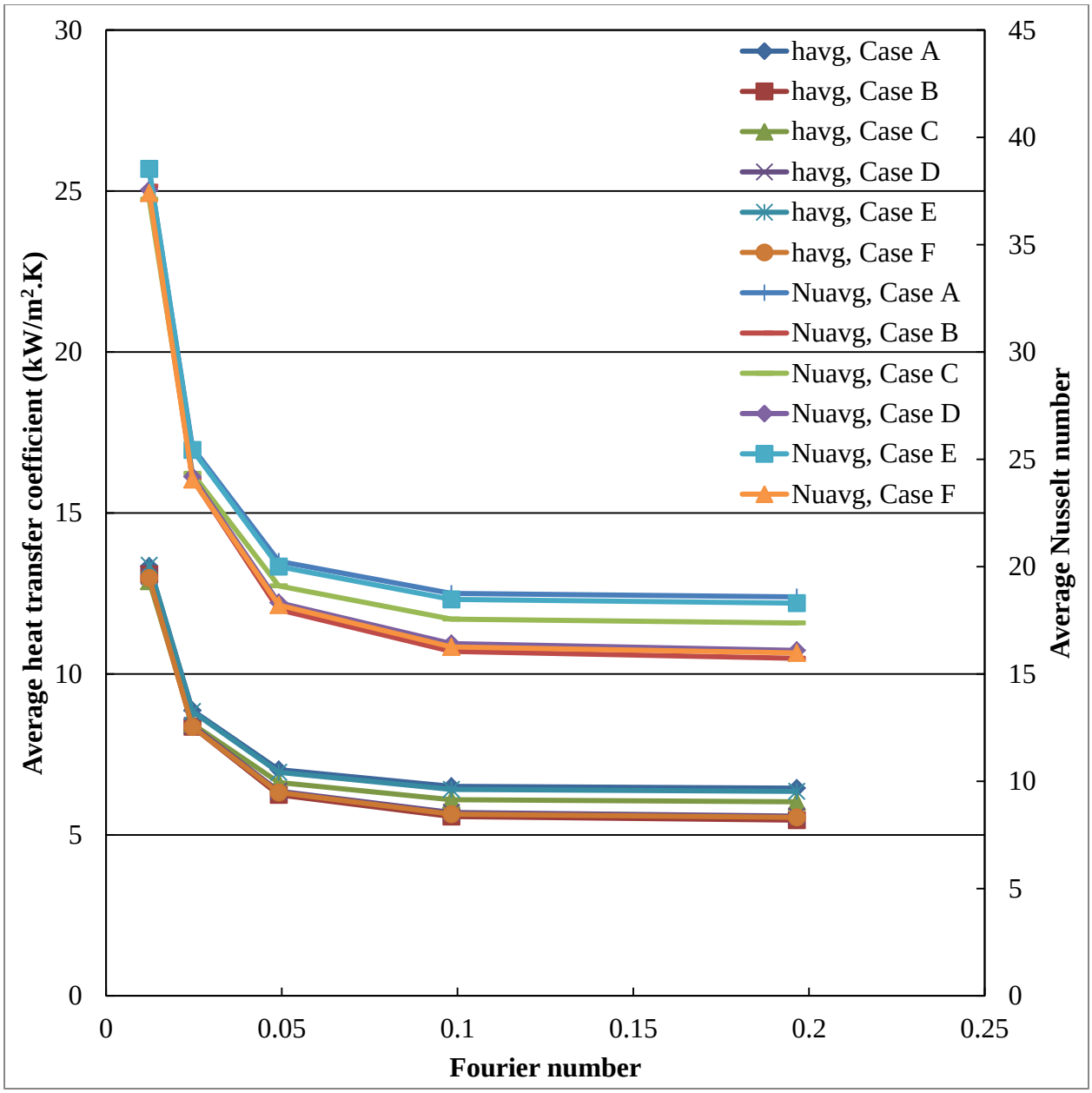

Figure 69: Variations of Average Heat Transfer Coefficient and Average Nusselt Number for Silicon Plate at Re = 500

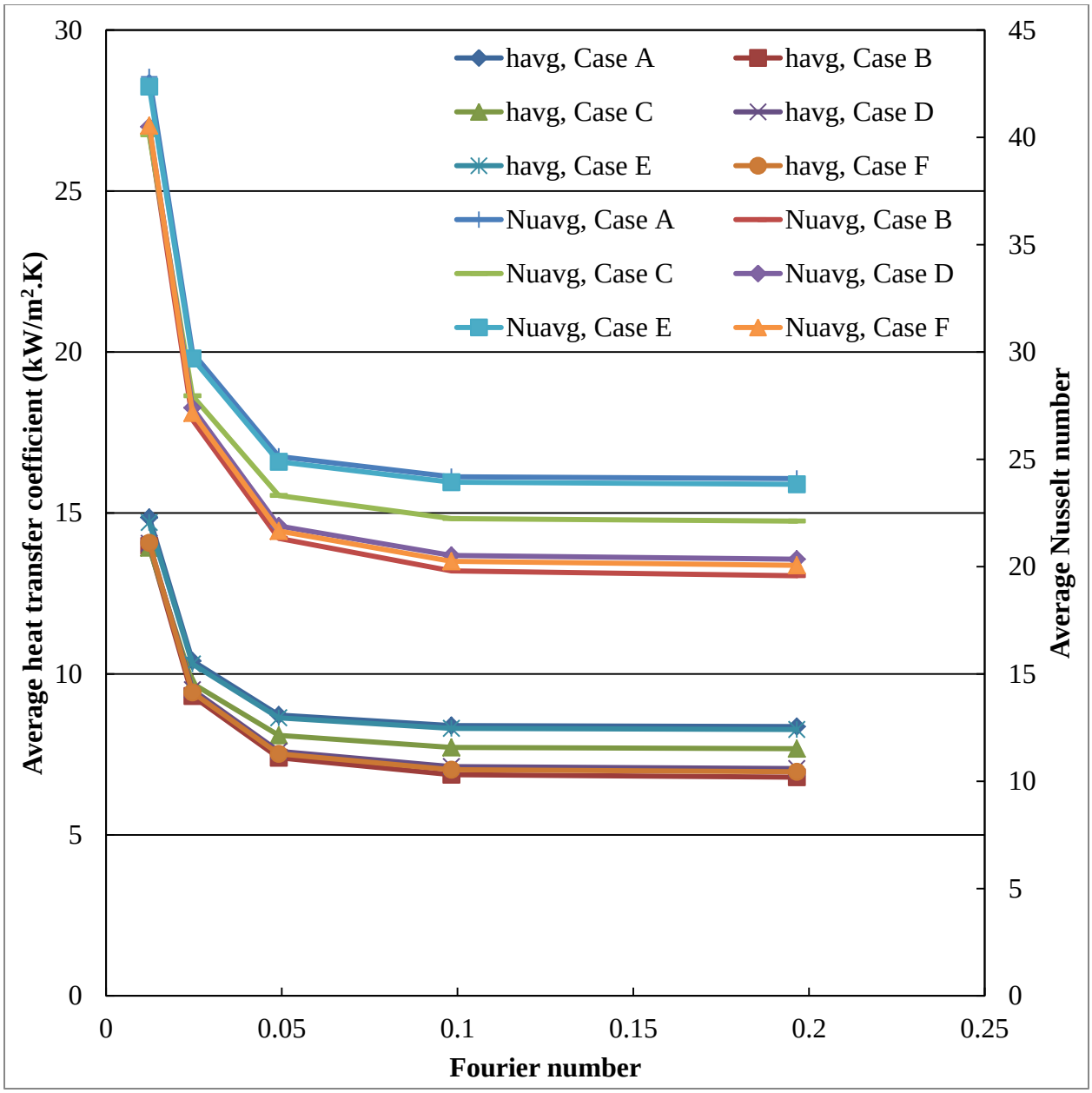

Figure 70: Variations of Average Heat Transfer Coefficient and Average Nusselt Number for Silicon Plate at Re = 1000

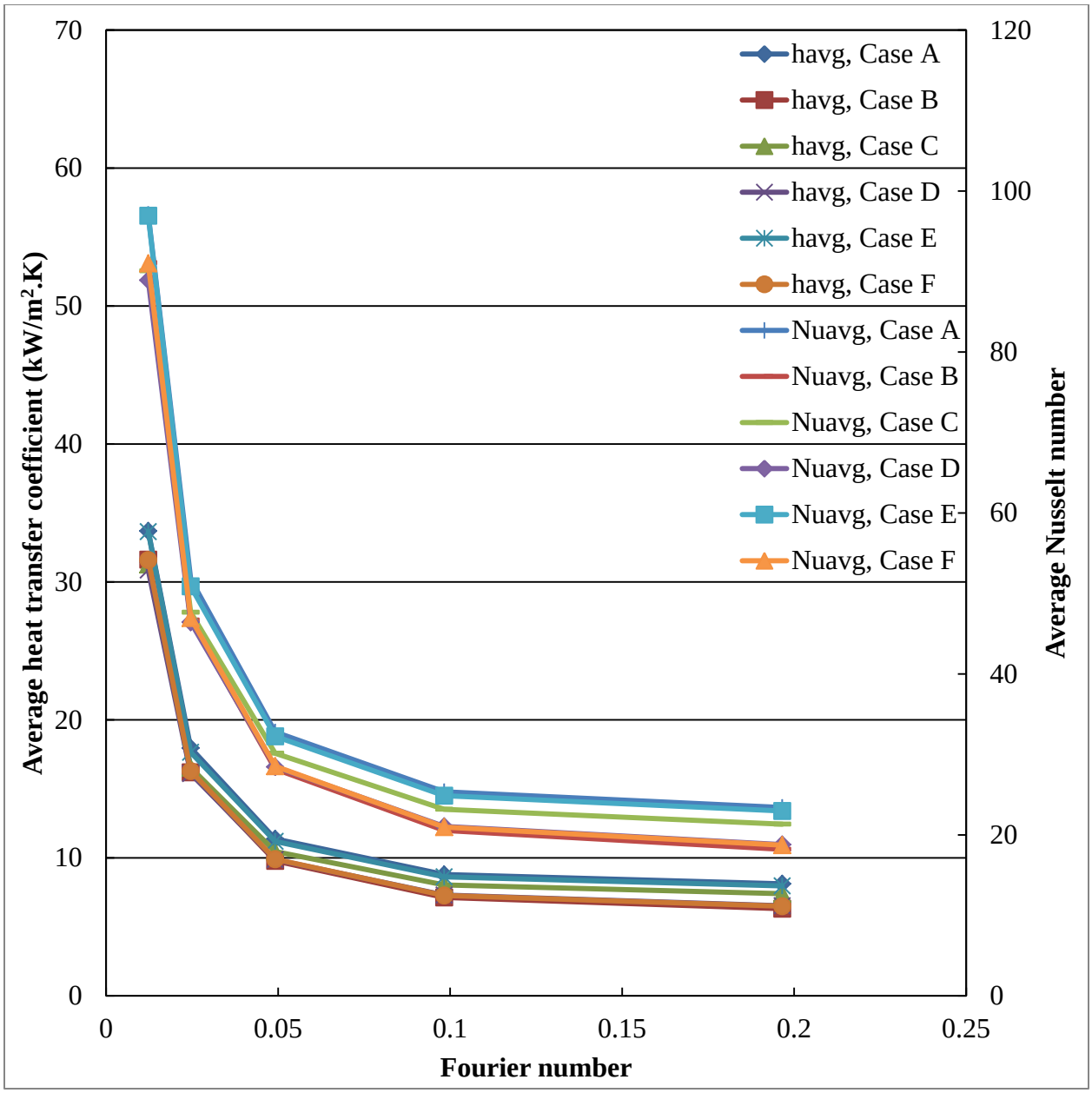

Figure 71: Variations of Average Heat Transfer Coefficient and Average Nusselt Number for Constantan Plate at Re = 750

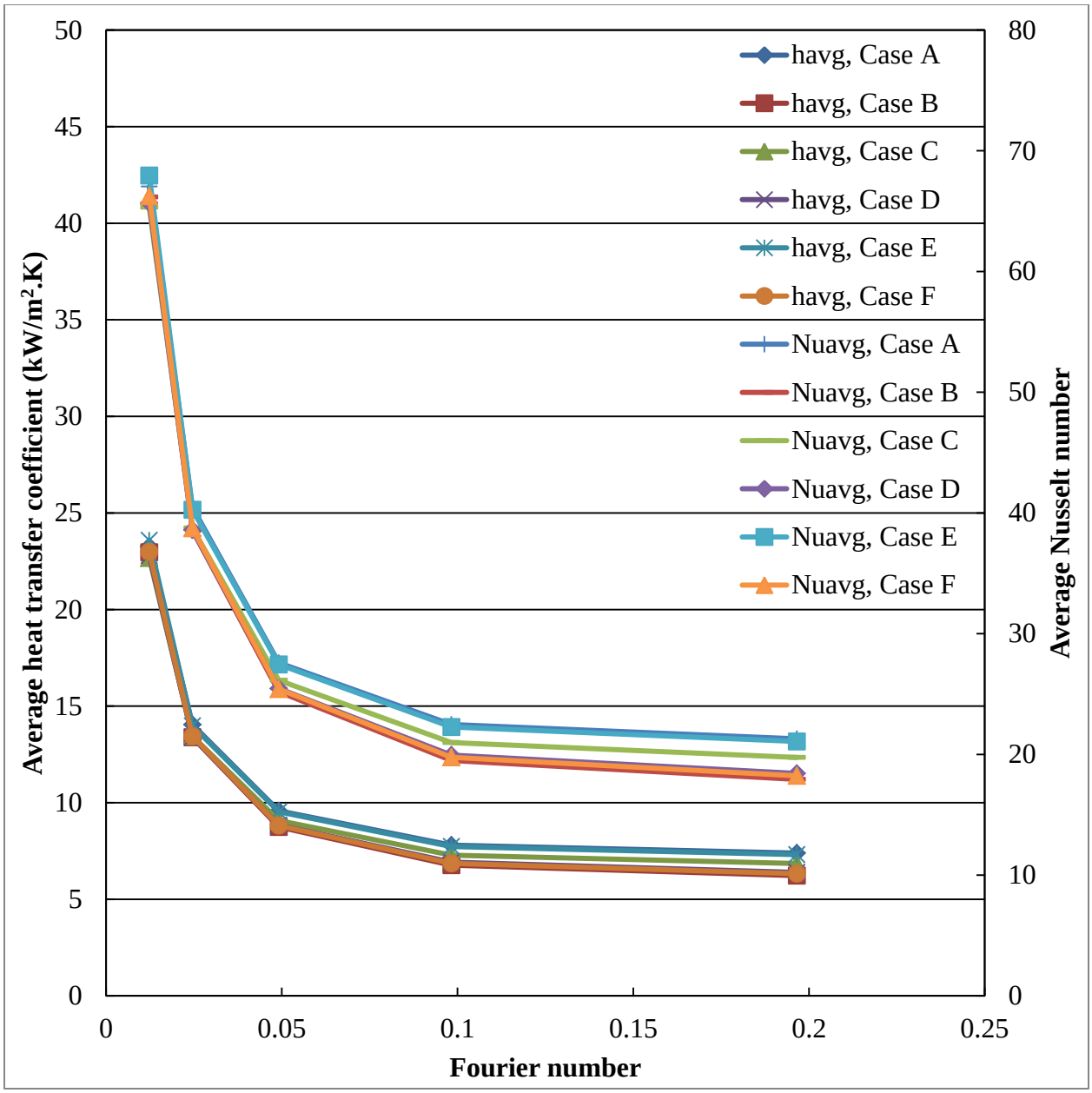

Figure 72: Variations of Average Heat Transfer Coefficient and Average Nusselt Number for Copper Plate at Re = 750

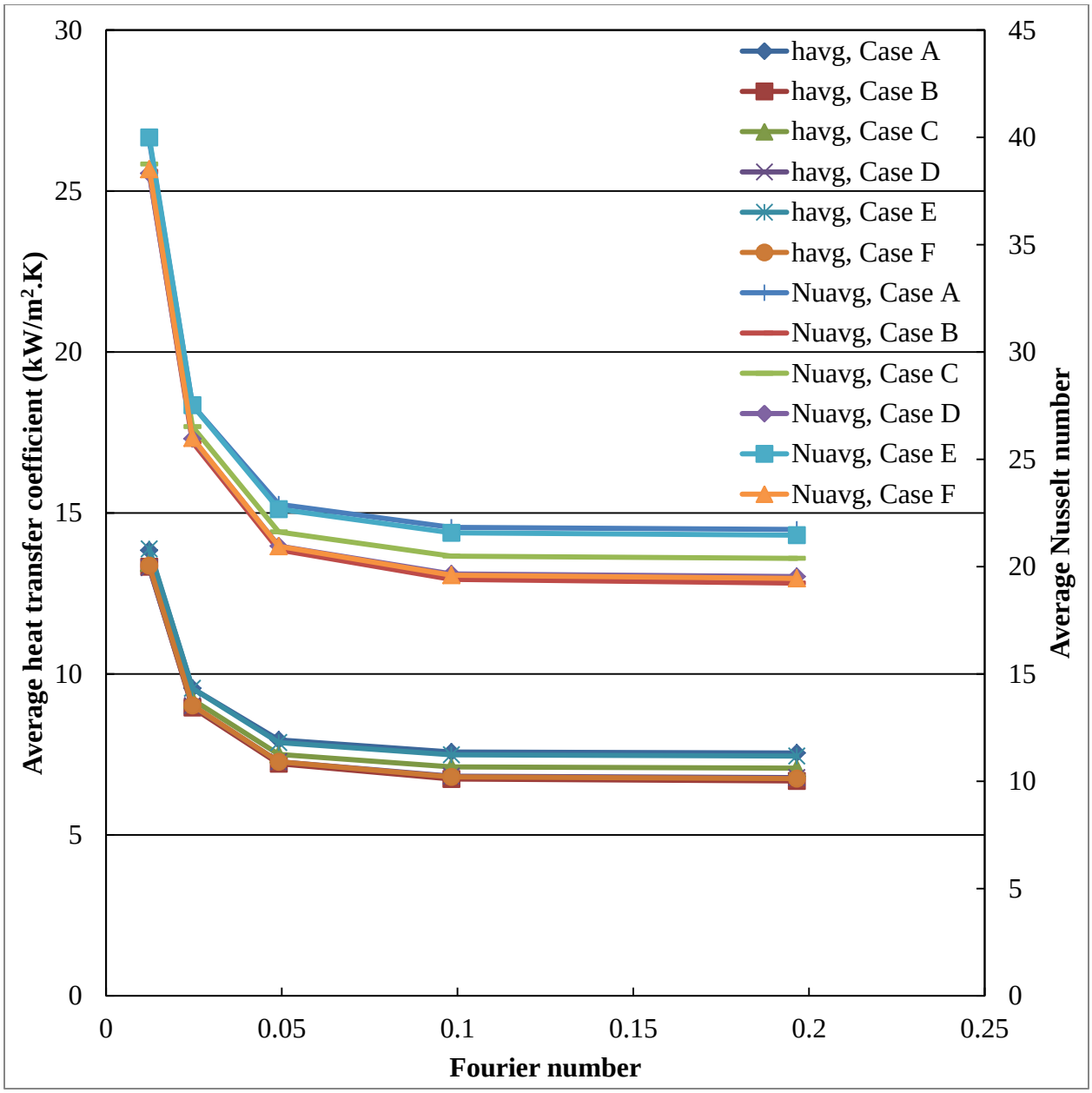

Figure 73: Variations of Average Heat Transfer Coefficient and Average Nusselt Number for Silicon Plate at Re = 750 with a = 0.000125 m

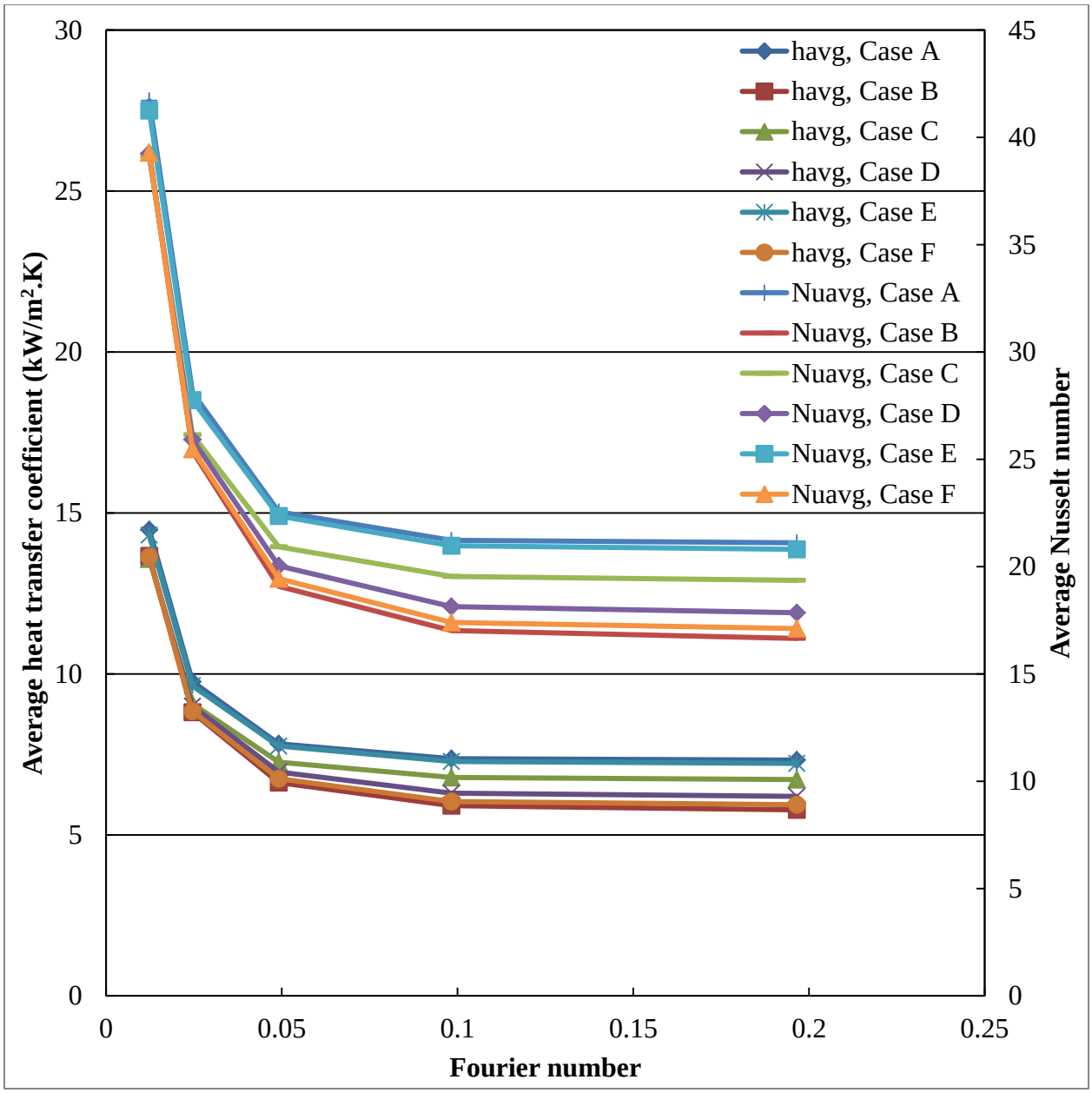

Figure 74: Variations of Average Heat Transfer Coefficient and Average Nusselt Number for Silicon Plate at Re = 750 with a = 0.000375 m

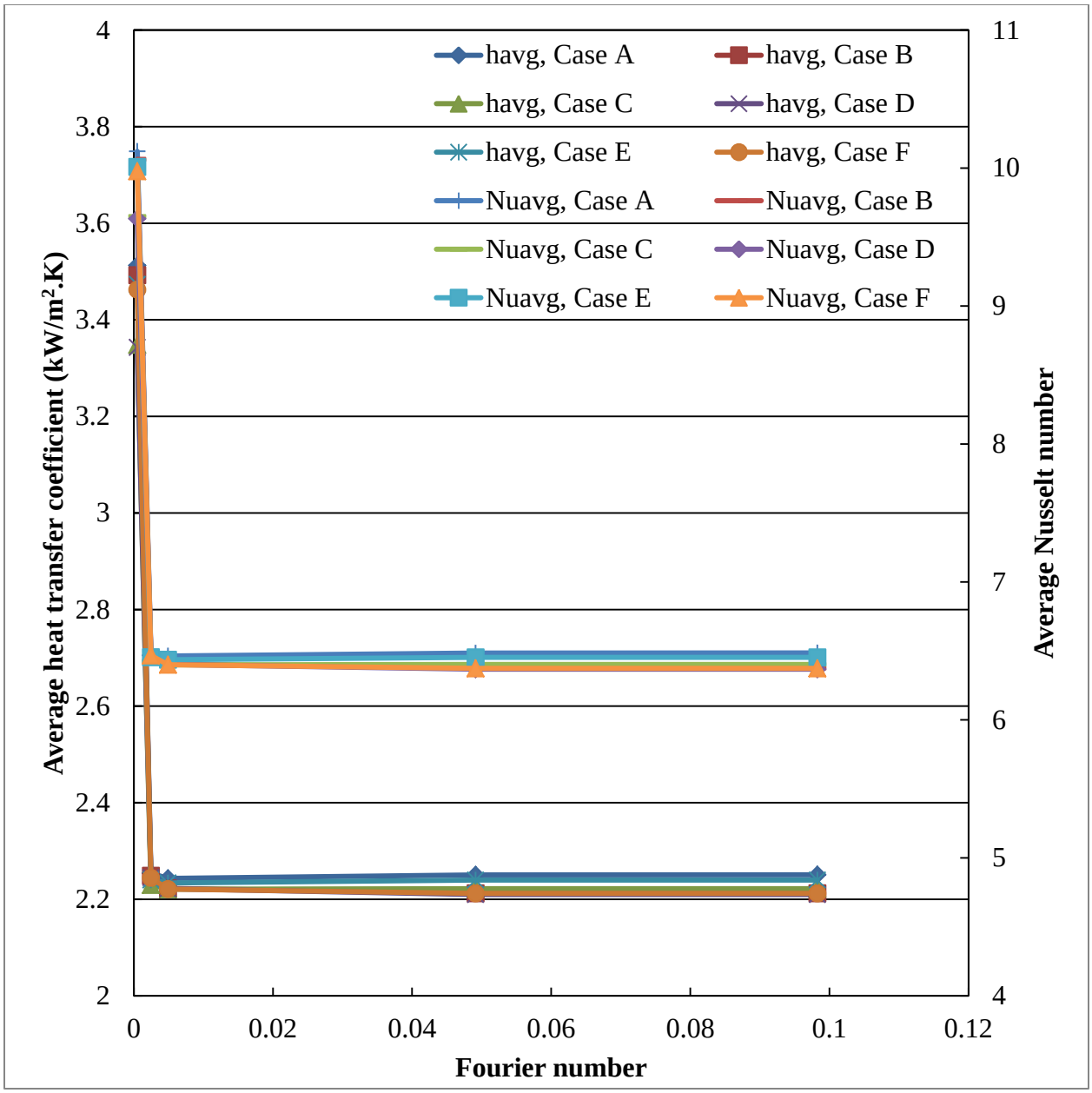

Figure 75: Variations of Average Heat Transfer Coefficient and Average Nusselt Number for Silicon Plate at Re = 750 with Isothermal Boundary Condition

CHAPTER 4: CONCLUSIONS AND FUTURE RECOMMENDATIONS

The effects of surface roughness on free surface jet impingement heat transfer were investigated in this research and few conclusions can be made. Steady state heat transfer results show that impinging the jet nozzle directly onto the steps improves the overall heat transfer compared to impinging the jet nozzle in between steps for all cases. The increase in Reynolds number decreases the overall temperature of the plate; therefore, it enhances the heat transfer. High thermal conductivity materials exhibit more uniform temperature distribution across the length of the plate. The increase in step height decreases the local heat transfer coefficient and local Nusselt number. The variations between all cases become smaller in isothermal boundary condition compared to constant heat flux boundary condition.

Few conclusions can be made based on the study conducted for the transient heat transfer. The local and average heat transfer coefficient and the local and average Nusselt number decrease with time until the steady state condition is reached. Highest rates of heat transfer are located at areas that experience no fluid recirculation. Case A shows the most advantageous geometry for impinging the jet directly onto the step due to the increase in surface area between the fluid and the solid. On the other hand, case D shows the most advantageous geometry for impinging the jet in between the steps due to the enhancement in fluid circulation. The increase in the height of the steps increases the time required to reach steady state condition. Materials with higher thermal diffusivity reach the steady state condition with less time. It

requires less time to reach steady state condition when changing the constant heat flux boundary condition to isothermal boundary condition.

Due to the lack of experimental research conducted for laminar free surface slot jet impinging onto roughened surfaces, it was not possible to compare the numerical results to experimental results found in the literature. The trends of the results are very comparable to the heat transfer behavior found in the literature. Future research recommendations are to experimentally investigate the free surface slot jet impingement for laminar flow using water as the cooling fluid. The plate length and thickness can be investigated as well to see the effects of those parameters. Finally, the jet nozzle height and width can be taken into considerations for the completeness of the work.

LIST OF REFERENCES

[1] S. Inada, Y. Miyasaka, R. Izumi, A study on the laminar-flow heat transfer between a two-dimensional water jet and a flat surface, *JSME* 24(196)(1981) 1803-1810.

[2] C.F. Ma, Y.H. Zhao, T. Masuoka, T. Gomi, Analytical study on impingement heat transfer with single-phase free-surface circular liquid jets, *J. of Thermal Science* 5(4)(1996) 271-277.

[3] C.F. Ma, Q. Zheng, H. Sun, K. Wu, T. Gomi, B.W. Webb, Local characteristics of impingement heat transfer with oblique round free-surface jets of large Prandtl number liquid, *Int. J. Heat Mass Transfer* 40(10)(1997) 2249-2259.

[4] W.M. Chakroun, A.A. Abdel-Rahman, S.F. Al-Fahed, Heat transfer augmentation for air jet impinging on a rough surface, *Applied Thermal Engineering* 18(1998) 1225-1241.

[5] A.J. Bula, M.M. Rahman, J.E. Leland, Axial steady free surface jet impingement over a flat disk with discrete heat sources, *Int. J. Heat and Fluid Flow* 21(2000) 11-21.

[6] A.J. Bula, M.M. Rahman, J.E. Leland, Numerical modeling of conjugate heat transfer during impingement of free liquid jet issuing from slot nozzle, *Numerical Heat Transfer* 38(2000) 45-66.

[7] C. Gau, I.C. Lee, Flow and impingement cooling heat transfer along triangular rib-roughened walls,*Int. J. Heat Mass Transfer* 43(2000) 4405-4418.

[8] S.V. Ekkad, D. Kontrovitz, Jet impingement heat transfer on dimpled target surfaces, *Int. J. Heat and Fluid Flow* 23(2002) 22–28.

[9] D. Sahoo, M.A.R. Sharif, Numerical modeling of slot-jet impingement cooling of a constant heat flux surface confined by a parallel wall, *International Journal of Thermal Sciences* 43(2004) 877–887.

[10] Y.C. Chen, C.F. Ma, M. Qin, Y.X. Li, Theoretical study on impingement heat transfer with single-phase free-surface slot jets, *International Journal of Heat and Mass Transfer* 48(2005) 3381–3386.

[11] X. Li, J.L. Gaddis, T. Wang, Multiple flow patterns and heat transfer in confined jet impingement, *Int. J. Heat and Fluid Flow* 26(2005) 746–754.

[12] Z.Q. Lou, A.S. Mujumdar, C. Yap, Effects of geometric parameters on confined impinging jet heat transfer, *Applied Thermal Engineering* 25(2005) 2687–2697.

[13] V. Katti, S.V. Prabhu, Heat transfer enhancement on a flat surface with axisymmetric detached ribs by normal impingement of circular air jet, *International Journal of Heat and Fluid Flow* 29(2008) 1279–1294.

[14] L.-x. Zhang, G.-x. Hu, Z.-g. Wang, Study on liquid-jet cooling and heating of the moving SMA actuator, *International Journal of Thermal Sciences* 47(2008) 306–314.

[15] Y.E. Akansu, M. Sarioglu, K. Kuvvet, T. Yavuz, Flow field and heat transfer characteristics in an oblique slot jet impinging on a flat plate, *International Communications in Heat and Mass Transfer* 35(2008) 873–880.

[16] K. Ibuki, T. Umeda, H. Fujimoto, H. Takuda, Heat transfer characteristics of a planar water jet impinging normally or obliquely on a flat surface at relatively low Reynolds numbers, *Experimental Thermal and Fluid Science* 33(2009) 1226–1234.

[17] P. Naphon, S. Wongwises, Investigation on the jet liquid impingement heat transfer for the central processing unit of personal computers, *International Communications in Heat and Mass Transfer* 37(2010) 822–826.

[18] K.S. Choo, S.J. Kim, Comparison of thermal characteristics of confined and unconfined impinging jets, *International Journal of Heat and Mass Transfer* 53(2010) 3366–3371.

[19] Y. Xing, S. Spring, B. Weigand, Experimental and numerical investigation of impingement heat transfer on a flat and micro-rib roughened plate with different crossflow schemes, *International Journal of Thermal Sciences* 50(2011) 1293-1307.

[20] D.H. Lee, H.J. Park, P. Ligrani, Milliscale confined impinging slot jets: Laminar heat transfer characteristics for an isothermal flat plate, *International Journal of Heat and Mass Transfer* 55(2012) 2249–2260.

[21] Y.-H. Liu, S.-J. Song, Y.-H. Lo, Jet impingement heat transfer on target surfaces with longitudinal and transverse grooves, *International Journal of Heat and Mass Transfer* 58(2013) 292–299.

[22] L. Tan, J.-Z. Zhang, H.-S. Xu, Jet impingement on a rib-roughened wall inside semi-confined channel, *International Journal of Thermal Sciences* 86(2014) 210-218.

[23] H. Fujimoto, H. Takuda, N. Hatta, R. Viskanta, Numerical simulation of transient cooling of a hot solid by an impinging free surface jet, *Numerical Heat Transfer* 36(1999) 767-780.

[24] M.M. Rahman, A.J. Bula, J.E. Leland, Analysis of transient conjugate heat transfer to a free impinging jet, *Journal of Thermophysics and Heat Transfer* 14(3)(2000) 330-339.

[25] L.-K. Liu, W.-S. Su, Y.-H. Hung, Transient convective heat transfer of air jet impinging onto a confined ceramic-based MCM disk, *Journal of Electronic Packaging* 126(2004) 159-172.

[26] Y.-T. Yang, S.-Y. Tsai, Numerical study of transient conjugate heat transfer of a turbulent impinging jet, *International Journal of Heat and Mass Transfer* 50(2007) 799–807.

[27] M.M. Rahman, J.C. Lallave, Transient conjugate heat transfer during free liquid jet impingement on a rotating solid disk, *Numerical Heat Transfer* 55(2009) 229-251.

[28] N. Karwa, T. Gambaryan-Roisman, P. Stephan, C. Tropea, Experimental investigation of circular free-surface jet impingement quenching: Transient hydrodynamics and heat transfer, *Experimental Thermal and Fluid Science* 35(2011) 1435–1443.

[29] M.M. Rahman, C.F. Hernandez, Transient conjugate heat transfer from a hemispherical plate during free liquid jet impingement on the convex surface, *Heat Mass Transfer* 47(2011) 69–80.

[30] D.H. Lee, J.R. Bae, H.J. Park, J.S. Lee, P. Ligrani,Confined, milliscale unsteady laminar impinging slot jets and surface Nusselt numbers, *International Journal of Heat and Mass Transfer* 54(2011) 2408–2418.

[31] L. Yang, Y. Li, P.M. Ligrani, J. Ren, H. Jiang, Unsteady heat transfer and flow structure of a row of laminar impingement jets, including vortex development, *International Journal of Heat and Mass Transfer* 88(2015) 149–164.

[32] W. Kays, M. Crawford, B. Weigand, Convective Heat and Mass Transfer, Fourth Edition, *McGraw-Hill* (2005).

[33] M. Necati Ozisik, Heat Conduction, Second Edition, *John Wiley & Sons* (1993).

[34] A.J. Bula Silvera, Numerical modeling of conjugate heat transfer during free liquid jet impingement, *Ph.D. Dissertation* (1999).

[35] M.M. Dobbertean, Steady and transient heat transfer for jet impingement on patterned surfaces, *M.S. Thesis* (2011).

[36] FIDAP v8.7.4 (Fluid Dynamics Analysis Package), *Fluent Inc*, Lebanon, NH.

[37] A. Bejan, Convection heat transfer, Fourth Edition, *John Wiley & Sons* (2013).

APPENDIX A: LIST OF SYMBOLS

a	Step height [m]
b	Thickness of the plate [m]
c_p	Specific heat at constant pressure [kJ/kg.K]
F_o	Fourier number
g	Acceleration due to gravity [m/s^2]
h	Heat transfer coefficient [$W/m^2.K$]
H_n	Height of the nozzle from impingement surface [m]
k	Thermal conductivity [W/m.K]
n	Coordinate normal to the free surface [m]
Nu	Nusselt number
p	Pressure [Pa]
q	Heat flux [W/m^2]
Re	Reynolds number
T	Temperature [K]
υ	Velocity [m/s]
$\vec{V}$	Velocity vector [m/s]
W	Nozzle width [m]
x	Horizontal coordinate [m]
y	Vertical coordinate [m]

Greek Symbols

δ	Free surface height [m]
η	Coordinate perpendicular to the solid-fluid interface [m]
μ	Dynamic viscosity [kg/m.s]
ρ	Density [kg/m^3]
ζ	Coordinate along the solid-fluid interface [m]
∇	Gradient operator [1/m]

Subscripts

atm	Atmospheric
avg	Average
f	Fluid
int	Interface
s	Solid
w	Bottom surface of plate

APPENDIX B: FIDAP CODE FOR CASE A

```
Title( )
Case A
FI-GEN(Elem = 1, POIN = 1, CURV = 1, SURF = 1, NODE = 0, MEDG= 1, MLOO = 1,
MFAC = 1, BEDG = 1, SPAV = 1, MSHE = 1, MSOL = 1, COOR = 1)
//Specifications
//Plate Thickness
$PlateT = 0.125
//Plate Length
$PlateL = 0.6475
//Nozzle width
$NozzleW = 0.085
//Nozzle height
$NozzleH = 0.55
//Depth of step
$Step = 0.025
//Creating basic geometry
//Points 1-8
POINT( ADD, COOR )
0 0
-$NozzleH 0
-$NozzleH $NozzleW
-0.18 0.17
-0.15 $PlateL
0 $PlateL
$PlateT $PlateL
$PlateT 0
//Lines 1-9
POINT( SELE, ID)
1
2
CURVE( ADD, LINE)
POINT( SELE, ID )
2
3
CURVE( ADD, LINE )
POINT(SELE, ID)
3
4
```

```
CURVE(ADD,LINE)
POINT(SELE, ID)
4
5
CURVE(ADD,LINE)
POINT(SELE,ID)
5
6
CURVE(ADD,LINE)
POINT(SELE,ID)
6
7
CURVE(ADD,LINE)
POINT(SELE,ID)
7
8
CURVE(ADD,LINE)
POINT(SELE,ID)
8
1
CURVE(ADD,LINE)
CURVE(SELE,ID)
3
4
CURVE(ADD, FILL, RADI=0.2)
//Interface Geometry
//Points 11-16
POINT(ADD, COOR)
-$Step 0
-$Step 0.032375
0 0.032375
0 0.615125
-$Step 0.615125
-$Step $PlateL
POINT(SELE,ID)
1
11
CURVE(ADD,LINE)
POINT(SELE,ID)
11
12
CURVE(ADD,LINE)
POINT(SELE,ID)
12
13
CURVE(ADD,LINE)
```

```
POINT(SELE,ID)
13
1
CURVE(ADD,LINE)
POINT(SELE,ID)
13
14
CURVE(ADD,LINE)
POINT(SELE,ID)
14
15
CURVE(ADD,LINE)
POINT(SELE,ID)
15
16
CURVE(ADD,LINE)
POINT(SELE,ID)
16
6
CURVE(ADD,LINE)
POINT(SELE,ID)
6
14
CURVE(ADD,LINE)
POINT(SELE,ID)
12
15
CURVE(ADD,LINE)
POINT(SELE,ID)
5
16
CURVE(ADD,LINE)
POINT(SELE,ID)
11
2
CURVE(ADD,LINE)
//surface
POINT(ADD,COOR)
-$NozzleH $PlateL
POINT(SELE,ID)
17
7
2
8
SURFACE(ADD,POINTS, ROWW=2, NOAD)
//mesh edges
```

```
CURVE(SELE,ID)
2
MEDGE(ADD, SUCC, INTE=30, RATI=0, 2RAT=0, PCEN=0)
CURVE(SELE,ID)
3
MEDGE(ADD, SUCC, INTE=6, RATI=0, 2RAT=0, PCEN=0)
CURVE(SELE,ID)
9
MEDGE(ADD, SUCC, INTE=34, RATI=0, 2RAT=0, PCEN=0)
CURVE(SELE,ID)
4
MEDGE(ADD, SUCC, INTE=70, RATI=0, 2RAT=0, PCEN=0)
CURVE(SELE,ID)
21
MEDGE(ADD, FRSTLAST, INTE=30, RATI=0.6, 2RAT=0, PCEN=0)
CURVE(SELE,ID)
20
MEDGE(ADD, LSTFIRST, INTE=30, RATI=0.4, 2RAT=0, PCEN=0)
CURVE(SELE, ID)
10
11
12
13
15
16
17
18
MEDGE(ADD, SUCC, INTE=10, RATI=0, 2RAT=0, PCEN=0)
CURVE(SELE,ID)
19
MEDGE(ADD, SUCC, INTE=120, RATI=0, 2RAT=0, PCEN=0)
CURVE(SELE,ID)
14
MEDGE(ADD, SUCC, INTE=120, RATI=0, 2RAT=0, PCEN=0)
CURVE(SELE,ID)
8
6
MEDGE(ADD, SUCC, INTE=25, RATI=0, 2RAT=0, PCEN=0)
CURVE(SELE,ID)
7
MEDGE(ADD, SUCC, INTE=140, RATI=0, 2RAT=0, PCEN=0)
//mesh loops
CURVE(SELE,ID)
21
2
3
```

```
9
4
20
16
19
11
MLOOP(ADD, MAP, VISI, NOSH, EDG1=1, EDG2=4, EDG3=1, EDG4=3)
CURVE(SELE,ID)
10
11
12
13
MLOOP(ADD, MAP, VISI, NOSH, EDG1=1, EDG2=1, EDG3=1, EDG4=1)
CURVE(SELE,ID)
12
14
15
19
MLOOP(ADD, MAP, VISI, NOSH, EDG1=1, EDG2=1, EDG3=1, EDG4=1)
CURVE(SELE,ID)
15
16
17
18
MLOOP(ADD, MAP, VISI, NOSH, EDG1=1, EDG2=1, EDG3=1, EDG4=1)
CURVE(SELE,ID)
8
13
14
18
6
7
MLOOP(ADD, MAP, VISI, NOSH, EDG1=1, EDG2=3, EDG3=1, EDG4=1)
//mesh faces
SURFACE(SELE,ID=1)
MLOOP(SELE,ID=1)
MFACE(ADD)
SURFACE(SELE,ID=1)
MLOOP(SELE,ID=2)
MFACE(ADD)
SURFACE(SELE,ID=1)
MLOOP(SELE,ID=3)
MFACE(ADD)
SURFACE(SELE,ID=1)
MLOOP(SELE,ID=4)
MFACE(ADD)
```

```
SURFACE(SELE,ID=1)
MLOOP(SELE,ID=5)
MFACE(ADD)
//meshing
MFACE(SELE,ID)
1
3
ELEMENT(SETD, QUAD, NODE=4)
MFACE(MESH, MAP, ENTI="fluid")
MFACE(SELE,ID)
2
4
5
ELEMENT(SETD,QUAD,NODE=4)
MFACE(MESH,MAP,ENTI="solid")
ELEMENT(SETD, EDGE, NODE=2)
MEDGE(SELE,ID)
1
MEDGE(MESH,MAP,ENTI="inlet")
MEDGE(SELE,ID)
6
MEDGE(MESH,MAP,ENTI="outlet")
MEDGE(SELE,ID)
5
MEDGE(MESH,MAP,ENTI="axis")
MEDGE(SELE,ID)
2
3
4
MEDGE(MESH,MAP,ENTI="freesurf")
MEDGE(SELE,ID)
8
9
16
11
12
MEDGE(MESH,MAP,ENTI="interface")
MEDGE(SELE,ID)
13
18
MEDGE(MESH,MAP,ENTI="edge")
MEDGE(SELE,ID)
19
MEDGE(MESH,MAP,ENTI="bottom")
MEDGE(SELE,ID)
7
```

```
17
MEDGE(MESH,MAP,ENTI="axiss")
END( )
FIPREP( )
//PROPERTIES
DENSITY( ADD, SET = "water", CONS = 0.9982 )
CONDUCTIVITY( ADD, SET = "water", CONS = 0.001409 )
VISCOSITY( ADD, SET = "water", CONS = 0.01002)
SPECIFICHEAT( ADD, SET = "water", CONS = 0.99952 )
SURFACETENSION( ADD, SET = "water", CONS = 72.8 )
DENSITY( ADD, SET = "silicon", CONS = 2.33 )
CONDUCTIVITY( ADD, SET = "silicon", CONS = 0.365434 )
SPECIFICHEAT( ADD, SET = "silicon", CONS = 0.168021 )
//ENTITIES
ENTITY(ADD, NAME="fluid", FLUI, PROP="water")
ENTITY( ADD, NAME = "solid", SOLI, PROP = "silicon" )
ENTITY(ADD, NAME="outlet", PLOT)
ENTITY(ADD, NAME="inlet", PLOT)
ENTITY(ADD, NAME="axis", PLOT)
ENTITY(ADD, NAME="freesurf", SURF, DEPT = 31, SPIN, STRA, ANG1=10, ANG2=180)
ENTITY(ADD, NAME="axiss", PLOT)
ENTITY(ADD, NAME="edge", PLOT)
ENTITY(ADD, NAME="bottom", PLOT)
ENTITY( ADD, NAME = "interface", PLOT, ATTA = "solid", NATT = "fluid" )
BODYFORCE(ADD, CONS, FX=981, FY=0, FZ=0)
PRESSURE(ADD, MIXE=1.0E-11, DISC)
OPTIONS(ADD, UPWINDING)
UPWINDING(ADD, STRE)
RELAXATION(  )
  0.3, 0.3, 0.3, 0, 0.5, 0.25
//BC
BCNODE(ADD, COOR, NODE=2)
BCNODE(ADD, SURF, NODE=2, ZERO)
BCNODE(ADD, VELO, NODE=2, ZERO)
BCNODE(ADD, UT, NODE=2, ZERO)
BCNODE(ADD, UX, ENTI="inlet", CONS=44.29)
BCNODE(ADD, UY, ENTI="inlet", ZERO)
BCNODE(ADD, UY, ENTI="axis", ZERO)
BCNODE(ADD, VELO, ENTI="interface", ZERO)
BCNODE(ADD, VELO, ENTI="bottom", ZERO)
BCNODE(ADD, VELO, ENTI="edge", ZERO)
BCNODE(ADD, VELO, ENTI="axiss", ZERO)
BCNODE( ADD, VELO, ENTI = "solid", ZERO )
BCNODE( ADD, TEMP, ENTI = "inlet", CONS = 20 )
BCFLUX( ADD, HEAT, ENTI = "bottom", CONS = 1.5 )
```

```
PROBLEM( ADD, 2-d, INCOMP, TRAN, LAMI, NONL, NEWT, MOME, ENERGY, FREE,
SING )
SOLUTION( ADD, N.R. = 50, KINE = 25, VELC = 1e-4, RESC = 1e-4, SURF = 1e-3 )
TIMEINTEGRATION( ADD, BACK, NSTE = 501, TSTA = 0, DT = 0.0001, VARI, WIND =
9, NOFI = 12 )
POSTPROCESS( NBLO = 2 )
   1,   101,     1
 101,   501,     2
CLIPPING( ADD, MINI )
   0,     0,     0,     0,    20,     0
ICNODE( ADD, UX, ENTI = "fluid", CONS = 44.29 )
ICNODE( ADD, TEMP, ENTI = "fluid", CONS = 20 )
ICNODE( ADD, TEMP, ENTI = "solid", CONS = 20 )
EXECUTION(ADD, NEWJ)
PRINTOUT(ADD, NONE, BOUN)
DATAPRINT(ADD, CONT)
END( )
CREATE(FISO)
RUN(FISOLV, BACK, AT="", TIME="NOW", COMP)
```

APPENDIX C: FIDAP CODE FOR CASE B

```
Title( )
Case B
FI-GEN(Elem = 1, POIN = 1, CURV = 1, SURF = 1, NODE = 0, MEDG= 1, MLOO = 1,
MFAC = 1, BEDG = 1, SPAV = 1, MSHE = 1, MSOL = 1, COOR = 1)
//Specifications
//Plate Thickness
$PlateT = 0.125
//Plate Length
$PlateL = 0.6475
//Nozzle width
$NozzleW = 0.085
//Nozzle height
$NozzleH = 0.55
//Depth of step
$Step = 0.025
//Creating basic geometry
//Points 1-8
POINT( ADD, COOR )
0 0
-$NozzleH 0
-$NozzleH $NozzleW
-0.18 0.17
-0.15 $PlateL
0 $PlateL
$PlateT $PlateL
$PlateT 0
//Lines 1-9
POINT( SELE, ID)
1
2
CURVE( ADD, LINE)
POINT( SELE, ID )
2
3
CURVE( ADD, LINE )
POINT(SELE, ID)
3
4
```

```
CURVE(ADD,LINE)
POINT(SELE, ID)
4
5
CURVE(ADD,LINE)
POINT(SELE,ID)
5
6
CURVE(ADD,LINE)
POINT(SELE,ID)
6
7
CURVE(ADD,LINE)
POINT(SELE,ID)
7
8
CURVE(ADD,LINE)
POINT(SELE,ID)
8
1
CURVE(ADD,LINE)
CURVE(SELE,ID)
3
4
CURVE(ADD, FILL, RADI=0.2)
//Interface Geometry
//Points 11-16
POINT(ADD, COOR)
-$Step 0
-$Step 0.291375
-$Step 0.356125
0 0.356125
0 0.291375
-$Step $PlateL
POINT(SELE,ID)
1
11
CURVE(ADD,LINE)
POINT(SELE,ID)
11
12
CURVE(ADD,LINE)
POINT(SELE,ID)
12
15
CURVE(ADD,LINE)
```

```
POINT(SELE,ID)
15
1
CURVE(ADD,LINE)
POINT(SELE,ID)
12
13
CURVE(ADD,LINE)
POINT(SELE,ID)
13
14
CURVE(ADD,LINE)
POINT(SELE,ID)
14
15
CURVE(ADD,LINE)
POINT(SELE,ID)
13
16
CURVE(ADD,LINE)
POINT(SELE,ID)
16
6
CURVE(ADD,LINE)
POINT(SELE,ID)
6
14
CURVE(ADD,LINE)
POINT(SELE,ID)
5
16
CURVE(ADD,LINE)
POINT(SELE,ID)
11
2
CURVE(ADD,LINE)
//surface
POINT(ADD,COOR)
-$NozzleH $PlateL
POINT(SELE,ID)
17
7
2
8
SURFACE(ADD,POINTS, ROWW=2, NOAD)
//mesh edges
```

```
CURVE(SELE,ID)
2
MEDGE(ADD, SUCC, INTE=30, RATI=0, 2RAT=0, PCEN=0)
CURVE(SELE,ID)
3
MEDGE(ADD, SUCC, INTE=6, RATI=0, 2RAT=0, PCEN=0)
CURVE(SELE,ID)
9
MEDGE(ADD, SUCC, INTE=34, RATI=0, 2RAT=0, PCEN=0)
CURVE(SELE,ID)
4
MEDGE(ADD, SUCC, INTE=70, RATI=0, 2RAT=0, PCEN=0)
CURVE(SELE,ID)
21
MEDGE(ADD, FRSTLAST, INTE=30, RATI=0.6, 2RAT=0, PCEN=0)
CURVE(SELE,ID)
20
MEDGE(ADD, LSTFIRST, INTE=30, RATI=0.4, 2RAT=0, PCEN=0)
CURVE(SELE, ID)
10
12
15
18
MEDGE(ADD, SUCC, INTE=10, RATI=0, 2RAT=0, PCEN=0)
CURVE(SELE,ID)
11
13
17
19
MEDGE(ADD, SUCC, INTE=60, RATI=0, 2RAT=0, PCEN=0)
CURVE(SELE,ID)
14
16
MEDGE(ADD, SUCC, INTE=20, RATI=0, 2RAT=0, PCEN=0)
CURVE(SELE,ID)
8
6
MEDGE(ADD, SUCC, INTE=25, RATI=0, 2RAT=0, PCEN=0)
CURVE(SELE,ID)
7
MEDGE(ADD, SUCC, INTE=140, RATI=0, 2RAT=0, PCEN=0)
//mesh loops
CURVE(SELE,ID)
21
2
3
```

```
9
4
20
17
14
11
MLOOP(ADD, MAP, VISI, NOSH, EDG1=1, EDG2=4, EDG3=1, EDG4=3)
CURVE(SELE,ID)
10
11
12
13
MLOOP(ADD, MAP, VISI, NOSH, EDG1=1, EDG2=1, EDG3=1, EDG4=1)
CURVE(SELE,ID)
12
14
15
16
MLOOP(ADD, MAP, VISI, NOSH, EDG1=1, EDG2=1, EDG3=1, EDG4=1)
CURVE(SELE,ID)
15
17
18
19
MLOOP(ADD, MAP, VISI, NOSH, EDG1=1, EDG2=1, EDG3=1, EDG4=1)
CURVE(SELE,ID)
8
13
16
19
6
7
MLOOP(ADD, MAP, VISI, NOSH, EDG1=1, EDG2=3, EDG3=1, EDG4=1)
//mesh faces
SURFACE(SELE,ID=1)
MLOOP(SELE,ID=1)
MFACE(ADD)
SURFACE(SELE,ID=1)
MLOOP(SELE,ID=2)
MFACE(ADD)
SURFACE(SELE,ID=1)
MLOOP(SELE,ID=3)
MFACE(ADD)
SURFACE(SELE,ID=1)
MLOOP(SELE,ID=4)
MFACE(ADD)
```

```
SURFACE(SELE,ID=1)
MLOOP(SELE,ID=5)
MFACE(ADD)
//meshing
MFACE(SELE,ID)
1
2
4
ELEMENT(SETD, QUAD, NODE=4)
MFACE(MESH, MAP, ENTI="fluid")
MFACE(SELE,ID)
3
5
ELEMENT(SETD,QUAD,NODE=4)
MFACE(MESH,MAP,ENTI="solid")
ELEMENT(SETD, EDGE, NODE=2)
MEDGE(SELE,ID)
1
MEDGE(MESH,MAP,ENTI="inlet")
MEDGE(SELE,ID)
6
10
MEDGE(MESH,MAP,ENTI="outlet")
MEDGE(SELE,ID)
5
7
MEDGE(MESH,MAP,ENTI="axis")
MEDGE(SELE,ID)
2
3
4
MEDGE(MESH,MAP,ENTI="freesurf")
MEDGE(SELE,ID)
12
8
15
9
14
MEDGE(MESH,MAP,ENTI="interface")
MEDGE(SELE,ID)
18
MEDGE(MESH,MAP,ENTI="edge")
MEDGE(SELE,ID)
19
MEDGE(MESH,MAP,ENTI="bottom")
MEDGE(SELE,ID)
```

```
17
MEDGE(MESH,MAP,ENTI="axiss")
END( )
FIPREP( )
//PROPERTIES
DENSITY( ADD, SET = "water", CONS = 0.9982 )
CONDUCTIVITY( ADD, SET = "water", CONS = 0.001409 )
VISCOSITY( ADD, SET = "water", CONS = 0.01002)
SPECIFICHEAT( ADD, SET = "water", CONS = 0.99952 )
SURFACETENSION( ADD, SET = "water", CONS = 72.8 )
DENSITY( ADD, SET = "silicon", CONS = 2.33 )
CONDUCTIVITY( ADD, SET = "silicon", CONS = 0.365434 )
SPECIFICHEAT( ADD, SET = "silicon", CONS = 0.168021 )
//ENTITIES
ENTITY(ADD, NAME="fluid", FLUI, PROP="water")
ENTITY( ADD, NAME = "solid", SOLI, PROP = "silicon" )
ENTITY(ADD, NAME="outlet", PLOT)
ENTITY(ADD, NAME="inlet", PLOT)
ENTITY(ADD, NAME="axis", PLOT)
ENTITY(ADD, NAME="freesurf", SURF, DEPT = 31, SPIN, STRA, ANG1=10, ANG2=180)
ENTITY(ADD, NAME="axiss", PLOT)
ENTITY(ADD, NAME="edge", PLOT)
ENTITY(ADD, NAME="bottom", PLOT)
ENTITY( ADD, NAME = "interface", PLOT, ATTA = "solid", NATT = "fluid" )
BODYFORCE(ADD, CONS, FX=981, FY=0, FZ=0)
PRESSURE(ADD, MIXE=1.0E-11, DISC)
OPTIONS(ADD, UPWINDING)
UPWINDING(ADD, STRE)
RELAXATION(  )
  0.3, 0.3, 0.3, 0, 0.5, 0.25
//BC
BCNODE(ADD, COOR, NODE=2)
BCNODE(ADD, SURF, NODE=2, ZERO)
BCNODE(ADD, VELO, NODE=2, ZERO)
BCNODE(ADD, UT, NODE=2, ZERO)
BCNODE(ADD, UX, ENTI="inlet", CONS=44.29)
BCNODE(ADD, UY, ENTI="inlet", ZERO)
BCNODE(ADD, UY, ENTI="axis", ZERO)
BCNODE(ADD, VELO, ENTI="interface", ZERO)
BCNODE(ADD, VELO, ENTI="bottom", ZERO)
BCNODE(ADD, VELO, ENTI="edge", ZERO)
BCNODE(ADD, VELO, ENTI="axiss", ZERO)
BCNODE( ADD, VELO, ENTI = "solid", ZERO )
BCNODE( ADD, TEMP, ENTI = "inlet", CONS = 20 )
BCFLUX( ADD, HEAT, ENTI = "bottom", CONS = 1.5 )
```

```
PROBLEM( ADD, 2-d, INCOMP, TRAN, LAMI, NONL, NEWT, MOME, ENERGY, FREE,
SING )
SOLUTION( ADD, N.R. = 50, KINE = 25, VELC = 1e-4, RESC = 1e-4, SURF = 1e-3 )
TIMEINTEGRATION( ADD, BACK, NSTE = 501, TSTA = 0, DT = 0.0001, VARI, WIND =
9, NOFI = 12 )
POSTPROCESS( NBLO = 2 )
   1,   101,     1
 101,   501,     2
CLIPPING( ADD, MINI )
   0,     0,     0,     0,    20,     0
ICNODE( ADD, UX, ENTI = "fluid", CONS = 44.29 )
ICNODE( ADD, TEMP, ENTI = "fluid", CONS = 20 )
ICNODE( ADD, TEMP, ENTI = "solid", CONS = 20 )
EXECUTION(ADD, NEWJ)
PRINTOUT(ADD, NONE, BOUN)
DATAPRINT(ADD, CONT)
END( )
CREATE(FISO)
RUN(FISOLV, BACK, AT="", TIME="NOW", COMP)
```

APPENDIX D: FIDAP CODE FOR CASE C

```
Title( )
Case C
FI-GEN(Elem = 1, POIN = 1, CURV = 1, SURF = 1, NODE = 0, MEDG= 1, MLOO = 1,
MFAC = 1, BEDG = 1, SPAV = 1, MSHE = 1, MSOL = 1, COOR = 1)
//Specifications
//Plate Thickness
$PlateT = 0.125
//Plate Length
$PlateL = 0.6475
//Nozzle width
$NozzleW = 0.085
//Nozzle height
$NozzleH = 0.55
//Depth of step
$Step = 0.025
//Creating basic geometry
//Points 1-8
POINT( ADD, COOR )
0 0
-$NozzleH 0
-$NozzleH $NozzleW
-0.18 0.17
-0.15 $PlateL
0 $PlateL
$PlateT $PlateL
$PlateT 0
//Lines 1-9
POINT(SELE, ID)
1
2
CURVE(ADD,LINE)
POINT(SELE,ID)
2
3
CURVE(ADD,LINE)
POINT(SELE,ID)
3
4
```

```
CURVE(ADD,LINE)
POINT(SELE,ID)
4
5
CURVE(ADD,LINE)
POINT(SELE,ID)
5
6
CURVE(ADD,LINE)
POINT(SELE,ID)
6
7
CURVE(ADD,LINE)
POINT(SELE,ID)
7
8
CURVE(ADD,LINE)
POINT(SELE,ID)
8
1
CURVE(ADD,LINE)
CURVE(SELE,ID)
3
4
CURVE(ADD,FILL,RADI=0.2)
//Interface Geometry
//Points 11-18
POINT(ADD, COOR)
-$Step 0
0 0.032375
$Step 0.032375
$Step 0
0 0.615125
-$Step $PlateL
$Step $PlateL
$Step 0.615125
POINT(SELE,ID)
14
11
CURVE(ADD,LINE)
POINT(SELE,ID)
11
12
CURVE(ADD,LINE)
POINT(SELE,ID)
12
```

13
CURVE(ADD,LINE)
POINT(SELE,ID)
13
14
CURVE(ADD,LINE)
POINT(SELE,ID)
12
15
CURVE(ADD,LINE)
POINT(SELE,ID)
15
16
CURVE(ADD,LINE)
POINT(SELE,ID)
16
17
CURVE(ADD,LINE)
POINT(SELE,ID)
17
18
CURVE(ADD,LINE)
POINT(SELE,ID)
18
15
CURVE(ADD,LINE)
POINT(SELE,ID)
11
16
CURVE(ADD,LINE)
POINT(SELE,ID)
13
18
CURVE(ADD,LINE)
POINT(SELE,ID)
5
16
CURVE(ADD,LINE)
POINT(SELE,ID)
11
2
CURVE(ADD,LINE)
POINT(SELE,ID)
17
7
CURVE(ADD,LINE)

```
POINT(SELE,ID)
14
8
CURVE(ADD,LINE)
//surface
POINT(ADD,COOR)
-$NozzleH $PlateL
POINT(SELE,ID)
19
7
2
8
SURFACE(ADD,POINTS, ROWW=2, NOAD)
//mesh edges
CURVE(SELE,ID)
2
MEDGE(ADD, SUCC, INTE=25, RATI=0, 2RAT=0, PCEN=0)
CURVE(SELE,ID)
3
MEDGE(ADD, SUCC, INTE=5, RATI=0, 2RAT=0, PCEN=0)
CURVE(SELE,ID)
9
MEDGE(ADD, SUCC, INTE=30, RATI=0, 2RAT=0, PCEN=0)
CURVE(SELE,ID)
4
MEDGE(ADD, SUCC, INTE=60, RATI=0, 2RAT=0, PCEN=0)
CURVE(SELE,ID)
22
MEDGE(ADD, FRSTLAST, INTE=30, RATI=0.6, 2RAT=0, PCEN=0)
CURVE(SELE,ID)
21
MEDGE(ADD, LSTFIRST, INTE=30, RATI=0.4, 2RAT=0, PCEN=0)
CURVE(SELE, ID)
10
11
12
13
15
16
17
18
MEDGE(ADD, SUCC, INTE=10, RATI=0, 2RAT=0, PCEN=0)
CURVE(SELE,ID)
19
MEDGE(ADD, SUCC, INTE=120, RATI=0, 2RAT=0, PCEN=0)
CURVE(SELE,ID)
```

```
14
20
MEDGE(ADD, SUCC, INTE=120, RATI=0, 2RAT=0, PCEN=0)
CURVE(SELE,ID)
24
23
MEDGE(ADD, SUCC, INTE=20, RATI=0, 2RAT=0, PCEN=0)
CURVE(SELE,ID)
7
MEDGE(ADD, SUCC, INTE=140, RATI=0, 2RAT=0, PCEN=0)
//mesh loops
CURVE(SELE,ID)
22
2
3
9
4
21
19
MLOOP(ADD, MAP, VISI, NOSH, EDG1=1, EDG2=4, EDG3=1, EDG4=1)
CURVE(SELE,ID)
10
11
12
13
MLOOP(ADD, MAP, VISI, NOSH, EDG1=1, EDG2=1, EDG3=1, EDG4=1)
CURVE(SELE,ID)
11
14
15
19
MLOOP(ADD, MAP, VISI, NOSH, EDG1=1, EDG2=1, EDG3=1, EDG4=1)
CURVE(SELE,ID)
15
16
17
18
MLOOP(ADD, MAP, VISI, NOSH, EDG1=1, EDG2=1, EDG3=1, EDG4=1)
CURVE(SELE,ID)
12
20
18
14
MLOOP(ADD, MAP, VISI, NOSH, EDG1=1, EDG2=1, EDG3=1, EDG4=1)
CURVE(SELE,ID)
24
```

```
13
20
17
23
7
MLOOP(ADD, MAP, VISI, NOSH, EDG1=1, EDG2=3, EDG3=1, EDG4=1)
//mesh faces
SURFACE(SELE,ID=1)
MLOOP(SELE,ID=1)
MFACE(ADD)
SURFACE(SELE,ID=1)
MLOOP(SELE,ID=2)
MFACE(ADD)
SURFACE(SELE,ID=1)
MLOOP(SELE,ID=3)
MFACE(ADD)
SURFACE(SELE,ID=1)
MLOOP(SELE,ID=4)
MFACE(ADD)
SURFACE(SELE,ID=1)
MLOOP(SELE,ID=5)
MFACE(ADD)
SURFACE(SELE,ID=1)
MLOOP(SELE,ID=6)
MFACE(ADD)
//meshing
MFACE(SELE,ID)
1
3
ELEMENT(SETD, QUAD, NODE=4)
MFACE(MESH, MAP, ENTI="fluid")
MFACE(SELE,ID)
2
4
5
6
ELEMENT(SETD,QUAD,NODE=4)
MFACE(MESH,MAP,ENTI="solid")
ELEMENT(SETD, EDGE, NODE=2)
MEDGE(SELE,ID)
1
MEDGE(MESH,MAP,ENTI="inlet")
MEDGE(SELE,ID)
6
MEDGE(MESH,MAP,ENTI="outlet")
MEDGE(SELE,ID)
```

```
5
MEDGE(MESH,MAP,ENTI="axis")
MEDGE(SELE,ID)
2
3
4
MEDGE(MESH,MAP,ENTI="freesurf")
MEDGE(SELE,ID)
8
16
11
MEDGE(MESH,MAP,ENTI="interface")
MEDGE(SELE,ID)
12
19
MEDGE(MESH,MAP,ENTI="edge")
MEDGE(SELE,ID)
20
MEDGE(MESH,MAP,ENTI="bottom")
MEDGE(SELE,ID)
7
18
MEDGE(MESH,MAP,ENTI="axiss")
END( )
FIPREP( )
//PROPERTIES
DENSITY( ADD, SET = "water", CONS = 0.9982 )
CONDUCTIVITY( ADD, SET = "water", CONS = 0.001409 )
VISCOSITY( ADD, SET = "water", CONS = 0.01002)
SPECIFICHEAT( ADD, SET = "water", CONS = 0.99952 )
SURFACETENSION( ADD, SET = "water", CONS = 72.8 )
DENSITY( ADD, SET = "silicon", CONS = 2.33 )
CONDUCTIVITY( ADD, SET = "silicon", CONS = 0.365434 )
SPECIFICHEAT( ADD, SET = "silicon", CONS = 0.168021 )
//ENTITIES
ENTITY(ADD, NAME="fluid", FLUI, PROP="water")
ENTITY( ADD, NAME = "solid", SOLI, PROP = "silicon" )
ENTITY(ADD, NAME="outlet", PLOT)
ENTITY(ADD, NAME="inlet", PLOT)
ENTITY(ADD, NAME="axis", PLOT)
ENTITY(ADD, NAME="freesurf", SURF, DEPT = 31, SPIN, STRA, ANG1=10, ANG2=180)
ENTITY(ADD, NAME="axiss", PLOT)
ENTITY(ADD, NAME="edge", PLOT)
ENTITY(ADD, NAME="bottom", PLOT)
ENTITY( ADD, NAME = "interface", PLOT, ATTA = "solid", NATT = "fluid" )
BODYFORCE(ADD, CONS, FX=981, FY=0, FZ=0)
```

```
PRESSURE(ADD, MIXE=1.0E-11, DISC)
OPTIONS(ADD, UPWINDING)
UPWINDING(ADD, STRE)
RELAXATION(  )
  0.3, 0.3, 0.3, 0, 0.5, 0.25
//BC
BCNODE(ADD, COOR, NODE=2)
BCNODE(ADD, SURF, NODE=2, ZERO)
BCNODE(ADD, VELO, NODE=2, ZERO)
BCNODE(ADD, UT, NODE=2, ZERO)
BCNODE(ADD, UX, ENTI="inlet", CONS=44.29)
BCNODE(ADD, UY, ENTI="inlet", ZERO)
BCNODE(ADD, UY, ENTI="axis", ZERO)
BCNODE(ADD, VELO, ENTI="interface", ZERO)
BCNODE(ADD, VELO, ENTI="bottom", ZERO)
BCNODE(ADD, VELO, ENTI="edge", ZERO)
BCNODE(ADD, VELO, ENTI="axiss", ZERO)
BCNODE( ADD, VELO, ENTI = "solid", ZERO )
BCNODE( ADD, TEMP, ENTI = "inlet", CONS = 20 )
BCFLUX( ADD, HEAT, ENTI = "bottom", CONS = 1.5 )
PROBLEM( ADD, 2-d, INCOMP, TRAN, LAMI, NONL, NEWT, MOME, ENERGY, FREE,
SING )
SOLUTION( ADD, N.R. = 50, KINE = 25, VELC = 1e-4, RESC = 1e-4, SURF = 1e-3 )
TIMEINTEGRATION( ADD, BACK, NSTE = 501, TSTA = 0, DT = 0.0001, VARI, WIND =
9, NOFI = 12 )
POSTPROCESS( NBLO = 2 )
   1,   101,     1
 101,   501,     2
CLIPPING( ADD, MINI )
   0,     0,     0,     0,    20,     0
ICNODE( ADD, UX, ENTI = "fluid", CONS = 44.29 )
ICNODE( ADD, TEMP, ENTI = "fluid", CONS = 20 )
ICNODE( ADD, TEMP, ENTI = "solid", CONS = 20 )
EXECUTION(ADD, NEWJ)
PRINTOUT(ADD, NONE, BOUN)
DATAPRINT(ADD, CONT)
END( )
CREATE(FISO)
RUN(FISOLV, BACK, AT="", TIME="NOW", COMP)
```

APPENDIX E: FIDAP CODE FOR CASE D

```
Title( )
Case D
FI-GEN(Elem = 1, POIN = 1, CURV = 1, SURF = 1, NODE = 0, MEDG= 1, MLOO = 1,
MFAC = 1, BEDG = 1, SPAV = 1, MSHE = 1, MSOL = 1, COOR = 1)
//Specifications
//Plate Thickness
$PlateT = 0.125
//Plate Length
$PlateL = 0.6475
//Nozzle width
$NozzleW = 0.085
//Nozzle height
$NozzleH = 0.55
//Depth of step
$Step = 0.025
//Creating basic geometry
//Points 1-8
POINT( ADD, COOR )
0 0
-$NozzleH 0
-$NozzleH $NozzleW
-0.18 0.17
-0.15 $PlateL
0 $PlateL
$PlateT $PlateL
$PlateT 0
//Lines 1-9
POINT( SELE, ID)
1
2
CURVE( ADD, LINE)
POINT( SELE, ID )
2
3
CURVE( ADD, LINE )
POINT(SELE, ID)
3
4
```

```
CURVE(ADD,LINE)
POINT(SELE, ID)
4
5
CURVE(ADD,LINE)
POINT(SELE,ID)
5
6
CURVE(ADD,LINE)
POINT(SELE,ID)
6
7
CURVE(ADD,LINE)
POINT(SELE,ID)
7
8
CURVE(ADD,LINE)
POINT(SELE,ID)
8
1
CURVE(ADD,LINE)
CURVE(SELE,ID)
3
4
CURVE(ADD, FILL, RADI=0.2)
//Interface Geometry
//Points 11-18
POINT(ADD, COOR)
-$Step 0
-$Step 0.32375
0 0.291375
0 0.356125
$Step 0.32375
-$Step $PlateL
$Step $PlateL
$Step 0
POINT(SELE,ID)
1
11
CURVE(ADD,LINE)
POINT(SELE,ID)
11
12
CURVE(ADD,LINE)
POINT(SELE,ID)
12
```

13
CURVE(ADD,LINE)
POINT(SELE,ID)
13
1
CURVE(ADD,LINE)
POINT(SELE,ID)
12
14
CURVE(ADD,LINE)
POINT(SELE,ID)
14
6
CURVE(ADD,LINE)
POINT(SELE,ID)
6
16
CURVE(ADD,LINE)
POINT(SELE,ID)
16
12
CURVE(ADD,LINE)
POINT(SELE,ID)
14
15
CURVE(ADD,LINE)
POINT(SELE,ID)
15
17
CURVE(ADD,LINE)
POINT(SELE,ID)
17
6
CURVE(ADD,LINE)
POINT(SELE,ID)
13
15
CURVE(ADD,LINE)
POINT(SELE,ID)
15
18
CURVE(ADD,LINE)
POINT(SELE,ID)
18
1
CURVE(ADD,LINE)

```
POINT(SELE,ID)
16
5
CURVE(ADD,LINE)
POINT(SELE,ID)
11
2
CURVE(ADD,LINE)
POINT(SELE,ID)
18
8
CURVE(ADD,LINE)
POINT(SELE,ID)
17
7
CURVE(ADD,LINE)
//surface
POINT(ADD,COOR)
-$NozzleH $PlateL
POINT(SELE,ID)
19
7
2
8
SURFACE(ADD,POINTS, ROWW=2, NOAD)
//mesh edges
CURVE(SELE,ID)
2
MEDGE(ADD, SUCC, INTE=30, RATI=0, 2RAT=0, PCEN=0)
CURVE(SELE,ID)
3
MEDGE(ADD, SUCC, INTE=6, RATI=0, 2RAT=0, PCEN=0)
CURVE(SELE,ID)
9
MEDGE(ADD, SUCC, INTE=34, RATI=0, 2RAT=0, PCEN=0)
CURVE(SELE,ID)
4
MEDGE(ADD, SUCC, INTE=70, RATI=0, 2RAT=0, PCEN=0)
CURVE(SELE,ID)
25
MEDGE(ADD, FRSTLAST, INTE=30, RATI=0.6, 2RAT=0, PCEN=0)
CURVE(SELE,ID)
24
MEDGE(ADD, LSTFIRST, INTE=30, RATI=0.4, 2RAT=0, PCEN=0)
CURVE(SELE, ID)
10
```

```
12
14
16
20
18
21
23
MEDGE(ADD, SUCC, INTE=10, RATI=0, 2RAT=0, PCEN=0)
CURVE(SELE,ID)
11
13
22
17
15
19
MEDGE(ADD, SUCC, INTE=70, RATI=0, 2RAT=0, PCEN=0)
CURVE(SELE,ID)
26
27
MEDGE(ADD, SUCC, INTE=20, RATI=0, 2RAT=0, PCEN=0)
CURVE(SELE,ID)
7
MEDGE(ADD, SUCC, INTE=140, RATI=0, 2RAT=0, PCEN=0)
//mesh loops
CURVE(SELE,ID)
25
2
3
9
4
24
17
11
MLOOP(ADD, MAP, VISI, NOSH, EDG1=1, EDG2=4, EDG3=1, EDG4=2)
CURVE(SELE,ID)
10
11
12
13
MLOOP(ADD, MAP, VISI, NOSH, EDG1=1, EDG2=1, EDG3=1, EDG4=1)
CURVE(SELE,ID)
12
14
18
21
MLOOP(ADD, MAP, VISI, NOSH, EDG1=1, EDG2=1, EDG3=1, EDG4=1)
```

```
CURVE(SELE,ID)
14
17
16
15
MLOOP(ADD, MAP, VISI, NOSH, EDG1=1, EDG2=1, EDG3=1, EDG4=1)
CURVE(SELE,ID)
18
15
20
19
MLOOP(ADD, MAP, VISI, NOSH, EDG1=1, EDG2=1, EDG3=1, EDG4=1)
CURVE(SELE,ID)
23
13
21
22
MLOOP(ADD, MAP, VISI, NOSH, EDG1=1, EDG2=1, EDG3=1, EDG4=1)
CURVE(SELE,ID)
26
22
19
27
7
MLOOP(ADD, MAP, VISI, NOSH, EDG1=1, EDG2=2, EDG3=1, EDG4=1)
//mesh faces
SURFACE(SELE,ID=1)
MLOOP(SELE,ID=1)
MFACE(ADD)
SURFACE(SELE,ID=1)
MLOOP(SELE,ID=2)
MFACE(ADD)
SURFACE(SELE,ID=1)
MLOOP(SELE,ID=3)
MFACE(ADD)
SURFACE(SELE,ID=1)
MLOOP(SELE,ID=4)
MFACE(ADD)
SURFACE(SELE,ID=1)
MLOOP(SELE,ID=5)
MFACE(ADD)
SURFACE(SELE,ID=1)
MLOOP(SELE,ID=6)
MFACE(ADD)
SURFACE(SELE,ID=1)
MLOOP(SELE,ID=7)
```

```
MFACE(ADD)
//meshing
MFACE(SELE,ID)
1
2
4
ELEMENT(SETD, QUAD, NODE=4)
MFACE(MESH, MAP, ENTI="fluid")
MFACE(SELE,ID)
3
5
6
7
ELEMENT(SETD,QUAD,NODE=4)
MFACE(MESH,MAP,ENTI="solid")
ELEMENT(SETD, EDGE, NODE=2)
MEDGE(SELE,ID)
1
MEDGE(MESH,MAP,ENTI="inlet")
MEDGE(SELE,ID)
6
10
MEDGE(MESH,MAP,ENTI="outlet")
MEDGE(SELE,ID)
5
7
MEDGE(MESH,MAP,ENTI="axis")
MEDGE(SELE,ID)
2
3
4
MEDGE(MESH,MAP,ENTI="freesurf")
MEDGE(SELE,ID)
16
8
9
19
MEDGE(MESH,MAP,ENTI="interface")
MEDGE(SELE,ID)
11
22
MEDGE(MESH,MAP,ENTI="edge")
MEDGE(SELE,ID)
23
MEDGE(MESH,MAP,ENTI="bottom")
MEDGE(SELE,ID)
```

```
14
21
MEDGE(MESH,MAP,ENTI="axiss")
END( )
FIPREP( )
//PROPERTIES
DENSITY( ADD, SET = "water", CONS = 0.9982 )
CONDUCTIVITY( ADD, SET = "water", CONS = 0.001409 )
VISCOSITY( ADD, SET = "water", CONS = 0.01002)
SPECIFICHEAT( ADD, SET = "water", CONS = 0.99952 )
SURFACETENSION( ADD, SET = "water", CONS = 72.8 )
DENSITY( ADD, SET = "silicon", CONS = 2.33 )
CONDUCTIVITY( ADD, SET = "silicon", CONS = 0.365434 )
SPECIFICHEAT( ADD, SET = "silicon", CONS = 0.168021 )
//ENTITIES
ENTITY(ADD, NAME="fluid", FLUI, PROP="water")
ENTITY( ADD, NAME = "solid", SOLI, PROP = "silicon" )
ENTITY(ADD, NAME="outlet", PLOT)
ENTITY(ADD, NAME="inlet", PLOT)
ENTITY(ADD, NAME="axis", PLOT)
ENTITY(ADD, NAME="freesurf", SURF, DEPT = 31, SPIN, STRA, ANG1=10, ANG2=180)
ENTITY(ADD, NAME="axiss", PLOT)
ENTITY(ADD, NAME="edge", PLOT)
ENTITY(ADD, NAME="bottom", PLOT)
ENTITY( ADD, NAME = "interface", PLOT, ATTA = "solid", NATT = "fluid" )
BODYFORCE(ADD, CONS, FX=981, FY=0, FZ=0)
PRESSURE(ADD, MIXE=1.0E-11, DISC)
OPTIONS(ADD, UPWINDING)
UPWINDING(ADD, STRE)
RELAXATION(  )
  0.3, 0.3, 0.3, 0, 0.5, 0.25
//BC
BCNODE(ADD, COOR, NODE=2)
BCNODE(ADD, SURF, NODE=2, ZERO)
BCNODE(ADD, VELO, NODE=2, ZERO)
BCNODE(ADD, UT, NODE=2, ZERO)
BCNODE(ADD, UX, ENTI="inlet", CONS=44.29)
BCNODE(ADD, UY, ENTI="inlet", ZERO)
BCNODE(ADD, UY, ENTI="axis", ZERO)
BCNODE(ADD, VELO, ENTI="interface", ZERO)
BCNODE(ADD, VELO, ENTI="bottom", ZERO)
BCNODE(ADD, VELO, ENTI="edge", ZERO)
BCNODE(ADD, VELO, ENTI="axiss", ZERO)
BCNODE( ADD, VELO, ENTI = "solid", ZERO )
BCNODE( ADD, TEMP, ENTI = "inlet", CONS = 20 )
BCFLUX( ADD, HEAT, ENTI = "bottom", CONS = 1.5 )
```

```
PROBLEM( ADD, 2-d, INCOMP, TRAN, LAMI, NONL, NEWT, MOME, ENERGY, FREE,
SING )
SOLUTION( ADD, N.R. = 50, KINE = 25, VELC = 1e-4, RESC = 1e-4, SURF = 1e-3 )
TIMEINTEGRATION( ADD, BACK, NSTE = 501, TSTA = 0, DT = 0.0001, VARI, WIND =
9, NOFI = 12 )
POSTPROCESS( NBLO = 2 )
   1,   101,     1
 101,   501,     2
CLIPPING( ADD, MINI )
   0,     0,     0,     0,    20,     0
ICNODE( ADD, UX, ENTI = "fluid", CONS = 44.29 )
ICNODE( ADD, TEMP, ENTI = "fluid", CONS = 20 )
ICNODE( ADD, TEMP, ENTI = "solid", CONS = 20 )
EXECUTION(ADD, NEWJ)
PRINTOUT(ADD, NONE, BOUN)
DATAPRINT(ADD, CONT)
END( )
CREATE(FISO)
RUN(FISOLV, BACK, AT="", TIME="NOW", COMP)
```

APPENDIX F: FIDAP CODE FOR CASE E

```
Title( )
Case E
FI-GEN(Elem = 1, POIN = 1, CURV = 1, SURF = 1, NODE = 0, MEDG= 1, MLOO = 1,
MFAC = 1, BEDG = 1, SPAV = 1, MSHE = 1, MSOL = 1, COOR = 1)
//Specifications
//Plate Thickness
$PlateT = 0.125
//Plate Length
$PlateL = 0.6475
//Nozzle width
$NozzleW = 0.085
//Nozzle height
$NozzleH = 0.55
//Depth of step
$Step = 0.025
//Creating basic geometry
//Points 1-8
POINT( ADD, COOR )
0 0
-$NozzleH 0
-$NozzleH $NozzleW
-0.18 0.17
-0.15 $PlateL
0 $PlateL
$PlateT $PlateL
$PlateT 0
//Lines 1-9
POINT( SELE, ID)
1
2
CURVE( ADD, LINE)
POINT( SELE, ID )
2
3
CURVE( ADD, LINE )
POINT(SELE, ID)
3
4
```

```
CURVE(ADD,LINE)
POINT(SELE, ID)
4
5
CURVE(ADD,LINE)
POINT(SELE,ID)
5
6
CURVE(ADD,LINE)
POINT(SELE,ID)
6
7
CURVE(ADD,LINE)
POINT(SELE,ID)
7
8
CURVE(ADD,LINE)
POINT(SELE,ID)
8
1
CURVE(ADD,LINE)
CURVE(SELE,ID)
3
4
CURVE(ADD, FILL, RADI=0.2)
//Interface Geometry
//Points 11-16
POINT(ADD, COOR)
-$Step 0
-$Step 0.032375
0 0.0485625
0 0.5989375
-$Step 0.615125
-$Step $PlateL
POINT(SELE,ID)
1
11
CURVE(ADD,LINE)
POINT(SELE,ID)
11
12
CURVE(ADD,LINE)
POINT(SELE,ID)
12
13
CURVE(ADD,LINE)
```

```
POINT(SELE,ID)
13
1
CURVE(ADD,LINE)
POINT(SELE,ID)
13
14
CURVE(ADD,LINE)
POINT(SELE,ID)
14
15
CURVE(ADD,LINE)
POINT(SELE,ID)
15
16
CURVE(ADD,LINE)
POINT(SELE,ID)
16
6
CURVE(ADD,LINE)
POINT(SELE,ID)
6
14
CURVE(ADD,LINE)
POINT(SELE,ID)
12
15
CURVE(ADD,LINE)
POINT(SELE,ID)
5
16
CURVE(ADD,LINE)
POINT(SELE,ID)
11
2
CURVE(ADD,LINE)
//surface
POINT(ADD,COOR)
-$NozzleH $PlateL
POINT(SELE,ID)
17
7
2
8
SURFACE(ADD,POINTS, ROWW=2, NOAD)
//mesh edges
```

```
CURVE(SELE,ID)
2
MEDGE(ADD, SUCC, INTE=30, RATI=0, 2RAT=0, PCEN=0)
CURVE(SELE,ID)
3
MEDGE(ADD, SUCC, INTE=6, RATI=0, 2RAT=0, PCEN=0)
CURVE(SELE,ID)
9
MEDGE(ADD, SUCC, INTE=34, RATI=0, 2RAT=0, PCEN=0)
CURVE(SELE,ID)
4
MEDGE(ADD, SUCC, INTE=70, RATI=0, 2RAT=0, PCEN=0)
CURVE(SELE,ID)
21
MEDGE(ADD, FRSTLAST, INTE=35, RATI=0.6, 2RAT=0, PCEN=0)
CURVE(SELE,ID)
20
MEDGE(ADD, LSTFIRST, INTE=35, RATI=0.4, 2RAT=0, PCEN=0)
CURVE(SELE, ID)
10
11
12
13
15
16
17
18
MEDGE(ADD, SUCC, INTE=10, RATI=0, 2RAT=0, PCEN=0)
CURVE(SELE,ID)
19
MEDGE(ADD, SUCC, INTE=120, RATI=0, 2RAT=0, PCEN=0)
CURVE(SELE,ID)
14
MEDGE(ADD, SUCC, INTE=120, RATI=0, 2RAT=0, PCEN=0)
CURVE(SELE,ID)
8
6
MEDGE(ADD, SUCC, INTE=20, RATI=0, 2RAT=0, PCEN=0)
CURVE(SELE,ID)
7
MEDGE(ADD, SUCC, INTE=140, RATI=0, 2RAT=0, PCEN=0)
//mesh loops
CURVE(SELE,ID)
21
2
3
```

```
9
4
20
16
19
11
MLOOP(ADD, MAP, VISI, NOSH, EDG1=1, EDG2=4, EDG3=1, EDG4=3)
CURVE(SELE,ID)
10
11
12
13
MLOOP(ADD, MAP, VISI, NOSH, EDG1=1, EDG2=1, EDG3=1, EDG4=1)
CURVE(SELE,ID)
12
14
15
19
MLOOP(ADD, MAP, VISI, NOSH, EDG1=1, EDG2=1, EDG3=1, EDG4=1)
CURVE(SELE,ID)
15
16
17
18
MLOOP(ADD, MAP, VISI, NOSH, EDG1=1, EDG2=1, EDG3=1, EDG4=1)
CURVE(SELE,ID)
8
13
14
18
6
7
MLOOP(ADD, MAP, VISI, NOSH, EDG1=1, EDG2=3, EDG3=1, EDG4=1)
//mesh faces
SURFACE(SELE,ID=1)
MLOOP(SELE,ID=1)
MFACE(ADD)
SURFACE(SELE,ID=1)
MLOOP(SELE,ID=2)
MFACE(ADD)
SURFACE(SELE,ID=1)
MLOOP(SELE,ID=3)
MFACE(ADD)
SURFACE(SELE,ID=1)
MLOOP(SELE,ID=4)
MFACE(ADD)
```

```
SURFACE(SELE,ID=1)
MLOOP(SELE,ID=5)
MFACE(ADD)
//meshing
MFACE(SELE,ID)
1
3
ELEMENT(SETD, QUAD, NODE=4)
MFACE(MESH, MAP, ENTI="fluid")
MFACE(SELE,ID)
2
4
5
ELEMENT(SETD,QUAD,NODE=4)
MFACE(MESH,MAP,ENTI="solid")
ELEMENT(SETD, EDGE, NODE=2)
MEDGE(SELE,ID)
1
MEDGE(MESH,MAP,ENTI="inlet")
MEDGE(SELE,ID)
6
MEDGE(MESH,MAP,ENTI="outlet")
MEDGE(SELE,ID)
5
MEDGE(MESH,MAP,ENTI="axis")
MEDGE(SELE,ID)
2
3
4
MEDGE(MESH,MAP,ENTI="freesurf")
MEDGE(SELE,ID)
8
9
16
11
12
MEDGE(MESH,MAP,ENTI="interface")
MEDGE(SELE,ID)
13
18
MEDGE(MESH,MAP,ENTI="edge")
MEDGE(SELE,ID)
19
MEDGE(MESH,MAP,ENTI="bottom")
MEDGE(SELE,ID)
10
```

```
8
MEDGE(MESH,MAP,ENTI="axiss")
END( )
FIPREP( )
//PROPERTIES
DENSITY( ADD, SET = "water", CONS = 0.9982 )
CONDUCTIVITY( ADD, SET = "water", CONS = 0.001409 )
VISCOSITY( ADD, SET = "water", CONS = 0.01002)
SPECIFICHEAT( ADD, SET = "water", CONS = 0.99952 )
SURFACETENSION( ADD, SET = "water", CONS = 72.8 )
DENSITY( ADD, SET = "silicon", CONS = 2.33 )
CONDUCTIVITY( ADD, SET = "silicon", CONS = 0.365434 )
SPECIFICHEAT( ADD, SET = "silicon", CONS = 0.168021 )
//ENTITIES
ENTITY(ADD, NAME="fluid", FLUI, PROP="water")
ENTITY( ADD, NAME = "solid", SOLI, PROP = "silicon" )
ENTITY(ADD, NAME="outlet", PLOT)
ENTITY(ADD, NAME="inlet", PLOT)
ENTITY(ADD, NAME="axis", PLOT)
ENTITY(ADD, NAME="freesurf", SURF, DEPT = 31, SPIN, STRA, ANG1=10, ANG2=180)
ENTITY(ADD, NAME="axiss", PLOT)
ENTITY(ADD, NAME="edge", PLOT)
ENTITY(ADD, NAME="bottom", PLOT)
ENTITY( ADD, NAME = "interface", PLOT, ATTA = "solid", NATT = "fluid" )
BODYFORCE(ADD, CONS, FX=981, FY=0, FZ=0)
PRESSURE(ADD, MIXE=1.0E-11, DISC)
OPTIONS(ADD, UPWINDING)
UPWINDING(ADD, STRE)
RELAXATION(  )
  0.3, 0.3, 0.3, 0, 0.5, 0.25
//BC
BCNODE(ADD, COOR, NODE=2)
BCNODE(ADD, SURF, NODE=2, ZERO)
BCNODE(ADD, VELO, NODE=2, ZERO)
BCNODE(ADD, UT, NODE=2, ZERO)
BCNODE(ADD, UX, ENTI="inlet", CONS=44.29)
BCNODE(ADD, UY, ENTI="inlet", ZERO)
BCNODE(ADD, UY, ENTI="axis", ZERO)
BCNODE(ADD, VELO, ENTI="interface", ZERO)
BCNODE(ADD, VELO, ENTI="bottom", ZERO)
BCNODE(ADD, VELO, ENTI="edge", ZERO)
BCNODE(ADD, VELO, ENTI="axiss", ZERO)
BCNODE( ADD, VELO, ENTI = "solid", ZERO )
BCNODE( ADD, TEMP, ENTI = "inlet", CONS = 20 )
BCFLUX( ADD, HEAT, ENTI = "bottom", CONS = 1.5 )
```

```
PROBLEM( ADD, 2-d, INCOMP, TRAN, LAMI, NONL, NEWT, MOME, ENERGY, FREE,
SING )
SOLUTION( ADD, N.R. = 50, KINE = 25, VELC = 1e-4, RESC = 1e-4, SURF = 1e-3 )
TIMEINTEGRATION( ADD, BACK, NSTE = 501, TSTA = 0, DT = 0.0001, VARI, WIND =
9, NOFI = 12 )
POSTPROCESS( NBLO = 2 )
   1,   101,     1
 101,   501,     2
CLIPPING( ADD, MINI )
   0,     0,     0,     0,    20,     0
ICNODE( ADD, UX, ENTI = "fluid", CONS = 44.29 )
ICNODE( ADD, TEMP, ENTI = "fluid", CONS = 20 )
ICNODE( ADD, TEMP, ENTI = "solid", CONS = 20 )
EXECUTION(ADD, NEWJ)
PRINTOUT(ADD, NONE, BOUN)
DATAPRINT(ADD, CONT)
END( )
CREATE(FISO)
RUN(FISOLV, BACK, AT="", TIME="NOW", COMP)
```

APPENDIX G: FIDAP CODE FOR CASE F

```
Title( )
Case F
FI-GEN(Elem = 1, POIN = 1, CURV = 1, SURF = 1, NODE = 0, MEDG= 1, MLOO = 1,
MFAC = 1, BEDG = 1, SPAV = 1, MSHE = 1, MSOL = 1, COOR = 1)
//Specifications
//Plate Thickness
$PlateT = 0.125
//Plate Length
$PlateL = 0.6475
//Nozzle width
$NozzleW = 0.085
//Nozzle height
$NozzleH = 0.55
//Depth of step
$Step = 0.025
//Creating basic geometry
//Points 1-8
POINT( ADD, COOR )
0 0
-$NozzleH 0
-$NozzleH $NozzleW
-0.18 0.17
-0.15 $PlateL
0 $PlateL
$PlateT $PlateL
$PlateT 0
//Lines 1-9
POINT( SELE, ID)
1
2
CURVE( ADD, LINE)
POINT( SELE, ID )
2
3
CURVE( ADD, LINE )
POINT(SELE, ID)
3
4
```

```
CURVE(ADD,LINE)
POINT(SELE, ID)
4
5
CURVE(ADD,LINE)
POINT(SELE,ID)
5
6
CURVE(ADD,LINE)
POINT(SELE,ID)
6
7
CURVE(ADD,LINE)
POINT(SELE,ID)
7
8
CURVE(ADD,LINE)
POINT(SELE,ID)
8
1
CURVE(ADD,LINE)
CURVE(SELE,ID)
3
4
CURVE(ADD, FILL, RADI=0.2)
//Interface Geometry
//Points 11-16
POINT(ADD, COOR)
-$Step 0
-$Step 0.291375
-$Step 0.356125
0 0.3723125
0 0.2751875
-$Step $PlateL
POINT(SELE,ID)
1
11
CURVE(ADD,LINE)
POINT(SELE,ID)
11
12
CURVE(ADD,LINE)
POINT(SELE,ID)
12
15
CURVE(ADD,LINE)
```

```
POINT(SELE,ID)
15
1
CURVE(ADD,LINE)
POINT(SELE,ID)
12
13
CURVE(ADD,LINE)
POINT(SELE,ID)
13
14
CURVE(ADD,LINE)
POINT(SELE,ID)
14
15
CURVE(ADD,LINE)
POINT(SELE,ID)
13
16
CURVE(ADD,LINE)
POINT(SELE,ID)
16
6
CURVE(ADD,LINE)
POINT(SELE,ID)
6
14
CURVE(ADD,LINE)
POINT(SELE,ID)
5
16
CURVE(ADD,LINE)
POINT(SELE,ID)
11
2
CURVE(ADD,LINE)
//surface
POINT(ADD,COOR)
-$NozzleH $PlateL
POINT(SELE,ID)
17
7
2
8
SURFACE(ADD,POINTS, ROWW=2, NOAD)
//mesh edges
```

```
CURVE(SELE,ID)
2
MEDGE(ADD, SUCC, INTE=30, RATI=0, 2RAT=0, PCEN=0)
CURVE(SELE,ID)
3
MEDGE(ADD, SUCC, INTE=6, RATI=0, 2RAT=0, PCEN=0)
CURVE(SELE,ID)
9
MEDGE(ADD, SUCC, INTE=34, RATI=0, 2RAT=0, PCEN=0)
CURVE(SELE,ID)
4
MEDGE(ADD, SUCC, INTE=70, RATI=0, 2RAT=0, PCEN=0)
CURVE(SELE,ID)
21
MEDGE(ADD, FRSTLAST, INTE=30, RATI=0.6, 2RAT=0, PCEN=0)
CURVE(SELE,ID)
20
MEDGE(ADD, LSTFIRST, INTE=30, RATI=0.4, 2RAT=0, PCEN=0)
CURVE(SELE, ID)
10
12
15
18
MEDGE(ADD, SUCC, INTE=10, RATI=0, 2RAT=0, PCEN=0)
CURVE(SELE,ID)
11
13
17
19
MEDGE(ADD, SUCC, INTE=60, RATI=0, 2RAT=0, PCEN=0)
CURVE(SELE,ID)
14
16
MEDGE(ADD, SUCC, INTE=20, RATI=0, 2RAT=0, PCEN=0)
CURVE(SELE,ID)
8
6
MEDGE(ADD, SUCC, INTE=25, RATI=0, 2RAT=0, PCEN=0)
CURVE(SELE,ID)
7
MEDGE(ADD, SUCC, INTE=140, RATI=0, 2RAT=0, PCEN=0)
//mesh loops
CURVE(SELE,ID)
21
2
3
```

```
9
4
20
17
14
11
MLOOP(ADD, MAP, VISI, NOSH, EDG1=1, EDG2=4, EDG3=1, EDG4=3)
CURVE(SELE,ID)
10
11
12
13
MLOOP(ADD, MAP, VISI, NOSH, EDG1=1, EDG2=1, EDG3=1, EDG4=1)
CURVE(SELE,ID)
12
14
15
16
MLOOP(ADD, MAP, VISI, NOSH, EDG1=1, EDG2=1, EDG3=1, EDG4=1)
CURVE(SELE,ID)
15
17
18
19
MLOOP(ADD, MAP, VISI, NOSH, EDG1=1, EDG2=1, EDG3=1, EDG4=1)
CURVE(SELE,ID)
8
13
16
19
6
7
MLOOP(ADD, MAP, VISI, NOSH, EDG1=1, EDG2=3, EDG3=1, EDG4=1)
//mesh faces
SURFACE(SELE,ID=1)
MLOOP(SELE,ID=1)
MFACE(ADD)
SURFACE(SELE,ID=1)
MLOOP(SELE,ID=2)
MFACE(ADD)
SURFACE(SELE,ID=1)
MLOOP(SELE,ID=3)
MFACE(ADD)
SURFACE(SELE,ID=1)
MLOOP(SELE,ID=4)
MFACE(ADD)
```

```
SURFACE(SELE,ID=1)
MLOOP(SELE,ID=5)
MFACE(ADD)
//meshing
MFACE(SELE,ID)
1
2
4
ELEMENT(SETD, QUAD, NODE=4)
MFACE(MESH, MAP, ENTI="fluid")
MFACE(SELE,ID)
3
5
ELEMENT(SETD,QUAD,NODE=4)
MFACE(MESH,MAP,ENTI="solid")
ELEMENT(SETD, EDGE, NODE=2)
MEDGE(SELE,ID)
1
MEDGE(MESH,MAP,ENTI="inlet")
MEDGE(SELE,ID)
6
10
MEDGE(MESH,MAP,ENTI="outlet")
MEDGE(SELE,ID)
5
7
MEDGE(MESH,MAP,ENTI="axis")
MEDGE(SELE,ID)
2
3
4
MEDGE(MESH,MAP,ENTI="freesurf")
MEDGE(SELE,ID)
12
8
15
9
14
MEDGE(MESH,MAP,ENTI="interface")
MEDGE(SELE,ID)
18
MEDGE(MESH,MAP,ENTI="edge")
MEDGE(SELE,ID)
19
MEDGE(MESH,MAP,ENTI="bottom")
MEDGE(SELE,ID)
```

```
17
MEDGE(MESH,MAP,ENTI="axiss")
END( )
FIPREP( )
//PROPERTIES
DENSITY( ADD, SET = "water", CONS = 0.9982 )
CONDUCTIVITY( ADD, SET = "water", CONS = 0.001409 )
VISCOSITY( ADD, SET = "water", CONS = 0.01002)
SPECIFICHEAT( ADD, SET = "water", CONS = 0.99952 )
SURFACETENSION( ADD, SET = "water", CONS = 72.8 )
DENSITY( ADD, SET = "silicon", CONS = 2.33 )
CONDUCTIVITY( ADD, SET = "silicon", CONS = 0.365434 )
SPECIFICHEAT( ADD, SET = "silicon", CONS = 0.168021 )
//ENTITIES
ENTITY(ADD, NAME="fluid", FLUI, PROP="water")
ENTITY( ADD, NAME = "solid", SOLI, PROP = "silicon" )
ENTITY(ADD, NAME="outlet", PLOT)
ENTITY(ADD, NAME="inlet", PLOT)
ENTITY(ADD, NAME="axis", PLOT)
ENTITY(ADD, NAME="freesurf", SURF, DEPT = 31, SPIN, STRA, ANG1=10, ANG2=180)
ENTITY(ADD, NAME="axiss", PLOT)
ENTITY(ADD, NAME="edge", PLOT)
ENTITY(ADD, NAME="bottom", PLOT)
ENTITY( ADD, NAME = "interface", PLOT, ATTA = "solid", NATT = "fluid" )
BODYFORCE(ADD, CONS, FX=981, FY=0, FZ=0)
PRESSURE(ADD, MIXE=1.0E-11, DISC)
OPTIONS(ADD, UPWINDING)
UPWINDING(ADD, STRE)
RELAXATION(  )
  0.3, 0.3, 0.3, 0, 0.5, 0.25
//BC
BCNODE(ADD, COOR, NODE=2)
BCNODE(ADD, SURF, NODE=2, ZERO)
BCNODE(ADD, VELO, NODE=2, ZERO)
BCNODE(ADD, UT, NODE=2, ZERO)
BCNODE(ADD, UX, ENTI="inlet", CONS=44.29)
BCNODE(ADD, UY, ENTI="inlet", ZERO)
BCNODE(ADD, UY, ENTI="axis", ZERO)
BCNODE(ADD, VELO, ENTI="interface", ZERO)
BCNODE(ADD, VELO, ENTI="bottom", ZERO)
BCNODE(ADD, VELO, ENTI="edge", ZERO)
BCNODE(ADD, VELO, ENTI="axiss", ZERO)
BCNODE( ADD, VELO, ENTI = "solid", ZERO )
BCNODE( ADD, TEMP, ENTI = "inlet", CONS = 20 )
BCFLUX( ADD, HEAT, ENTI = "bottom", CONS = 1.5 )
```

```
PROBLEM( ADD, 2-d, INCOMP, TRAN, LAMI, NONL, NEWT, MOME, ENERGY, FREE,
SING )
SOLUTION( ADD, N.R. = 50, KINE = 25, VELC = 1e-4, RESC = 1e-4, SURF = 1e-3 )
TIMEINTEGRATION( ADD, BACK, NSTE = 501, TSTA = 0, DT = 0.0001, VARI, WIND =
9, NOFI = 12 )
POSTPROCESS( NBLO = 2 )
   1,   101,     1
 101,   501,     2
CLIPPING( ADD, MINI )
   0,     0,     0,     0,    20,     0
ICNODE( ADD, UX, ENTI = "fluid", CONS = 44.29 )
ICNODE( ADD, TEMP, ENTI = "fluid", CONS = 20 )
ICNODE( ADD, TEMP, ENTI = "solid", CONS = 20 )
EXECUTION(ADD, NEWJ)
PRINTOUT(ADD, NONE, BOUN)
DATAPRINT(ADD, CONT)
END( )
CREATE(FISO)
RUN(FISOLV, BACK, AT="", TIME="NOW", COMP)
```